AN EXPERIMENTAL STUDY OF WINDTURBINE NOISE

by

EDWARD N. MARCUS

S.B. (PHYSICS)
MASSACHUSETTS INSTITUTE OF TECHNOLOGY
(1981)

Submitted in Partial Fulfillment
of the Requirements
for the Degree of

MASTER OF SCIENCE IN AERONAUTICS

AND ASTRONAUTICS

at the

MASSACHUSETTS INSTITUTE OF TECHNOLOGY

August 1982

Signature of Author: Signature redacted .....
Department of Aeronautics and Astronautics August, 1982

Signature redacted

Certified by: .....
Wesley L. Harris, Thesis Supervisor

Signature redacted

Accepted by: ....
Chairman, Departmental Graduate Committee

AN EXPERIMENTAL STUDY of WINDTURBINE NOISE

by
EDWARD N. MARCUS

Submitted To The Department of Aeronautics and Astronautics in August 1982 in partial fulfillment of the requirements for the Degree of Master of Science in Aeronautics and Astronautics

Abstract

A program of experiments has been conducted to study the noise of a horizontal axis windturbine. These tests were performed on a 1/53 scale model of the D.O.E.-NASA MOD-1 windturbine. Experiments were performed in the MIT 5'x7 1/2' Anechoic Windtunnel facility.

The three forms of noise of particular interest to this study are broadband noise, Gutin noise, and the noise produced by blade tower wake interaction. The intensity of noise from blade tower wake interaction is predicted to increase with the fourth power of the RPM, and the second power of the tower drag to the oncoming wind. These predictions were confirmed in experiments. Broadband noise is predicted to increase with the fourth power of the RPM, the kinetic energy of incident turbulence, and with the ratio of the rotor span to the turbulent scale. These predictions could not be confirmed through experiment, and require the further effort of improved measurements and experimental techniques.

Thesis Supervisor: Professor Wesley L. Harris

Acknowledgements

There are many people without whose help, this work could not have been completed. I would like to thank Don Weiner and Al Shaw, who, throughout my experiments, were always ready with a helping hand. I thank James Wang for his enthusiastic work both in the windtunnel and on the computer. A special thanks to Rudi Martinez and Greg Tocci for fruitful discussions on the theory. Thanks to the members of the Acoustics and Vibration Lab for their patient instruction and help on the spectrum analyzer. A special thanks to Mark Drela for his work on the model blades.

Professor Harris was always sensitive to my work and its progress. I would like to thank him for his guidance, leadership, and support. I would also like to acknowledge the support of the Solar Energy Research Institute.

TABLE OF CONTENTS

LIST OF FIGURES

A complete catalog of all acoustic measurements can be found in Appendix C.

LIST OF SYMBOLS

A	Wake Amplitude
b	Span
B	Wake Half Width at Half Depth
c	Chord
c_o	Speed of Sound
F	Line Source Strength
J_m	Bessel Function of the First Kind (order m)
K_x, K_Y, K_Z	Cartesian Wavenumbers of the Turbulence
K	$(K_x^2 + K_Y^2)^{1/2}$
L	Turbulent Integral Scale
$\mathcal{L}$	Lift / Span
$\tilde{\mathcal{L}}$	Fourier Transform of $\mathcal{L}$
m	Harmonic Counter
n	Number of Blades
P	Acoustic Pressure
r	Radial Position
$\bar{r}$	r/b
R	Observer Distance
S	Aerodynamic Transfer Function
$W(x,Y,z)$	Axial Turbulent Velocity
$\tilde{W}(K_x, K_Y, K_z)$	Fourier Transform of W
$\overline{W^2}$	Mean Square Axial Velocity
U	Free Stream Velocity
α	$\mathrm{Tan}^{-1}(K_Y/K_x)$

Ω	Rotation Speed
ϕ_0	Initial Angular Blade Position
ρ	Density of Air
κ	KL
$\bar{\omega}$	Reduced Frequency $(\omega c / 2\Omega r)$
η	Azimuth Angle with Respect To The Windturbine Axis
SPL	20 Log $(P / 20\,\mu Pa)$
Φ_{ww}	Power Spectral Density of The Turbulence.
Λ	b/L
θ	Angle between the tower legs
$\langle\ \rangle$	Ensemble Average

CHAPTER 1

INTRODUCTION

Demand for the world's dwindling supplies of petroleum has motivated the search for alternative energy resources of the sun and wind. At present, the United States depends on petroleum for forty-four percent of its energy consumption (ref. 1). Thirty-six percent of this petroleum is imported. As the political and economic price of oil dependence increases, the incentive for energy self sufficiency has accelerated the developement of alternative energy resources. In this spirit, the first seeds of large scale solar and wind power facilities were planted in the energy conciousness of the late 1970's. During this time, as energy prices increased, a heat producing solar collector, or an electricity producing windturbine, became, in some cases, an attractive economic alternative to oil.

Compared to the inherent environmental dangers of nuclear power, oil, and coal, windturbines and solar collectors have only a mild influence on their surroundings. This is not to say, however, that alternative energy resources are without environmental impact. Recently, in the case of wind energy, it has been found that large scale windturbines produce sound of considerable annoyance to nearby neighbors. When DOE-NASA built the two megawatt MOD-1 windturbine in Boone, North Carolina, sound pressure levels of 86db were observed at a

residence one kilometer from the windturbine sight (ref. 17). Similiar noise problems have been observed for machines as small as fifty kilowatts (ref. 28). Windturbine noise is not only annoying to hear, but also, it is rich in low frequencies which excite structural resonances, and become a source of annoying vibration (ref. 21).

The three classic components of a noise control problem are the source, path and receiver of the acoustic field. For the case of windturbine noise, all of these components present important issues. Several authors have, with the help of field measurements, examined the issue of pathwise attenuation (refs. 21 & 26). In this problem, the geographic and atmospheric environment influence the geometric spreading characteristics of the sound as it approaches the receiver. Some of these papers also consider the insulating or amplifying effect of the receiver environment (ref. 21). In a specific noise control problem, the required transmission loss and resonant characteristics of a building must be considered in order to insure proper isolation of the observer from the sound. Even these issues are not straight forward. The human perception to low frequency sound is still a topic of research. Legal noise level thresholds are based on A-weighted filtering which tends to underestimate the annoying effects of windturbine noise.

Of course, the most desirable solution to the windturbine noise problem is an economic means of reducing the source of the noise at the windturbine itself. This approach requires

an understanding of the aerodynamic sources which theory and experiment have shown responsible for the annoying noise of a windturbine. Spectral density measurements have shown that windturbine noise consists of narrowband noise at harmonics of the blade passage frequency, and broadband noise whose frequency range lies both between and beyond the narrowband peaks. The relative magnitudes of broadband vs. narrowband noise depend on the specific case, but, simply stated, broadband noise is probably the result of blade interaction with a turbulent atmosphere. Narrowband noise, on the other hand, is the result of repeated blade interaction with a stationary structure such as a wake or boundary layer which the blade repeatedly encounters. In general, narrowband noise at the blade passage harmonics is impulsive, and therefore the more annoying of the two sounds.

The first theoretical model on low frequency narrowband noise was given by Martinez, Widnall, and Harris (ref. 9). This model employs unsteady aerodynamic theory to calculate the unsteady blade loads which occur with repeated blade passage through a tower wake. Knowing the periodic blade loading, the acoustic field can then be calculated from the classical theory of acoustics. A similiar approach was followed by Viterna (ref. 12) in his successful calculation of the noise produced by MOD-1. With slight modification, the narrowband theory of reference 9 will also be used here to compare the acoustic spectral densities which are measured for blade passage through the different wakes of our experiment.

The purpose of this thesis is to carry out a set of experiments in order to understand the important parameters which govern the production of aerodynamic windturbine noise. For the sake of intelligent comparison, these experiments are, when possible, conducted within the framework of theory. Among the many parameters which govern windturbine noise, those of specific interest to this study are,

1) RPM
2) Wind Velocity
3) Number of Blades
4) Blade Geometry
5) Tower Blade Separation
6) Blade Mounting (upwind/downwind)
7) Blade Loading
8) Ground Shear
9) Cross Flows
10) Incident Turbulence Intensity
11) Incident Turbulence Scale
12) Tower Wake

Our experiments were conducted on a 1/53 scale model of the MOD-1 windturbine tower and, these tests were conducted at the M.I.T. 5'x 7 1/2' Anechoic Windtunnel Facility. The small scale model provided the advantage of relative flexibility in the experimental procedure. The windturbine equipment and geometry were easy to manipulate. Also, it was found that the scale model provided an excellent tool for the study of narrowband noise at harmonics of the blade passage frequency. The measured spectral densities at these frequencies are believed representative of the spectral densities at the blade passage frequencies for the full scale MOD-1.

Unfortunately, the same correspondence which is found for narrowband noise, is believed not to hold for the broadband noise. Model noise at the blade passage harmonics is easily compared to similiar full scale noise by the ratio of the full

scale to the model rotation speed. Broadband noise is believed to scale, not only with the ratio of rotation speeds, but also with the ratio of the rotation speed to the frequencies of turbulent velocity fluctuations encountered by the rotor. Another important scaling factor for broadband noise is the ratio of the rotor span to the turbulent scale. Thus, it is easy to see that proper scale tests of broadband noise requires an experiment to simulate a number of different ratios. If these ratios are not identical, the shape of scale model broadband spectrum may be quite different from that of the full scale.

Another disadvantage of scale modeling in the windtunnel is the inability to simulate full scale Reynold's numbers. For example, the Reynold's number for flow around a tower leg of MOD-1 is 10^6. With the scale model at our disposal, and roughly equal free stream velocities, the Reynold's numbers for our tests were approximately,

$$Re = Re_{\substack{full \\ scale}} /50$$

The two major sections of this thesis are Chapter 2 and Chapter 4 which discuss the theory of windturbine noise and the results of windtunnel measurements respectively. The theory section tries to formulate scaling laws for broadband noise, Gutin noise and blade tower wake interaction noise, the three sources most responsible for windturbine noise. These

noise sources were observed in the windtunnel, and the results of these observations can be found in Chapter 4. Chapter 4 also contains comparisions of measurements with theoretical scaling predictions.

CHAPTER 2

THEORY

2.1 STATEMENT OF THE PROBLEM

The unsteady flow over the rotating airfoil of a windturbine induces fluctuating loads which radiate sound. When oscillating forces are the source of noise, the acoustic field will be of dipole form. It will exhibit the directionality expected from an acoustic dipole.

There are several mechanisms which are responsible for dipole noise of a windturbine. Among these are, blade interaction with atmospheric turbulence, blade tower wake interaction, and Gutin noise, the noise produced by steady loading on the blade. Although the analytic techniques to evaluate these sources are different, all these sources are of dipole form and so these problems share common elements. Among the factors to consider in any dipole rotor noise problem are 1) the loads which occur on the rotating blade and 2) the resulting acoustic field.

The loads on a windturbine blade may be classified as steady, or unsteady, and unsteady loads may be further classified as those which are random, and those loads which are not random but rather correlate to the angular position of the blade. Thus three classifications are responsible for the three kinds of dipole noises which are observed for a

windturbine. Steady loads are responsible for Gutin noise. Random unsteady loads are responsible for broadband noise, and finally, periodic non random blade loading is the source of noise at harmonics of the blade passage frequency. This noise is the result of periodic blade passage through a tower wake or boundary layer close to the earth's surface.

Once the blade loading is understood, a calculation of the acoustic field is theoretically simple, but its computation is difficult and expensive. This follows from the Doppler modulation of a dipole in rotation and the resulting complicated acoustic Green's function (ref. 4). Doppler modulation is the actual source of Gutin noise but, in the noise produced by unsteady blade forces, it only complicates the calculation of the acoustic field. Fortunately, in the case of blade tower wake interaction, the resulting noise is impulsive, and Doppler modulation is not believed to play a very important role. In the case of broadband noise, Morfey (ref. 5) showed , at the low Mach numbers of a windturbine blade, the noise of a rotating point dipole will be maximum in a direction perpendicular to the blade motion. In other words, broadband noise from a point source is a maximum in the direction which is free from Doppler modulation, and so a "worse case" for a broadband point source may be calculated in this direction with relative ease.

2.2 BROADBAND NOISE

As a windturbine rotates in a circular path, it encounters random gusts which are responsible for fluctuating forces on the windturbine blades. These forces react on the fluid as acoustic dipoles, and are therefore, to some extent, the source of broadband sound which is observed in the acoustic field. In this paper the sound produced by a windturbine in a turbulent atmosphere will be analyzed in a similiar method to that proposed by George and Homicz (ref. 3) in the analogous problem for helicopters. Namely, atmospheric turbulence will be characterized by a distribution of wavenumber scales. The acoustic field of one such wavenumber will be determined, whereby the total acoustic field can be calculated by superposition.

Consider a windturbine which is rotating in the $Z = 0$ plane. The windturbine encounters atmospheric velocity fluctuations (U, V, W) in the directions (X, Y, Z) respectively. In this theory, only the axial fluctuations W will be considered, for these are the fluctuations which are most responsible for unsteady loads on the blade. If, compared to the free stream velocity, the turbulent fluctuations are small, the turbulence may be modeled as frozen. In the convected coordinates, it may then be Fourier decomposed,

$$W(x', y', z') = \iiint_{-\infty}^{\infty} dK_x\, dK_y\, dK_z\, \tilde{W}(K_x, K_y, K_z)\, e^{i(K_x x' + K_y y' + K_z z')} \tag{2.1}$$

The relationship between the convected coordinates and the stationary coordinates is,

$$x' = x$$
$$Y' = Y \qquad (2.2)$$
$$z' = z + Ut$$

whereby, in the stationary coordinates, the turbulence has a convected time dependence,

$$W(x,Y,t) = \iiint_{-\infty}^{\infty} dK_x\, dK_Y\, dK_z\, \tilde{W}(K_x,K_Y,K_z)\, e^{i(K_x x + K_Y Y + K_z U t)} \qquad (2.3)$$

For later ease of computation, this integral can be written in cylindrical wavenumber coordinates.

$$W(x,Y,t) = \iiint_{-\infty}^{\infty} dK_x\, dK_Y\, dK_z\, \tilde{W}(K_x,K_Y,K_z)\, e^{i(K\cos\alpha\, x + K\sin\alpha\, Y + K_z U t)} \qquad (2.4)$$

where

$$K^2 = K_x^2 + K_Y^2 \quad , \qquad \alpha = \tan^{-1}\left(K_Y/K_x\right)$$

Now, consider the unsteady velocity experienced by an observer at radial position r on a rotating blade. This portion of the blade rotates in the $z=0$ plane, and its position is described by the parametric equations,

$$x = r\cos(\Omega t + \phi_o)$$

$$Y = r\sin(\Omega t + \phi_o) \qquad (2.5)$$

$$\phi_o = \text{initial blade angle}$$

Substituting these equations for the blade path into (2.4), the gust experienced on the rotating blade becomes,

$$W(r,t) = \iiint_{-\infty}^{\infty} dK_x dK_Y dK_z \, \tilde{W}(K_x, K_Y, K_z) \, e^{i\{Kr\cos(\Omega t + \phi_o - \alpha) + K_z U t\}} \qquad (2.6)$$

Using the well known identity,

$$e^{iKr\cos\phi} = \sum_{m=-\infty}^{\infty} (i)^m J_m(Kr) e^{im\phi} \qquad (2.7)$$

The gust history can be written,

$$W(r,t) = \iiint_{-\infty}^{\infty} dK_x dK_Y dK_z \left\{ \tilde{W}(K_x, K_Y, K_z) \right. \qquad (2.8)$$

$$\left. \sum_{m=-\infty}^{\infty} J_m(Kr) e^{i(m\Omega + K_z U)t} e^{im(\phi_o + \pi/2 - \alpha)} \right\}$$

It is seen that the gust frequencies on the blade occcur at sidebands of the rotation frequency harmonics. These sideband modulations occur at the convection frequency $K_z U$.

With an explicit expression for the gust velocity at position r on the blade, the spanwise lift distribution may be estimated from unsteady aerodynamics. Here, for lack of an appropriate theory for a rotating blade, a quasisteady aerodynamic model will be employed. The rotor blade will be treated as a flat plate airfoil in translation, and the unsteady lift assumed will be that of a quasisteady change in the angle of attack. Using a quasisteady model will tend to overestimate the high frequencies, but, as will be seen later, the simplicity of the quasisteady assumption highlights a simple scaling relationship for broadband noise.

With the quasisteady assumption the lift/span becomes,

$$\mathcal{L}(r,t) = \pi \rho c \Omega r \iiint_{-\infty}^{\infty} dK_x dK_y dK_z \left\{ \tilde{W}(K_x, K_y, K_z) \sum_{m=-\infty}^{\infty} J_m(Kr)\, e^{i(m\Omega + K_z U)t}\, e^{im(\phi_0 + \pi/2 - \alpha)} \right\} \quad (2.9)$$

This unsteady lift distribution can be pictured as a collection of acoustic dipoles which are rotating at the angular speed Ω. For each axial wavenumber K_z, a typical

portion of the blade consists of dipoles which are oscillating at the frequencies $m\Omega + K_z U$, and these dipoles travel a circular path of radius r .

The acoustic field of a rotating dipole is a well known problem whose solution can be found in a paper by Ffowcs Williams and Hawkings (Ref. 4). By virtue of its circular path, a rotating dipole produces an acoustic field which is modulated at the rotation speed. This is called Doppler modulation and is the result of repeated blade motion both towards and away from the observer.

In order to avoid the complication of Doppler modulation, it is convenient to calculate the acoustic far field along the windturbine axis. The on axis calculation is appropriate for two reasons. First, the atmospheric turbulence has an integral scale which is on the order of hundreds of meters (ref. 16). This means that the lift along the span of the turbine blade will be very well correlated and the entire spanwise lift distribution may be integrated to find the strength of an effective point dipole. Morfey (ref. 5) showed that, at low Mach numbers a rotating and randomly fluctuating point dipole will have maximum directionality along the dipole vector. In this way, if the fluctuating lift as on a windturbine blade is well correlated along the span, the on axis direction will a "worst case" direction. In this direction, the Doppler modulation may be ignored and the acoustic field is the simple spanwise integral,

$$P_{\substack{ON\\AXIS}}(R,t) = \frac{1}{4\pi c_o R} \int_0^b dr \, \frac{\partial \mathcal{L}(t - R/c_o)}{\partial t} \tag{2.10}$$

$$= \frac{i \rho c \Omega}{4 c_o R} \int_0^b dr\, r \iiint_{-\infty}^{\infty} dK_x dK_Y dK_z \left\{ \tilde{W}(K_x, K_Y, K_z) \right.$$

$$\left. \sum_{m=-\infty}^{\infty} (m\Omega + K_z U)\, J_m(Kr)\, e^{i(m\Omega + K_z U)(t - R/c_o) + im(\phi_o + \pi/2 - \alpha)} \right\}$$

Equation (2.10) is the far field on axis acoustic pressure produced by a single rotating blade. If the windturbine in multibladed, it might have "n" blades with equal angular separation.

$$\begin{aligned} \phi_{o_{BLADE\,1}} &= 0 \\ \phi_{o_{BLADE\,2}} &= 2\pi/n \\ &\vdots \\ \phi_{o_{BLADE\,n}} &= 2\pi(1 - 1/n) \end{aligned} \tag{2.11}$$

Adding the phase contribution of all the blades, it is found that only harmonics of the blade passage frequency and their sidebands will radiate. For "n" blades the far field pressure becomes,

$$P_{\substack{\text{ON}\\\text{AXIS}}}(R,t) = i\,\frac{\rho c n \Omega}{4 c_0 R} \int_c^b dr\, r \iiint_{-\infty}^{\infty} dK_x dK_Y dK_Z \Big\{ \tilde{W}(K_x, K_Y, K_Z)$$

(2.12)

$$\sum_{m=-\infty}^{\infty} (mn\Omega + K_Z U)\, J_{mn}(Kr)\, e^{i(mn\Omega + K_Z U)(t - R/c_0) + imn(\pi/2 - \alpha)} \Big\}$$

For comparison with experiment, one would like to calculate the mean square pressure $\overline{p^2} = \overline{\frac{pp^*}{2}}$

$$\overline{p^2} = \frac{1}{32}\left(\frac{\rho c n \Omega}{c_0 R}\right)^2 \iint_0^b dr\, dr'\, r\, r' \tag{2.13}$$

$$\iiiint\!\!\iint_{-\infty}^{\infty} dK_x dK_x' dK_Y dK_Y' dK_Z dK_Z' \Big\{ \tilde{W}(K_x, K_Y, K_Z)\, \tilde{W}^*(K_x', K_Y', K_Z')$$

$$\sum_{m=-\infty}^{\infty} \sum_{m'=-\infty}^{\infty} J_{mn}(Kr)\, J_{m'n}(K'r')\, (mn\Omega + K_Z U)(m'n\Omega + K_Z' U)$$

$$e^{i(mn\Omega + K_Z U - m'n\Omega - K_Z' U)(t - R/c_0)}\; e^{imn(\pi/2 - \alpha) - im'n(\pi/2 - \alpha)} \Big\}$$

Two relationships considerably simplify the integration. First is the time average relationship,

$$\overline{e^{i(mn\Omega + k_z v - m'n\Omega - k_z' v)(t - R/c_0)}} \tag{2.14}$$

$$= 1 \quad \text{IF} \quad \{(m-m')n\Omega + (k_z - k_z')v\} = 0$$

$$= 0 \quad \text{OTHERWISE}$$

A second simplification occurs if both sides of equation (2.13) are ensemble averaged. Here, the only quantity of independent statistical variation is the product of the two wavenumber distributions. Ensemble averaging this product, appendix A shows that, if the turbulence is homogeneous,

$$\langle \tilde{W}(k_x, k_y, k_z)\, \tilde{W}^*(k_x', k_y', k_z') \rangle \tag{2.15}$$

$$= \Phi_{ww}(k_x', k_y', k_z')\, \delta(k_x - k_x')\, \delta(k_y - k_y')\, \delta(k_z - k_z')$$

Where Φ_{ww} is the power spectral density of the turbulence. Substituting the two relationships (2.14) and (2.15), two of the integrals and one of the summations of (2.13) are eliminated, and the final ensemble averaged result becomes,

$$\langle \overline{p^2} \rangle = \frac{1}{32}\left(\frac{\rho c n \Omega}{c_0 R}\right)^2 \iiint_{-\infty}^{\infty} dK_x\, dK_r\, dK_z \left\{ \Phi_{ww}(K_x, K_r, K_z) \sum_{m=-\infty}^{\infty} (mn\Omega + K_z U)^2 \left| \int_0^b dr\, r\, J_{mn}(Kr) \right|^2 \right\} \tag{2.16}$$

If one is willing to forgo fine details of the spectrum, equation (2.16) may be simplified by lumping together some of the energy which is found in the neighborhood of the blade passage harmonics. This simplification follows because the turbulent scale of the atmosphere is large, and for a windturbine the free stream velocity is relatively small. Thus, for most wavenumbers of interest, the modulation frequency is much less than the rotation frequency.

$$K_z U \ll n\Omega \tag{2.17}$$

Most of the sideband energy is found in narrow regions about the blade passage harmonics. Equation (2.16) may then be integrated over the longitudinal wavenumber K_z and all the sideband energy of a particular harmonic is integrated to an effective power contribution from that harmonic.

At this point it is convenient to introduce a specific

form of the power spectral density and its integral over K_z. Here, the Liepmann (Ref. 15) spectrum will be chosen. Its integral over K_z was shown by Amiet (Ref. 6) to be,

$$\int_{-\infty}^{\infty} \Phi_{ww}(K_x, K_y, K_z)\, dK_z = \overline{w^2} \frac{3 K^2 L^4}{4\pi \left(1 + K^2 L^2\right)^{5/2}} \tag{2.18}$$

L = integral scale

$K^2 = K_x^2 + K_y^2$

With assumption (2.17), the summation in the integrand of (2.16) is symmetric and need only be taken for positive values and multiplied by two. Integrating (2.16) and substituting (2.18), the approximate mean square pressure becomes,

$$\langle \overline{p^2} \rangle = \frac{3}{32} \left(\frac{\rho c n^2 \Omega^2 b^2 \sqrt{\overline{w^2}}}{c_o R} \right)^2 \tag{2.19}$$

$$\sum_{m=1}^{\infty} m^2 \int_0^{\infty} dK \frac{K^3}{(1 + K^2)^{5/2}} \left| \int_0^1 d\bar{r}\, \bar{r}\, J_{mn}(K\Omega\bar{r}) \right|^2$$

where the substitution $2\pi K dK = dK_x dK_Y$ has been made, and the variables have been non dimensionalized,

$$\bar{r} = r/b$$

$$\kappa = KL$$

$$\Lambda = b/L$$

The proper non dimensionalization of the acoustic pressure can be seen in equation (2.19) where the following broadband noise relationships are concluded.

$$p^2 \propto M_{TIP}^4$$

$$\propto n^4$$

$$\propto \overline{W^2}$$

While these relationships determine the magnitude of the acoustic spectrum, the spectral distribution is exclusively determined by the parameter Λ , the ratio of the span to the turbulent scale. The influence of Λ on the spectrum shape can be seen in figure (2.1) which graphs the non dimensional

pressure as a function of harmonic number. Large values of Λ are seen to weight the higher frequencies. Small values of Λ accent the lower frequencies.

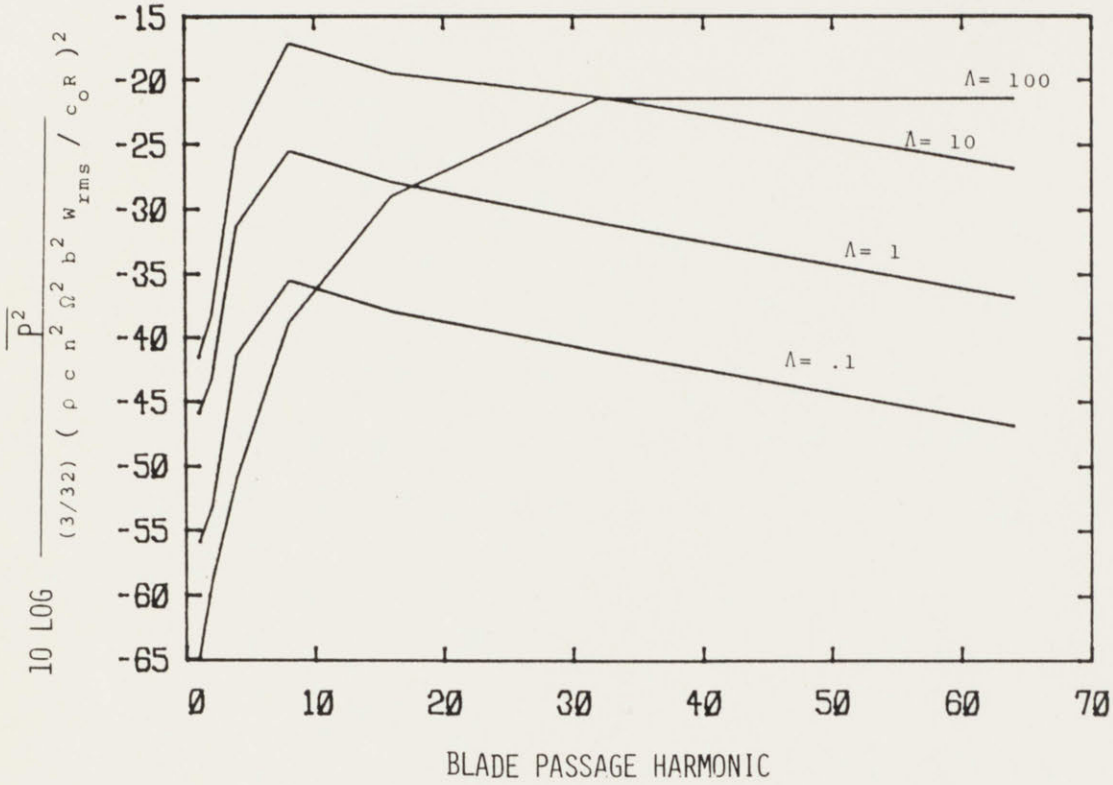

Fig 2.1 Broadband Spectra for Different Values of Λ
(points are connected for clarity)

High frequency broadband noise scales in direct proportion to the parameter Λ . This is a result which is observed in figure (2.1), and can be concluded from the following simple argument. Consider the transverse wavenumbers which contribute to the m'th blade passage harmonic. If m is large, then examination of high order Bessel functions shows that the range of contributing wavenumbers to a single harmonic is

narrow. Call this range $K_m \rightarrow K_m + dK_m$, and note that the position of the range, K_m , and its width, dK_m , can only be a function of the rotor span. It is then easy to conclude the proper scaling for K_m and dK_m

$$K_m \propto 1/b$$

$$dK_m \propto 1/b$$

Now, consider the turbulent energy which is contained in this small range of wavenumbers. As a result of the Liepmann spectrum,

$$\underset{K_m \rightarrow K_m + dK_m}{\text{turbulent energy}} \sim \frac{1}{(K_m L)^2} d(K_m L) \qquad (K_m L >> 1)$$

Substituting the scaling for K_m

$$\underset{K_m \rightarrow K_m + dK_m}{\text{turbulent energy}} \sim b/L = \Lambda$$

which is the result discovered in the computation.

The computations which are shown in figure (2.1) were

completed according to the program listed in Appendix B. Integration of equation (2.19) was done over a finite portion of the wavenumber spectrum in the neighborhood where the argument of the Bessel function equals the order. The increment of integration was chosen to be fairly small, but time did not permit a detailed study of proper sampling for the integration. Higher order Bessel functions are very oscillatory, which points to the weakness of the theory here presented, namely the calculations are difficult and expensive. The advantage of this theory lies in the parametric dependence of the spectrum on the single parameter Λ. Once equation 2.19 is computed for different values of Λ, the result is a family of spectra any one of which can be applied to a particular windturbine.

The spectral dependence on the parameter Λ is an artifact of a quasisteady approximation and is therefore only approximate. Here in lies a second weakness of the theory, the lack of an adequate aerodynamic model for a rotating blade. In Chapter 4, where broadband calculations are compared with experiment, a frequency rolloff was incorporated into the calculations in order to attenuate the higher frequencies. The frequency rolloff was estimated by the Sear's function behavior of the reduced frequency at the 75% span. This approach is somewhat sloppy because the Sear's function applies to a translating airfoil where as here, the turbine blade is rotating.

2.3 GUTIN NOISE

Although broadband noise is the consequence of unsteady blade loading, the steady loads which drive a windturbine are also a source of acoustic energy. By virtue of its circular path, the steady load on a particular portion of the blade creates an acoustic field which is Doppler modulated at the blade passage harmonics. Since the loading is steady, this means that the acoustic field occurs at the blade passage harmonics. This result was discovered by Gutin (ref. 2) and so the noise of a stationary dipole in rotation is called Gutin noise.

The magnitude $\overline{P_m P_m^*}$ of mth Gutin noise blade passage harmonic is,

$$\overline{P_m P_m^*} = \left\{ \frac{mn\Omega\cos\Omega}{2\pi c_0 R} \int_0^b \mathcal{L}_0 J_{mn}\left(\frac{mn\Omega r\sin\Omega}{c_0}\right) dr \right\}^2 \qquad (2.20)$$

where $\mathcal{L}_0$ is the spanwise load distribution.

It is interesting to notice that if the blade is subsonic, the argument of the Bessel function is less than its order, and this means that the integral of (2.20) is a decreasing function of the harmonic number. (See Ref. 24, Chapter 8) Most calculations of Gutin noise indeed show the lowest harmonic to have the highest amplitude. The amplitude

of the higher harmonics decreases rather rapidly.

The magnitude of the first harmonic of a two bladed windturbine may be estimated by approximating the Bessel function,

$$J_2\left(\frac{2\Omega r \sin\eta}{c_0}\right) \sim \frac{1}{2}\left(\frac{\Omega r \sin\eta}{c_0}\right)^2 \qquad (2.21)$$

whereby on substitution into (2.20)

$$\overline{P_1 P_1^*} = \left\{ \frac{\Omega^3 \cos\eta \sin^2\eta}{2\pi c_0^3 R} \int_0^b \mathcal{L}_0 r^2 dr \right\}^2 \qquad (2.22)$$

The acoustic intensity of Gutin noise is seen to have a sharp directionality and is also seen to increase as the sixth power of the rotation speed. This is a more sensitive rotation speed dependence than broadband noise which was found to increase with the fourth power of the RPM. As will now be seen, a third form of windturbine noise also increases as the fourth power of the RPM. This is the impulsive noise of blade tower wake interaction which, in certain cases, is the most annoying noise of a windturbine.

2.4 IMPULSIVE NOISE (Blade Tower Wake Interaction)

A windturbine which rotates downwind of its support tower, runs the danger of emitting impulsive noise which is the result of repeated blade passage in and out of the tower wake. The resulting acoustic signal is a repeated impulse, each impulse corresponding to a blade passage behind the tower. Like Gutin noise, the power spectral density of the sound field consists of sharp peaks at harmonics of the blade passage frequency. Unlike Gutin noise, tower wake impulse noise has, in most cases, a relatively slow harmonic rolloff. The relative importance of tower wake impulse noise to other forms of noise such as Gutin Noise depends on properties of the mean wake which are here examined.

It is convenient to analyze tower wake impulsive noise with a simple model of the tower wake. In this analysis the tower wake will be assumed a superposition of one or more Gaussian wake profiles. This assumption is convenient for two reasons. First, it is well known that the wake of a cylinder has an approximate Gaussian shape, and so the acoustic field produced by blade passage through the wake of a single cylinder may be conveniently analyzed. Secondly, such an understanding for a single cylinder, fosters a simple interpretation of the acoustic field produced by blade passage behind the multiple cylinders which make up a windturbine tower. The disadvantage of this simple assumption for the

wake is an inaccurate approximation of the fine details of the wake structure and the resulting higher frequencies in the acoustic field.

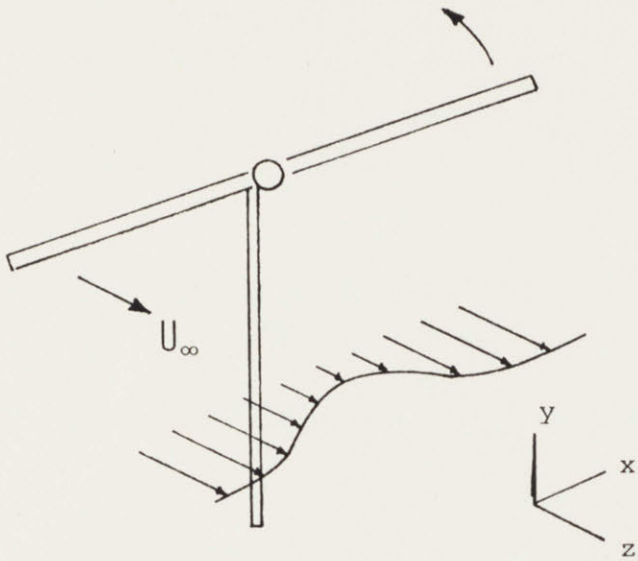

Fig 2.2 Cylindrical Support Tower

As shown in figure (2.2), consider a windturbine which is supported by a single cylindrical tower which is upwind of the rotation plane. The windturbine has "n" blades and rotates at angular velocity Ω . The blade passage frequency is then $n\Omega$. For analytic simplicity, assume the wake behind the tower to have a Gaussian profile. The wake is two dimensional and so it is independent of position "y" up the tower. Let the

wake profile be written,

$$W(x) = A U e^{-\ln 2\, x^2/B^2} \tag{2.23}$$

where

A = non dimensional amplitude

B = wake half width at half depth

At radial position "r", the blade is translating through the wake at the local blade speed Ωr . Substituting $x = \Omega r t$, the time history of the convected gust to an observer on the blade becomes,

$$W(r,t) = A U e^{-\ln 2\, \Omega^2 r^2 t^2/B^2} \tag{2.24}$$

In order to calculate the gust loading, it is necessary to Fourier decompose the gust.

$$\tilde{W}(r,\omega) = \frac{1}{2\pi} \int_{-\infty}^{\infty} W(r,t)\, e^{-i\omega t}\, dt \qquad (2.25)$$

$$= \frac{v}{2\sqrt{\pi \ln 2}} \left(\frac{AB}{\Omega r}\right) e^{-\left(\frac{\omega B}{2\Omega r}\right)^2 \frac{1}{\ln 2}}$$

The spectral density of the local lift/span can now be approximated by the Sear's function.

$$\tilde{L}(r,\omega) = \pi \rho c \Omega r\, \tilde{W}(r,\omega)\, S(r,\bar{\omega}) \qquad (2.26)$$

Where

$$S(r,\bar{\omega}) = \frac{1}{\sqrt{1 + 2\pi\bar{\omega}}}\, e^{i\bar{\omega}\left(1 - \pi^2/2 + 4\pi\bar{\omega}\right)}$$

$$\bar{\omega} = \frac{\omega c}{2\Omega r}$$

Equation (2.26) yields the Fourier transform of the loading impulse which acts on the blade, and correspondingly on the fluid in the wake. This impluse is the result of rapid passage of a single blade through the wake. With successive blade passage, this impulse is repeated, and, assuming the

wake retains its shape, the blade forces which react on the fluid repeat with subsequent blade passage, and are therefore periodic in harmonics of the blade passage frequency.

The acoustic field of repeated blade passage through the wake is easily calculated if the wake is assumed acoustically compact. The compactness assumption allows the rectangular region of the wake to be modeled as an equivalent acoustic line source down the wake's center. The time history of the dipole source which act along this line can then be made to follow the loading history of the blades which pass through the wake, and, for low frequencies, the acoustic effect should be the same.

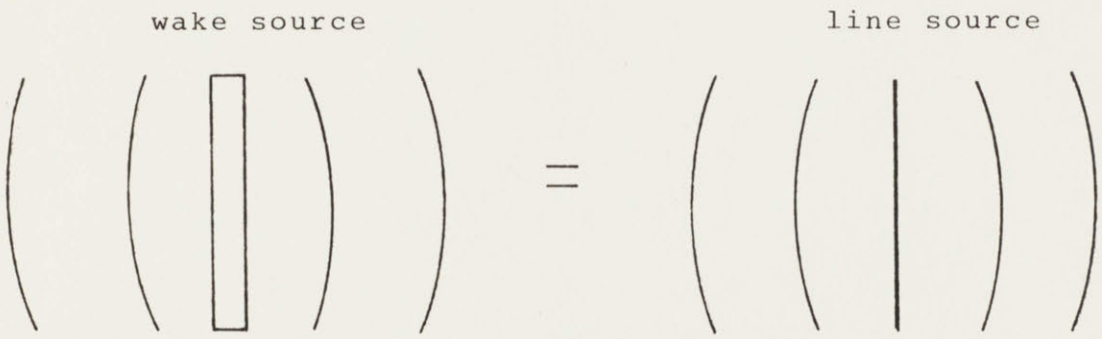

Fig 2.3 Compactness Assumption of the Wake

Having the Fourier transform of the loading for a single blade passage through the wake, the corresponding Fourier series for the fluid reaction in the wake may be calculated by the theorem of convolution. The narrow wake being compressed to an equivalent line source, the time history of the fluid loading may be considered as the successive response to the impulse of a blade passing through the wake. The impulse response is given by equation (2.26), and the resulting time history of fictitious dipole sources along the center line may then be modeled as a convolution of these impulses.

$$F(r,t)_{\text{line source}} = -\int \tilde{L}(r,\omega)e^{i\omega t}d\omega \quad X \quad \left(\delta(t) + \delta\left(t - \frac{2\pi}{n\Omega}\right) + \ldots\right)$$

Fig 2.4 Convolution Model of the Line Source

If the Fourier expansion of the periodic force/length is written

$$F(r,t) = \sum_{m=1}^{\infty} F_m(r) \cos(mn\Omega t) \tag{2.27}$$

then by the convolution theorem,

$$F_m(r) = 2\pi \left(\frac{n\Omega}{\pi}\right) \tilde{\mathcal{L}}(r, mn\Omega) \tag{2.28}$$

The time derivitive of the force/length serves as a local dipole strength along the line source, and the acoustic field is an integral superposition of this dipole distribution,

$$P(\vec{R},t) = \cos\Omega \int_0^b \left[\frac{\partial F(r,t)}{\partial t}\right] \frac{1}{|\vec{R}-\vec{r}|}\, dr \tag{2.29}$$

where

$$\left[\frac{\partial F(r,t)}{\partial t}\right] = \frac{\partial F\left(t - \frac{|\vec{R}-\vec{r}|}{c_0}\right)}{\partial t} \tag{2.30}$$

Combining equations (2.25), (2.26), (2.28),(2.29), and (2.30), the acoustic far field becomes,

$$P(\vec{R},t) = \sqrt{\frac{\pi}{\ln 2}}\ \rho\ U\ A B c\ \cos\Omega\,(n\Omega)^2 \qquad (2.31)$$

$$\sum_{m=1}^{\infty} m \int_0^b e^{-\left(\frac{mnB}{2r}\right)^2 1/\ln 2}\ S(\overline{mn\Omega})\ \frac{\sin mn\Omega\left(t-\frac{\vec{R}-\vec{r}}{c_0}\right)}{4\pi c_0 |\vec{R}-\vec{r}|}$$

The acoustic field is observed to have the following parametric dependence,

1) $P \propto AB$ — The pressure is proportional to the area of the Gaussian wake which, to first order is a direct measure of the cylinder drag coefficient.

2) $P \propto (n\Omega)^2$ — The pressure is proportional to the (blade passage frequency)^2.

3) rolloff $\sim m e^{-\left(\frac{mnB}{2r}\right)^2 1/\ln 2}$ — In most cases the wake width B is the critical parameter which governs harmonic rolloff with the increasing harmonic number n.

Equation (2.31) is a relatively simple calculation which may be performed with the computer program of Appendix B. In Chapter 4, a comparison is found between computed predictions, and the measured acoustic spectra for blade passage through the Gaussian wakes of three cylinders. The amplitude "A" and half width "B" were measured for these three cylinders, and

the computed results were found to agree quite well with the measurements. The next step of course, is to generalize the results from a single cylinder wake to the more complicated wake of a windturbine. This is a simple matter of superposition, and, as discussed is the next section, the frequency modulation observed in the spectrum of a full scale windturbine, is the result of subsequent blade passage through two or more Gaussian like wakes.

2.5 EXTENSIONS TO MORE COMPLICATED WAKES

(Frequency Modulation)

Most windturbine towers consist of three or four vertical supports which, at ground level, form a wide base, and, with increasing height, converge to the generator platform at the windturbine's hub. If these supports are fairly well spaced, their contribution to the tower wake can be seen as a series of distinct "bumps" in the wake profile. To some approximation, each bump may be modeled as Gaussian, that is each bump is characterized by its width "B" and nondimensional amplitude "A", and the corresponding sound field is given according to equation (2.31).

When two or more identical Gaussian peaks are present in the wake, their corresponding acoustic impulses are also identical, but time delayed by the transit time of the blade from one peak to the other. As will now be shown, this time delay produces a frequency modulation in the spectral density of the acoustic field.

Consider a four legged windturbine tower where two of these legs are located close to the rotor plane. The tower wake is then assumed to consist of two Gaussian peaks, the peaks corresponding to the two supports closest to the rotor. For simplicity, assume these supports form an angle θ with the hub.

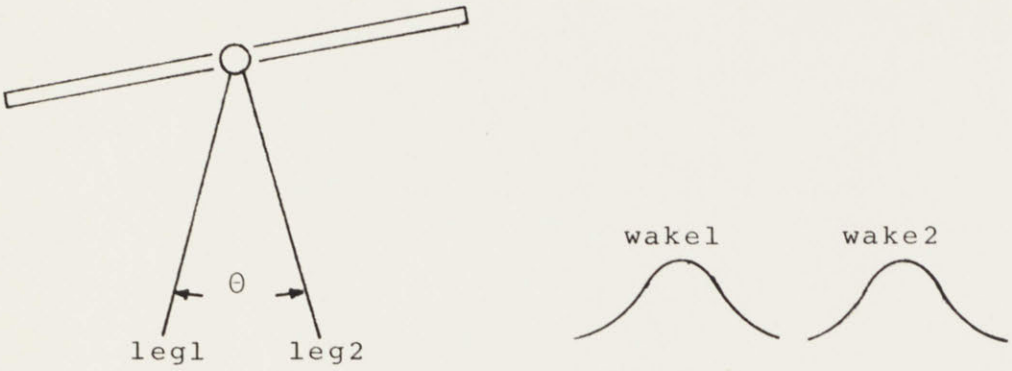

Fig 2.5 Model of the Tower Wake

Let P_m denote the amplitude of the mth harmonic radiated by blade passage through a single wake. The magnitude of P_m may be computed according to equation (2.31). If now, the acoustic fields of both wakes are combined, the m'th harmonic of the acoustic field becomes,

$$P_{m_{TOTAL}} = P_m \cos(mn\Omega t) + P_m \cos\left(mn\Omega\left(t - \frac{\theta}{\Omega}\right)\right) \tag{2.32}$$

The contribution from the second wake is identical to the first, only it is time delayed by the transit time $\frac{\Theta}{\Omega}$ between the tower legs. For the sake of comparison with spectral densities, the mean squared values of the pressure from different harmonics becomes,

$$\overline{p_{m_{TOTAL}}^2} = 2\cos^2\left(\frac{mn\Theta}{2}\right) p_m^2 \qquad (2.33)$$

This is the harmonic modulation which is often observed in the measured acoustic spectral densities of downwind machines. A particular harmonic of the acoustic field is enhanced or suppressed according to the constructive or destructive interference of the time delay between the towers. For the two legs considered here,

$\frac{mn\Theta}{2} \sim 0, \pi, 2\pi \ldots$ Spectral enhancement

$\frac{mn\Theta}{2} \sim \frac{\pi}{2}, \frac{3\pi}{2}, \frac{5\pi}{2} \ldots$ Spectral suppression

Tower angle Θ governs the modulation and subsequent enhancement or suppression of a particular harmonic. From a design standpoint, certain frequencies may then be suppressed with the design of a proper tower angle. Resonant frequencies of a nearby structure of even the structural frequencies of

the tower itself, may, with proper design, be avoided in the acoustic field. Of course suppression at one frequency is accomplished at the expense of enhancement at other frequencies, and adjusting the tower angle will have little effect on the overall noise.

CHAPTER 3

APPARATUS

Acoustic tests were conducted on a 1/53 scale model of the D.O.E. - NASA MOD-1 Windturbine. Instrumentation on the windturbine included a photo detector and counter for measuring rotation speed. A strain gauge was used to measure rotor torque. The windturbine was loaded by means of a current supply to a Volkswagon automobile generator. For some of the tests, the current supply was disconnected, and the windturbine was allowed to spin freely.

Rotation speeds were chosen to roughly simulate the tip Mach number of full scale MOD-1 which rotates at 35 RPM. In order to simulate tip speeds, the model should therefore rotate at 1650 RPM, but thoughout our tests, rotation speeds were varied well above and below this value. Unfortunately, the windturbine could not be loaded down to very low RPM, and it was often necessary to stall the blades in order to reach low rotation speed.

Our tests were conducted in the 5' x 7 1/2' test section of the Massachusetts Institute of Technology Anechoic Windtunnel Facility. This windtunnel is closed loop, and can provide tunnel speeds up to 75 MPH. The tunnel is considered anechoic down to 60 hz, at which point the acoustic modes of the chamber start to become excited. Figure (3.4) shows the acoustic noise floor for our experiments at a tunnel speed of

22.5 MPH. As can be seen, the low frequency noise is substantial, and overwhelmed some of the low frequency signal of our tests.

Acoustic equipment consisted of two B & K 4133 microphones with a frequency response of 20 hz - 20 khz. One of the microphones was located on the turbine rotation axis, the other off axis, and both microphones were powered by a B & K 2801 power supply. The microphones and recording equipment were calibrated by a B & K 4220 124dB SPL pistonphone. Overall sound pressure levels were measured on a B & K 2604 microphone amplifier. The acoustic signals were recorded on a Racal four channel 4 DS fm tape recorder. Both signals were tape recorded with a "wideband" bandwidth of D.C. - 5 khz. These tapes were later analyzed on a Hewlett Packard Structural Dynamics Analyzer.

All the acoustic data presented in this thesis is analyzed in the frequency range DC - 3.2 khz. This range provided a spectral resolution of 12.5 hz on the analyzer. Most all the data presented here are <u>not</u> acoustic spectral densities, but rather, <u>integrated values</u> of the acoustic spectral density over the individually resolved bins of the analyzer. Thus, the value, in decibels, for any one of the 256 analyzer bins, represents the total acoustic intensity contained in that particular 12.5 hz bin. Unless otherwise stated, the value in decibels of an acoustic measurement is

$$\text{SPL dB} = 10 \text{ Log} \int^{12.5 \text{ hz bin}} \frac{I(f)}{I_o} \, df$$

$I(f)$ = Acoustic Intensity / hz

I_o = 1 pW /m^2 which is the standard acoustic reference intensity for air.

In addition to acoustic measurements, some experiments required a number of instruments for the measurement of flow. The difference between static and dynamic pressure was used to measure free stream tunnel speed. An array of static and dynamic pressure sensors were used to measure the mean velocity gradients behind boundary layer spires. Finally, a hotwire was used both to record axial turbulence, and also measure the mean wake profiles behind cylinders. Prior to each measurement, the hotwire signal was first linearized and then calibrated against a pitostatic tube. One such calibration is shown in Figure 3.5 where the hotwire is seen to be linear over a velocity range of 0-30 MPH.

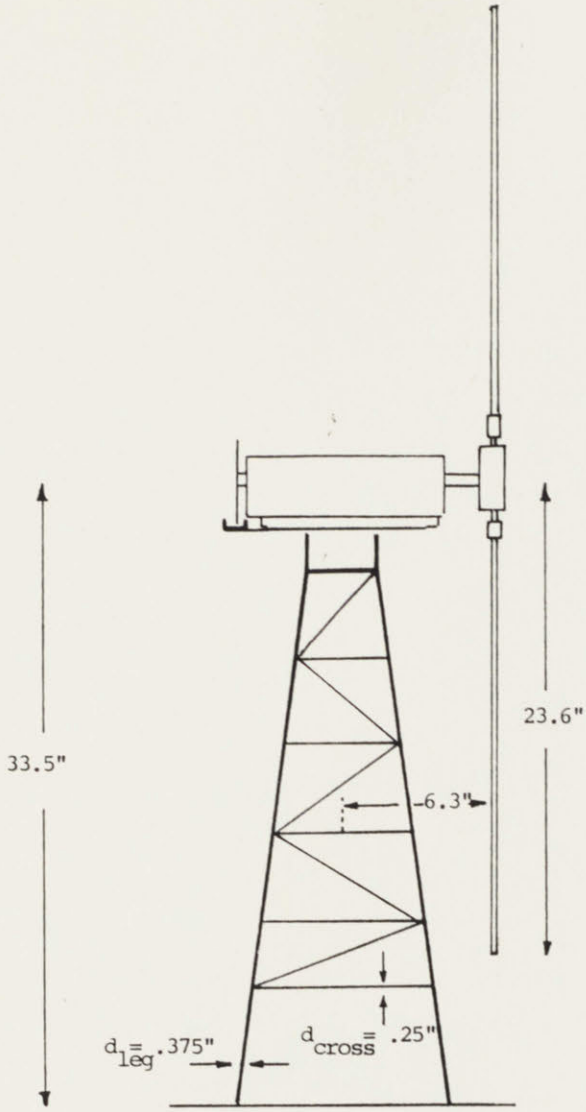

Fig 3.1 Scale Model

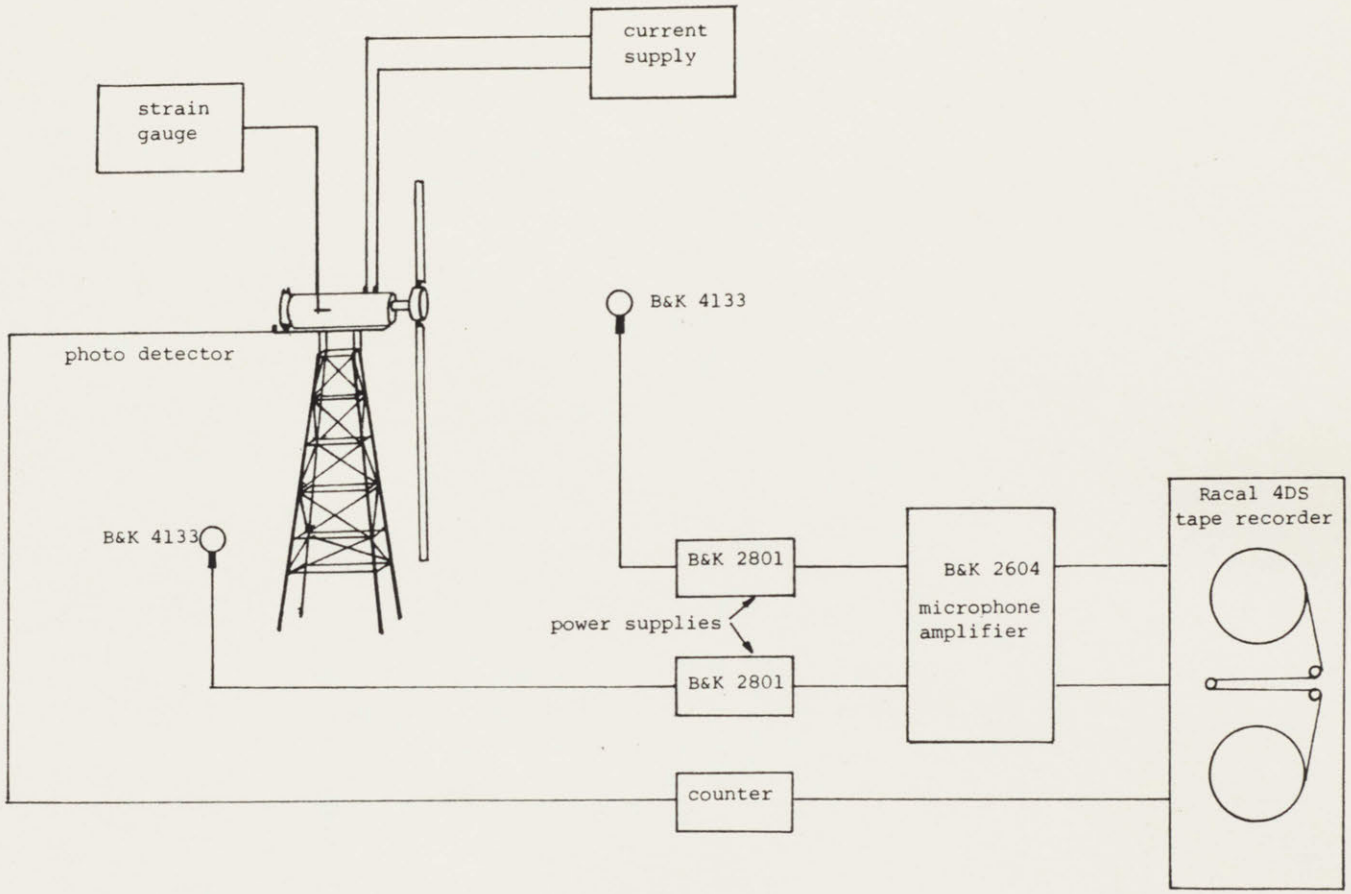

Fig 3.2 Instrumentation Diagram

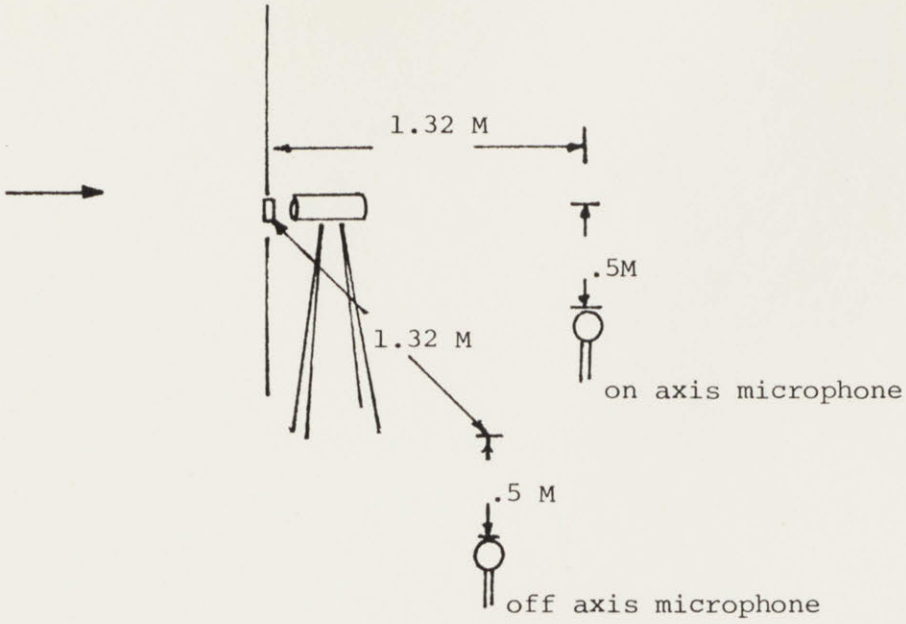

Microphone Position for Upwind Experiments
(cylinder tests, boundary layer tests, multiple blade tests)

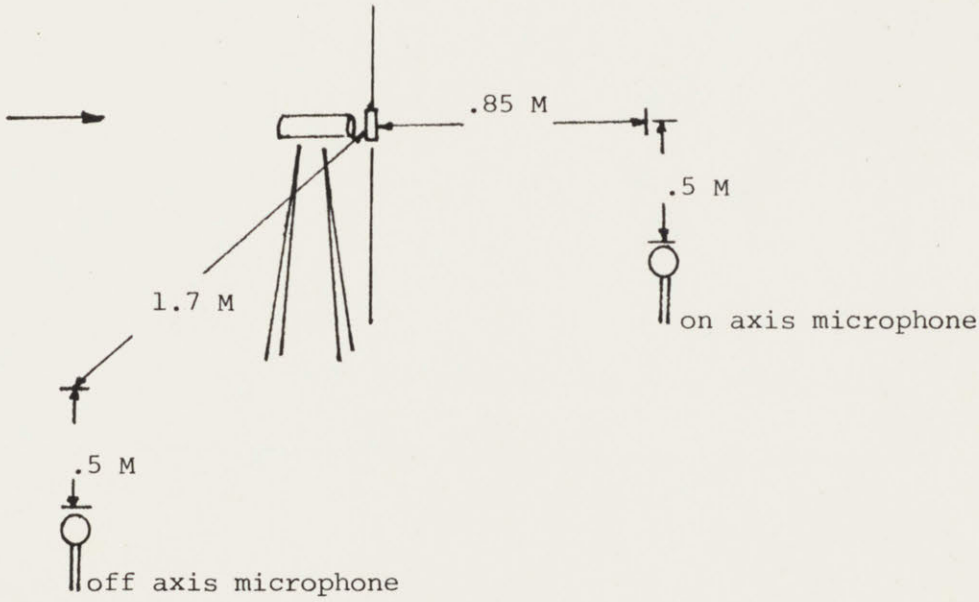

Microphone Position for Downwind Experiments
(RPM tests, tower shadow tests, loading tests)

Fig 3.3 Microphone Positions (Upwind and Downwind positions are different for comparison with previous experiments)

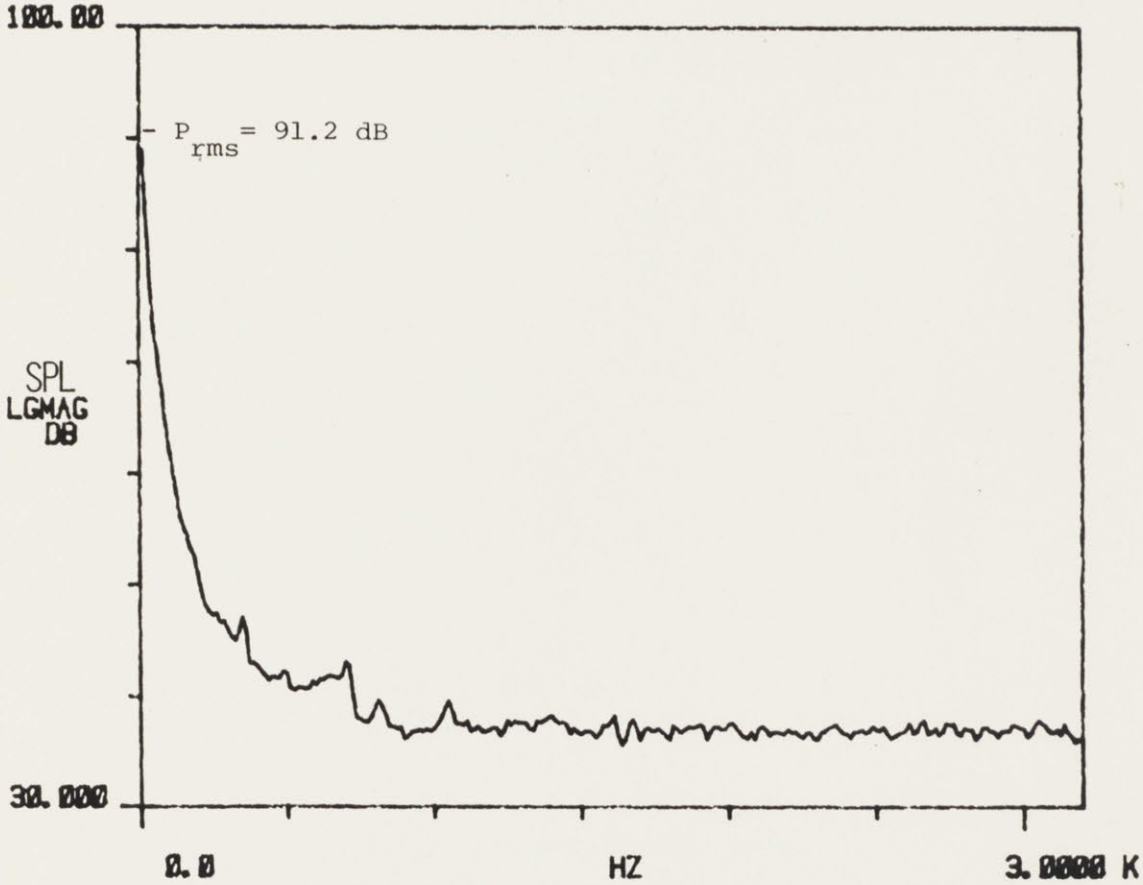

Fig 3.4 Backround Noise (Tunnel Speed = 22.5 MPH)

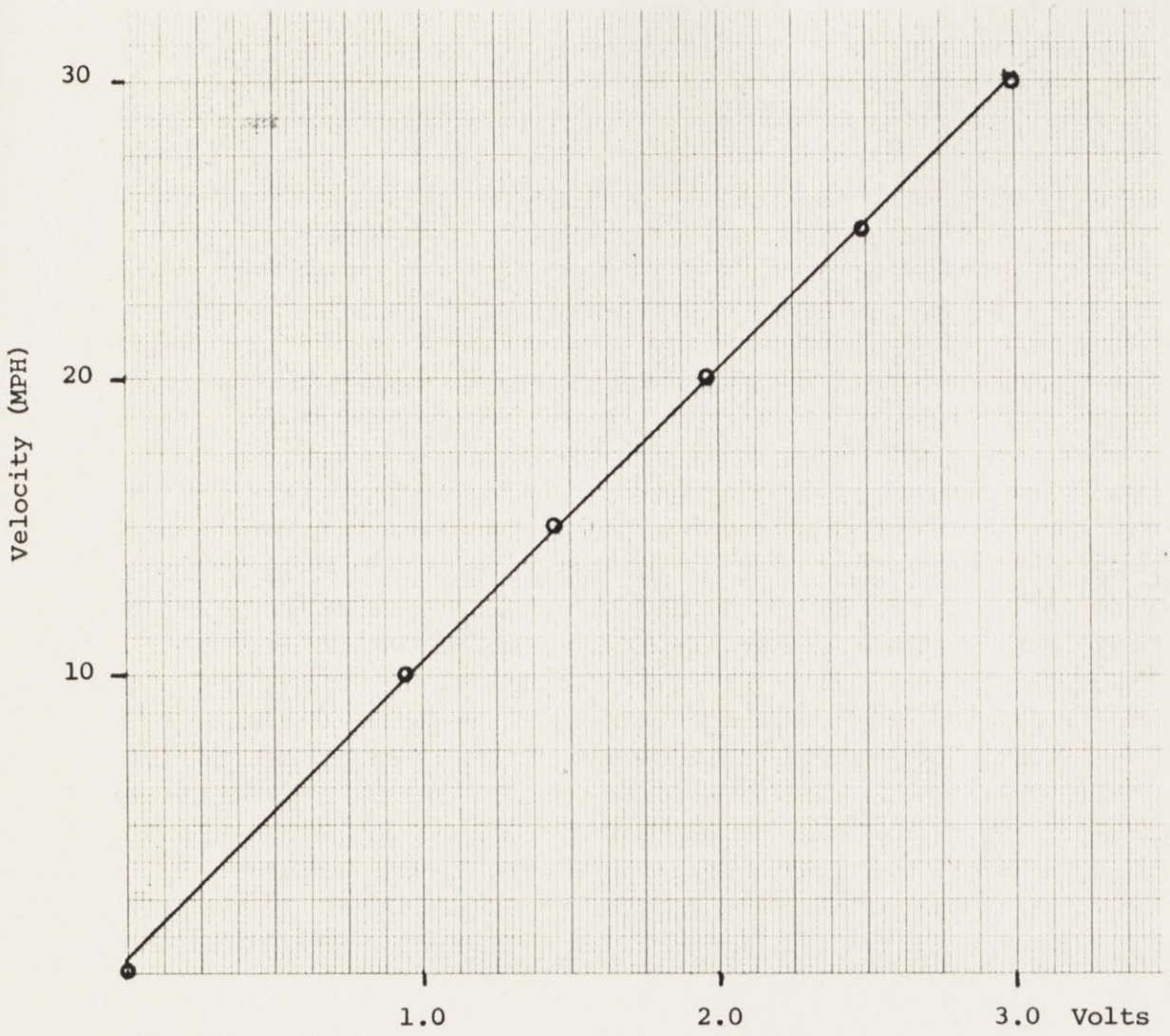

Fig 3.5 Hotwire Calibration

CHAPTER 4

EXPERIMENTAL RESULTS

The data which is presented here was gathered during two ten day sessions at the MIT anechoic windtunnel. The first few days of these test were dedicated to understanding the scale model performance whereby, in order to simulate MOD-1 advance ratio, it was decided that, whenever possible, acoustic measuremnts would be made at a tunnel speed of 22.5 MPH. For the sake of comparison, all tests (excluding RPM tests) are conducted at this same tunnel speed.

The contents of this chapter are split on a test by test basis. The data is therefore presented in sections each of which discuss a particular issue. In any section a small portion of measurements are presented to highlight the conclusionswhich are drawn on the particular issue at hand. A more complete acount of the measurments can be found in a Appendix C which catalogs all of the acoustic measurements.

4.1 COMPARISON OF THE ACOUSTIC SPECTRA

(Full Scale vs. Scale Model)

Figures 4.1 and 4.2 show acoustic spectra measured for the full scale MOD-1 and the 1/53 scale model respectively. Here, both windturbines have two blades which are rotating through the support tower wake. The full scale MOD-1 rotates at 35 RPM while the model is rotating at 1710 RPM. The ratio of rotation speeds is then 48.8. Both spectra are seen to have the identical characteristics of large peaks at the blade passage harmonics. In addition, both the model and the full scale spectra are seen to be modulated. This is the result of blade passage between the tower legs and so this modulation frequency should scale with the geometry and the rotation speed. The ratio of the scale model modulation frequency to that of full scale MOD-1 is,

$$500\text{hz} / 12\text{hz} = 41.6$$

which, as it should be, is close to 48.8, the ratio of rotation speeds.

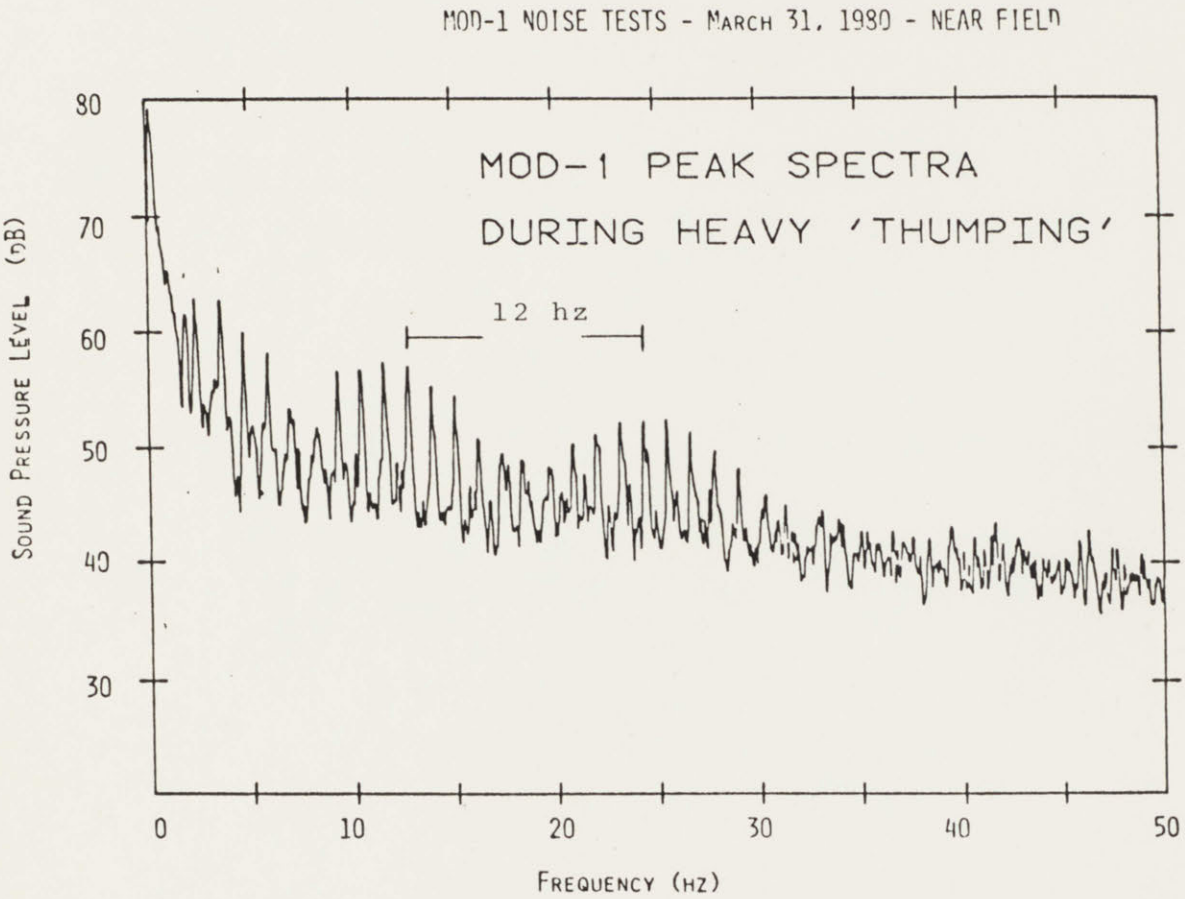

Fig 4.1 Acoustic Spectrum of Full Scale MOD-1*

* Figure borrowed from Reference 17

2 blades
1710 RPM
U = 22.5 MPH

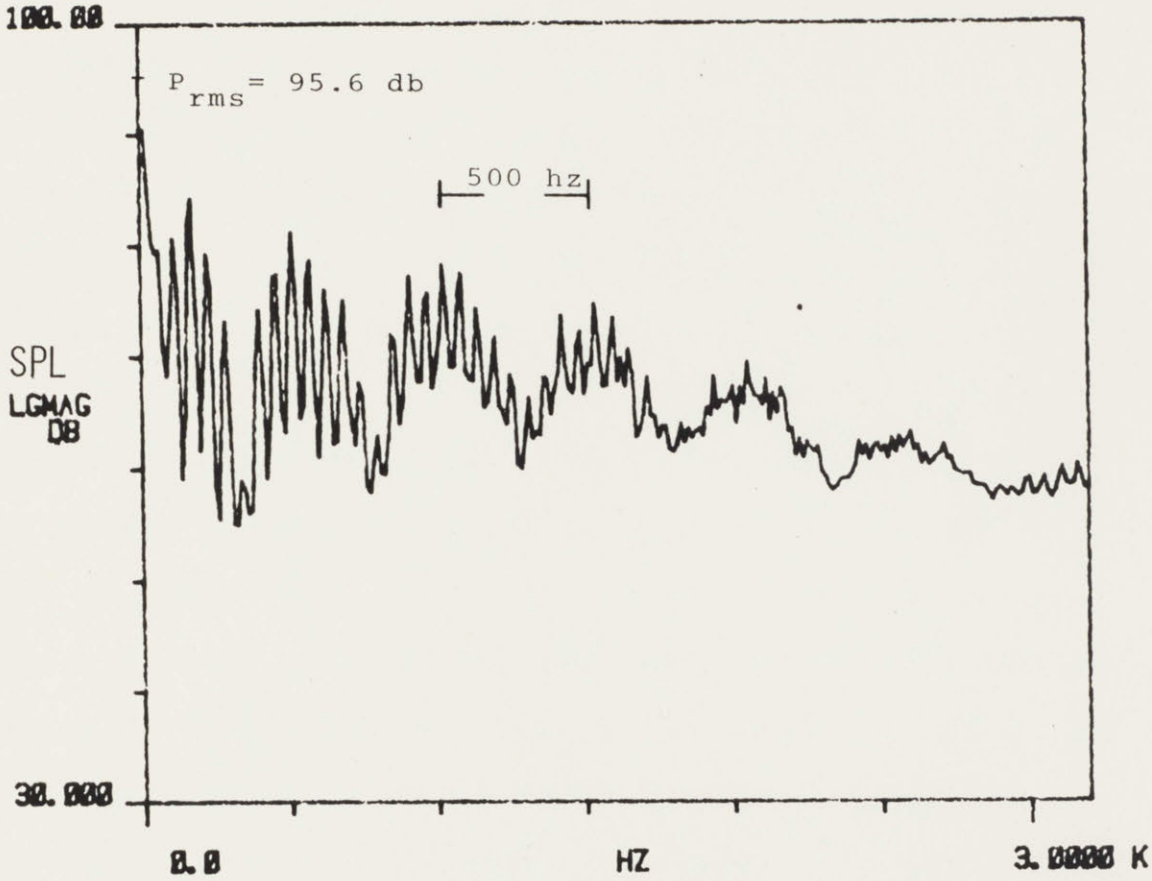

Fig 4.2 Acoustic Spectrum of the 1/53 Scale Model

4.2 DIRECTIONALITY

Although MOD-1 is a downwind machine, the 1/53 scale model provided the flexibility of both an upwind and downwind configuration. The on axis spectra for these two configurations can be compared in figure 4.3 where the upwind machine shows a considerable 10 - 20 decibel improvement over its downwind counterpart. Peaks at the blade passage harmonics are almost non existant for the upwind machine. Those peaks that do exist for the upwind machine are the result of blade passage through the slight upwind wake of the tower.

Figure 4.4 compares on axis and off axis measurements for the downwind configuration and it is seen that the downwind machine has a definite preference for on axis radiation. For the two directions measured here, this result is in agreement with the dipole line source model of chapter 2.

The directional characteristics of the upwind machine are shown in figure 4.5. Here, the upwind machine produces strong off axis radiation at the very lowest blade passage harmonics. These are the Gutin noise harmonics which can be seen in the off axis measurements of both the upwind and downwind machine. For example, in figure 4.6, the low frequency off axis peaks of both the upwind and downwind machines are seen to have identical sound pressure levels. This indicates that low frequency off axis noise is not the result of blade tower wake interaction. As the harmonic number increases, the Gutin noise is seen to rolloff rather quickly.

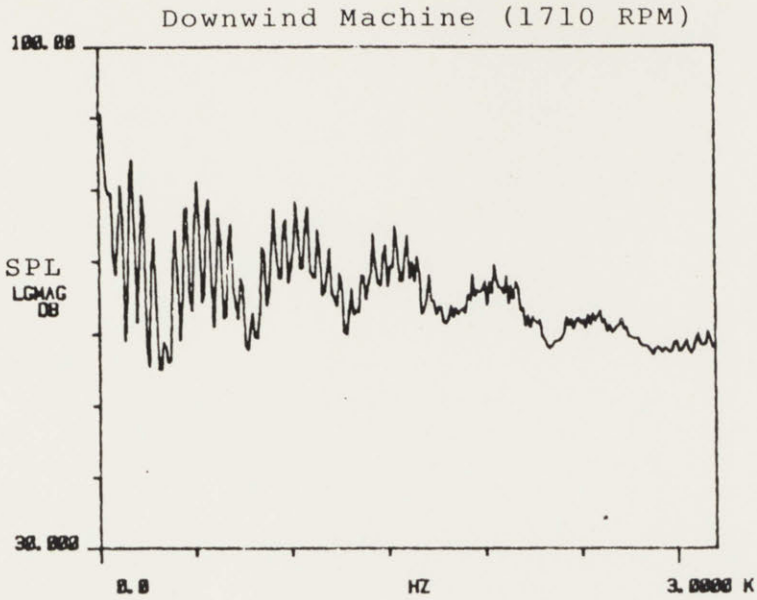

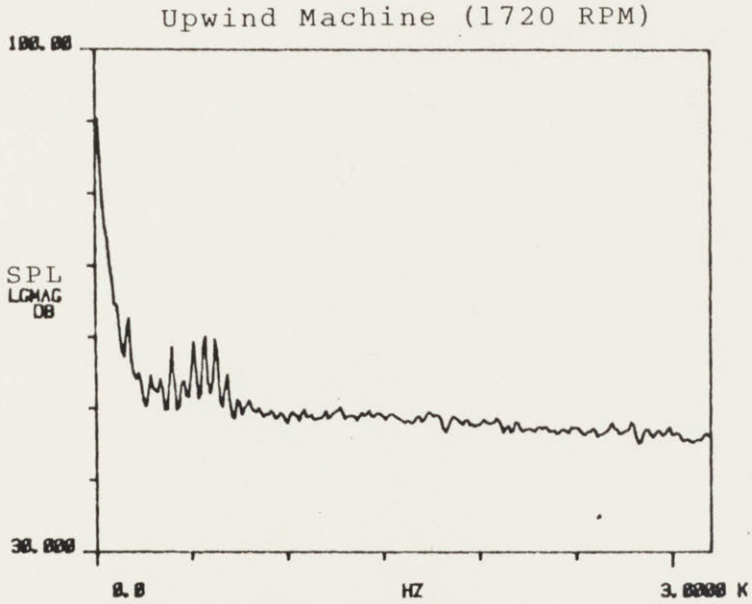

Fig 4.3 On Axis Microphone Comparison of an Upwind and Downwind Machine

2 blades
U = 22.5 MPH

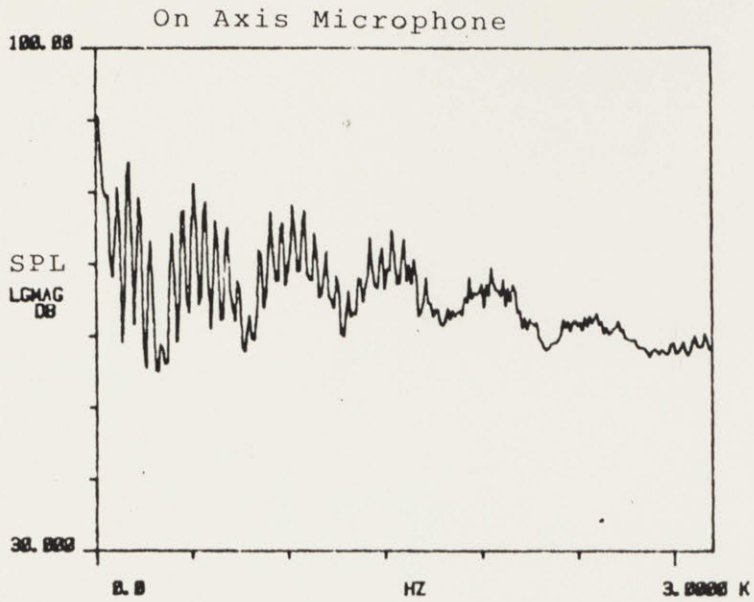

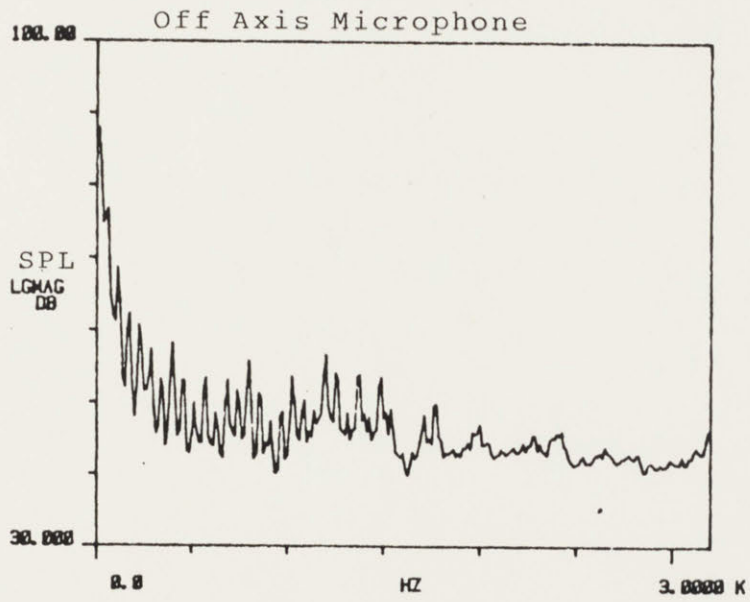

Fig 4.4 Comparison of On Axis and Off Axis Microphone for a Downwind Machine

2 blades
1710 RPM
U = 22.5 MPH

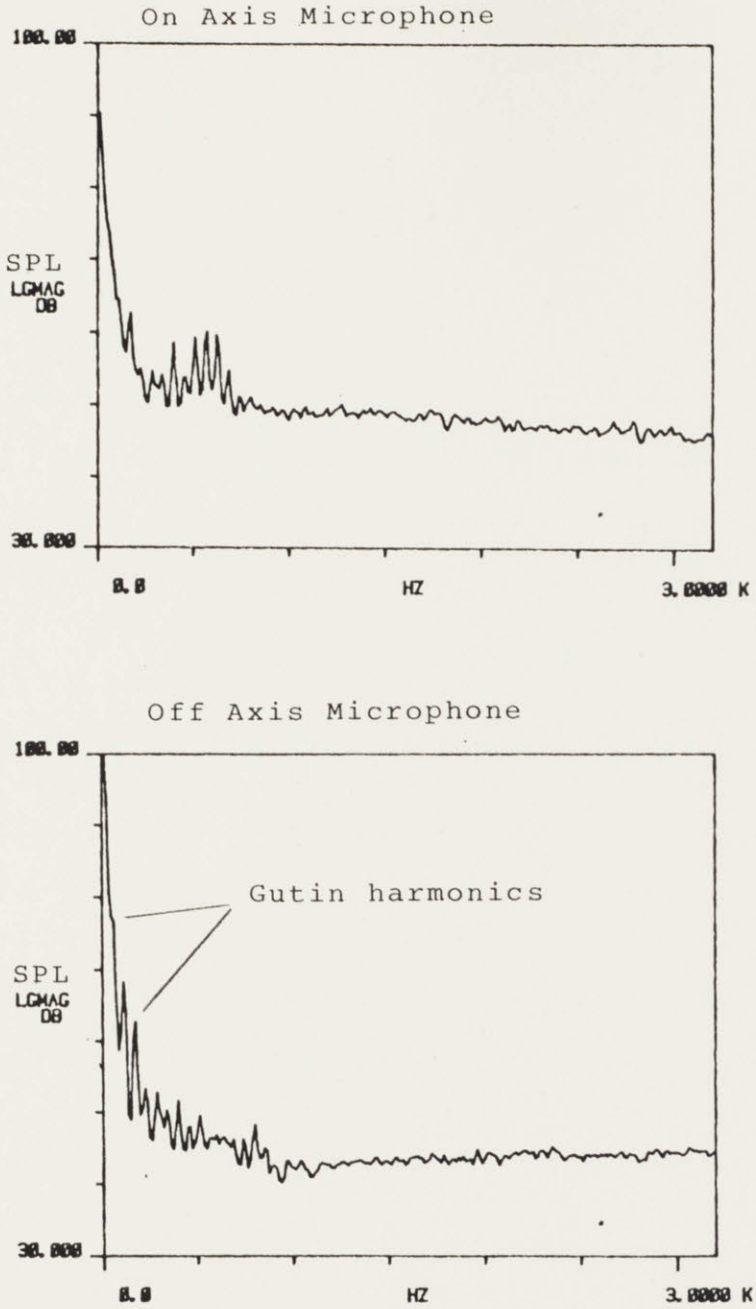

Fig 4.5 Comparison of On Axis and Off Axis Microphone for an Upwind Machine

2 blades
1720 RPM
U = 22.5 MPH

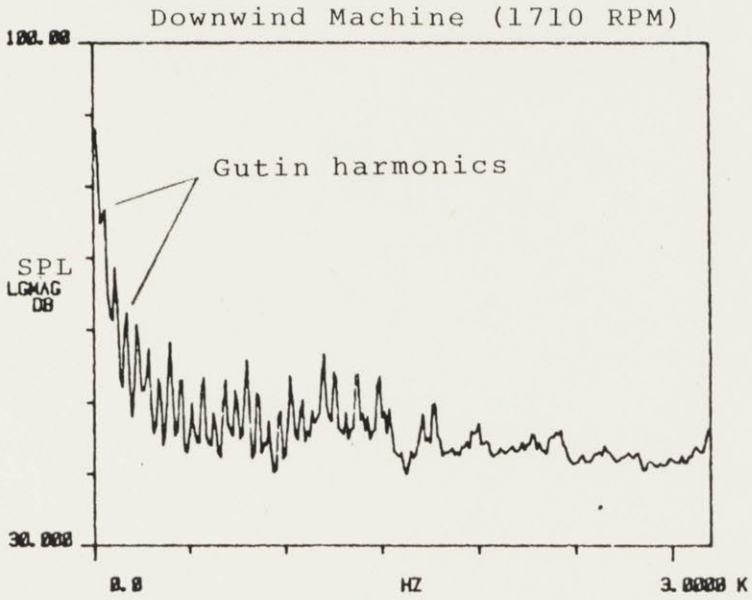

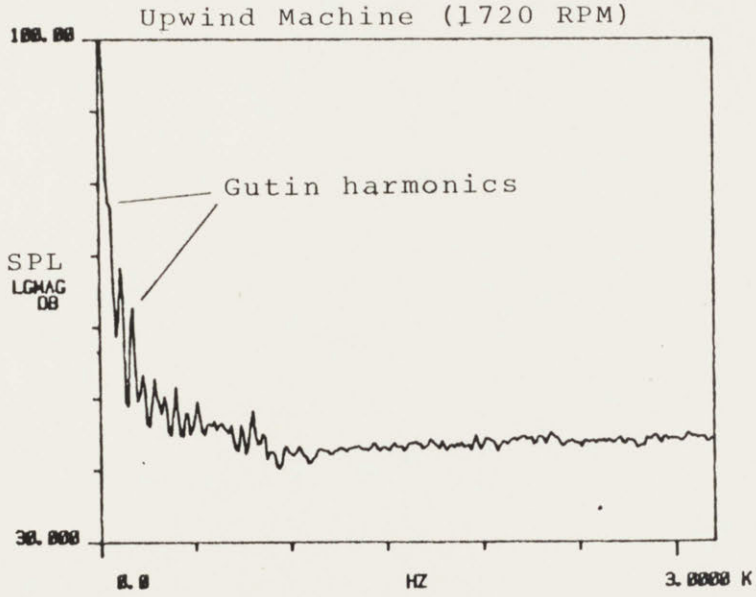

Fig 4.6 Off Axis Comparison of an Upwind and Downwind Machine

2 blades
U = 22.5 MPH

4.3 RPM TESTS

In the discussion of Chapter 2, the acoustic pressure of blade tower wake interaction was predicted to increase as the square of the rotation speed.

$$P \alpha (RPM)^2$$

$$\text{intensity} \alpha (RPM)^4$$

In order to investigate the pressure vs. RPM dependence, the windturbine was placed in a downwind configuration and acoustic spectra were measured for a number of rotation speeds.

Unfortunately, in order to reach very low rotation speeds, it was necessary to reduce the free stream velocity of the tunnel. Thus, not only the rotation speed, but also, the free stream velocity were reduced, and it then became necessary to plot the data via the theoretical prediction,

$$P \alpha U(RPM)^2$$

The results of this experiment are shown in figure 4.7, which is a plot of the sound power contained between 100 hz and 3.2 khz vs. Log U $(RPM)^2$. The sound power was integrated from 100 hz because, below this frequency, the tunnel noise makes a significant contribution.

By definition,

$$SPL = 20 \text{ Log}(P / Pref)$$

and so the log-log plot of figure 4.7 should have a slope of 20. Indeed, this is close to the value of 19.1 obtained

through least squares approximation to the data. A similar relationship is found in figure 4.8 which plots the magnitude of a single harmonic vs. Log U $(RPM)^2$.

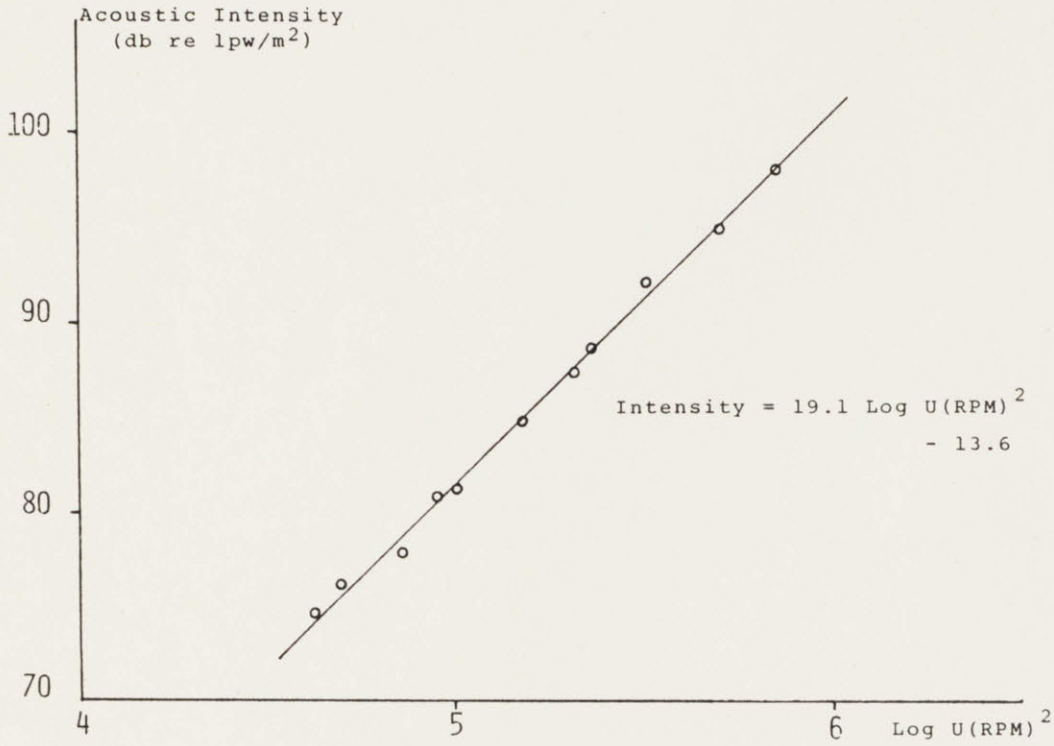

Fig 4.7 Integrated Acoustic Intensity (100 hz to 3.2 khz)

vs.

Log $U(RPM)^2$

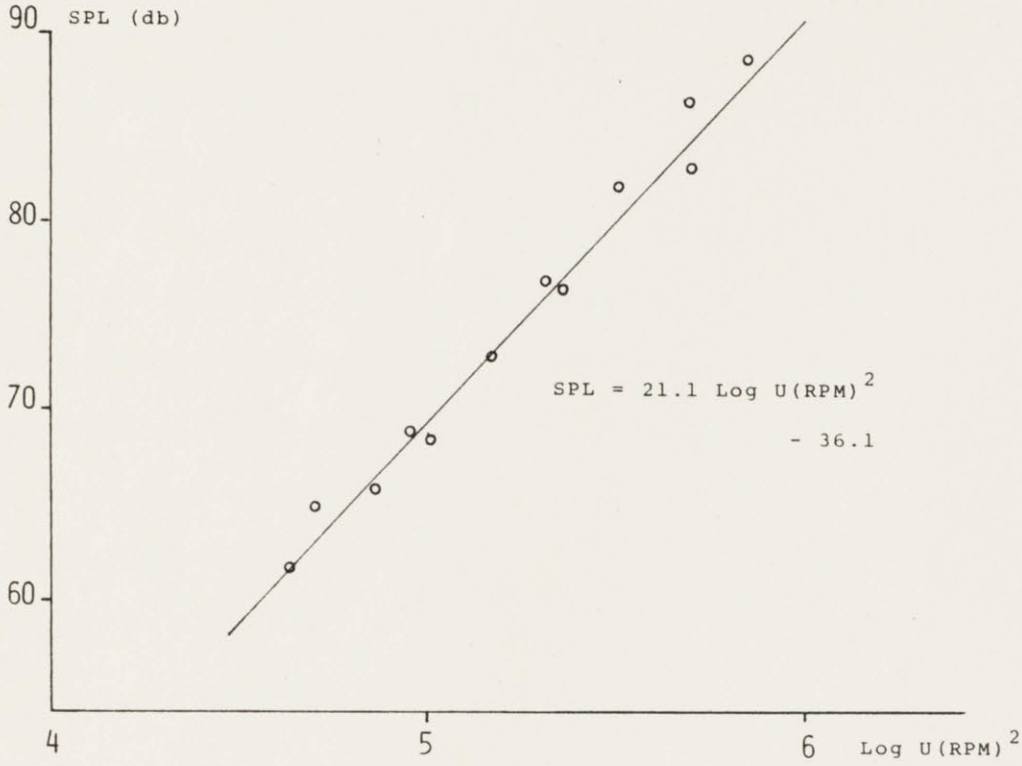

Fig 4.8 Sound Pressure Level of the Ninth Harmonic

vs.

Log U(RPM)^2

4.4 MULTIPLE BLADE TESTS

The number of blades on a windturbine has a marked influence on the spectrum of the acoustic intensity. This can be seen in figures 4.9 - 4.11 which show the acoustic spectra of a two, three and four bladed windturbine respectively. For all of these measurements, the windturbine is rotating in the wake of a 5/8" diameter cylinder which is located 15 diameters upstream of the rotor plane.

Figures 4.9 - 4.11 show that the spectral peaks at the blade passage harmonics progressively spread apart as the number of blades is increased. The blade number effectively rescales the frequency location of the harmonics. For example, if the frequency of the ninth harmonic of a two bladed windturbine is,

$$f9 = 597 \text{ hz} \quad (n = 2)$$

the corresponding frequency of a four bladed windturbine at the same speed is,

$$f9 = (2)(597) = 1194 \text{ hz} \quad (n = 4)$$

As the blade number increases, the spectral distribution is broadened, and this has a number of interesting and counteracting influences or the sound field. First, as a particular harmonic increases in frequency, the dipole radiation efficiency will also increase. Thus, the ninth

harmonic of a four bladed windturbine will, for a given magnitude of the unsteady load, radiate more efficiently than the same harmonic of a two bladed windturbine.

Counteracting the effect of improved radiation efficiency is the influence of spectral broadening which, with increasing blade number, tends to spread a given amount of power over a wider region of frequency. For example, if the spectra of figures 4.9 - 4.11 are integrated from 100 hz to 3.2 khz, the number of peaks there contained goes in inverse proportion to the number of blades.

Combining the effects of improved radiation efficiency with the influence of spectral broadening, it is not surprising that the integrated intensities are roughly equal for the two, three, and four bladed windtrubine.

# Blades	Integrated Intensity* (100 hz - 3.2 khz)
2	89.8 dB
3	89.8 dB
4	90.2 dB

The counteracting machanisms of increased blade number tend to cancel one another, and, as seen in the above table, the overall sound pressure level is roughly independent of the number of blades. This is a result which should also hold for a full scale windturbine.

* Lower integration limit of 100 hz chosen to avoid tunnel noise.

1990 RPM

U = 22.5 MPH

Cylinder is 15 diameters upstream of the rotor

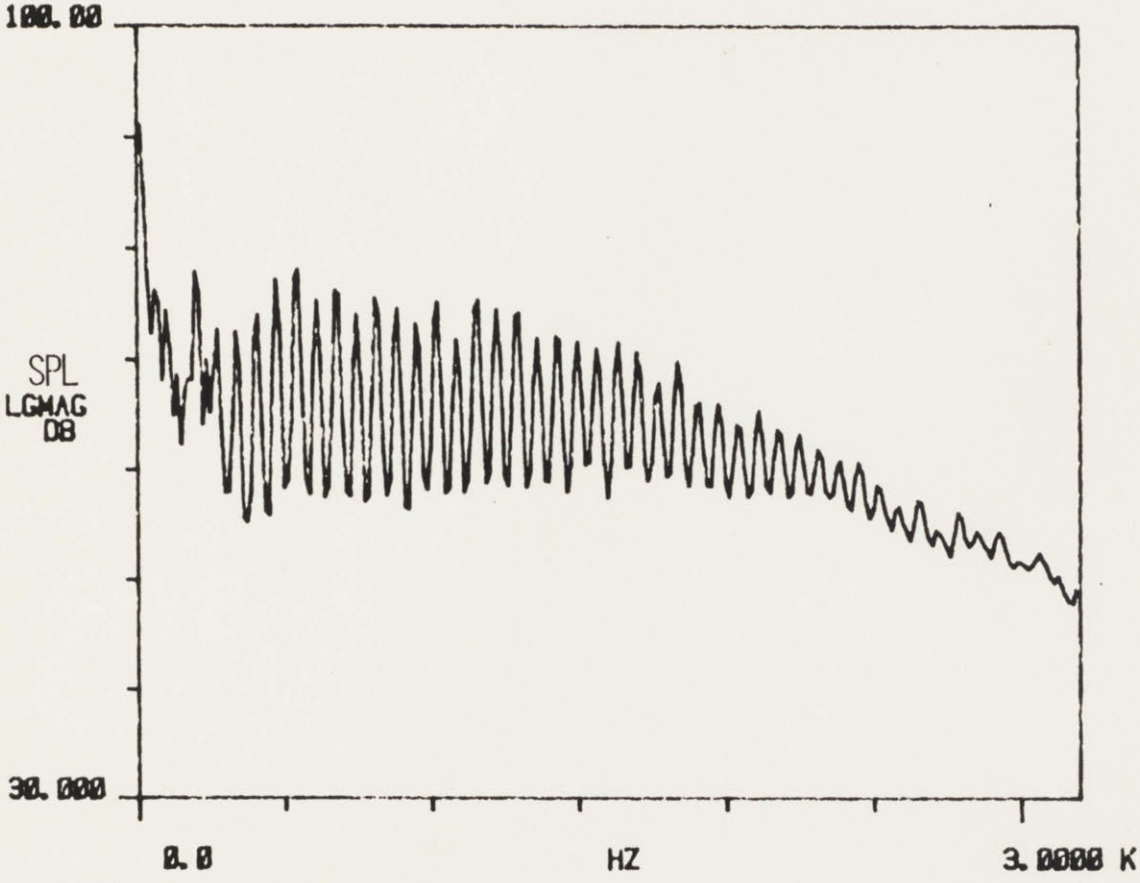

Fig 4.9 On Axis Microphone for a Two Bladed Windturbine Rotating in the Wake of a 5/8" Cylinder

1990 RPM

U = 22.5 MPH

Cylinder is 15 diameters upstream of the rotor

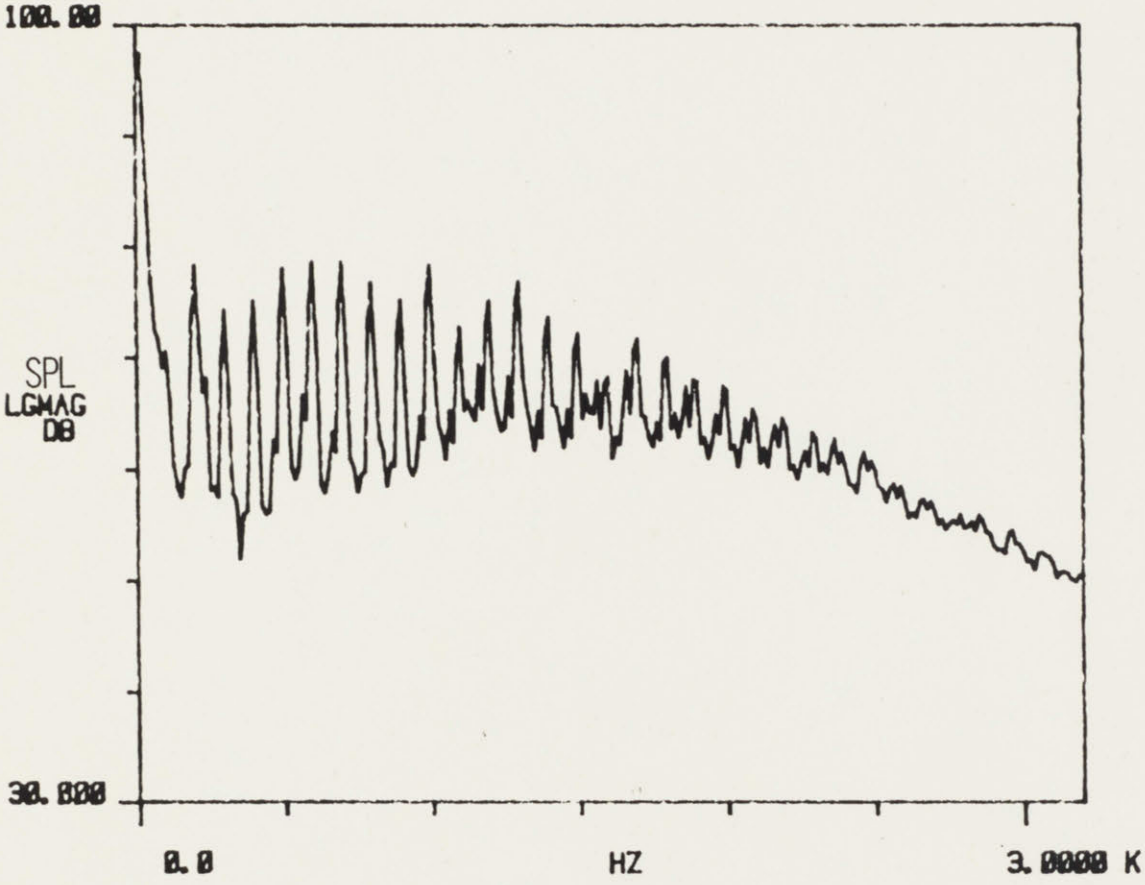

Fig 4.10 On Axis Microphone for a Three Bladed Windturbine Rotating in the Wake of a 5/8" cylinder

1970 RPM

U = 22.5 MPH

Cylinder is 15 diameters upstream of the rotor

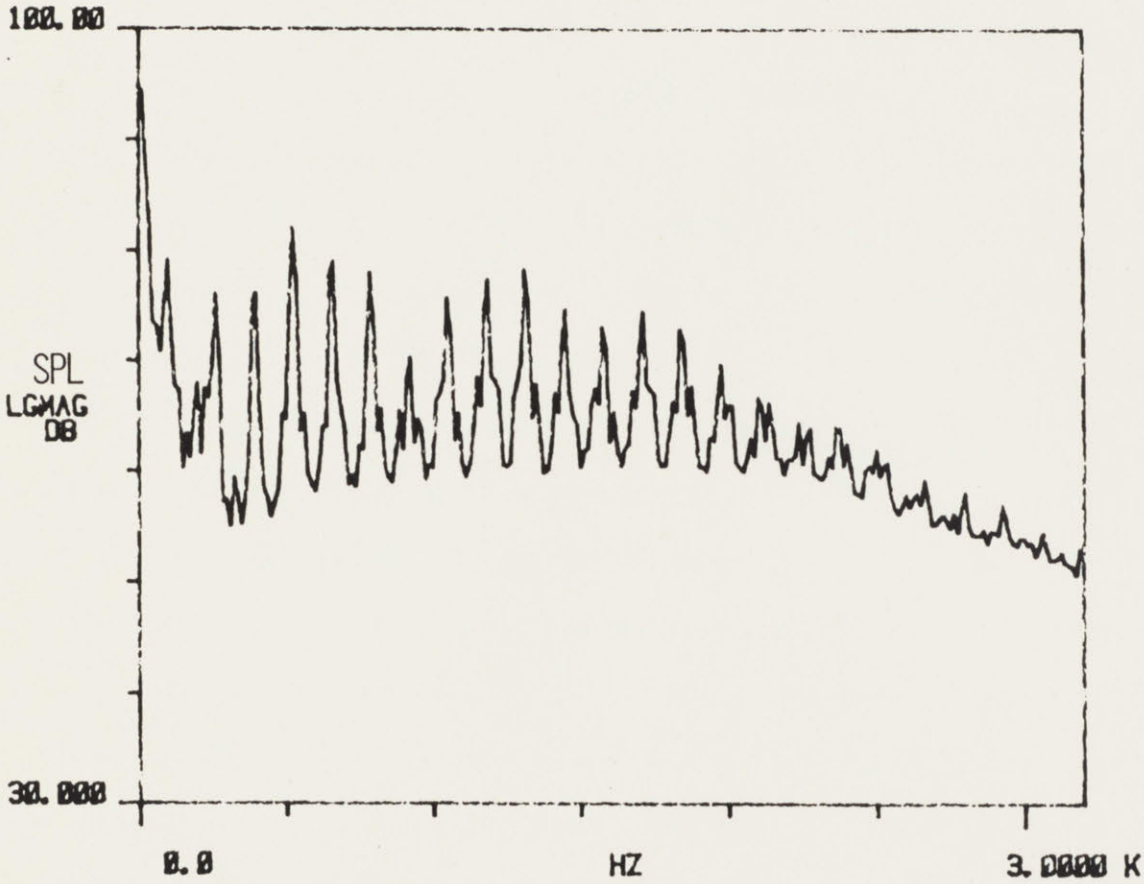

Fig 4.11 On Axis Microphone for a Four Bladed Windturbine Rotating in the wake of a 5/8" Cylinder

4.5 CYLINDER WAKE AND TOWER WAKE TESTS

Figure 4.12 shows the mean wake profiles measured fifteen diameters downstream of a 5/8", 1 1/4" and 2" diameter cylinder. As expected, these measurements show the cylinder to create a wake of near Gaussian profile. Each profile in figure 4.12 is then labeled with an approximate amplitude and halfwidth of an equivalent Gaussian wake. For the Reynold numbers of this test, the trend of the wake amplitude and width is to increase with the cylinder diameter.

After hotwire profiles were measured, the windturbine was made to operate in each of the wakes of figure 4.12, and the acoustic spectra were measured. These measurements are shown in figures 4.13 to 4.15 which also feature the harmonic levels predicted from the wake measurements (equation 2.31). It is encouraging that the low frequency predictions fall within three or four decibels of the measurements.

The most noticeable difference between three different cylinder wakes is the content of high frequency harmonics which are found in the acoustic field. The wider the cylinder, the less relative contribution is found from the higher harmonics. This phenomenon is the consequence of an inverse Fourier relationship between the bandwidth of the blade loading, and the time of blade passage through the wake. A wide wake prolongs the duration of the gust experienced by the blade, and conversely, the frequency content of the blade loading becomes narrow. In the time domain, the impulsive action of blade passage through the wake is "spread" over a

wider interval of time.

Figure 4.16 shows the mean velocity deficit behind the 1/53 scale model tower. This measurement was made at the position of 75% span, and it displays the two Gaussian-like peaks in the wake profile which extend the height of the windturbine. Near the blade tip, this pair of peaks describe an angle of .318 radians with the hub, and this angle determines the time delay for blade passage between the tower legs. This produces a modulation whose predicted pattern is shown alongside measurements in figure 4.17. At low frequencies, the predicted modulation is close to that which is measured. The actual harmonic levels are, however, overestimated. This is a descrepancy which is believed to result from the assumption of coherent blade motion through each of the two wakes. The actual tower legs do not meet at the hub, but rather, the tower legs are skewed to the motion of the blade, one portion of which leads the other through the wake.

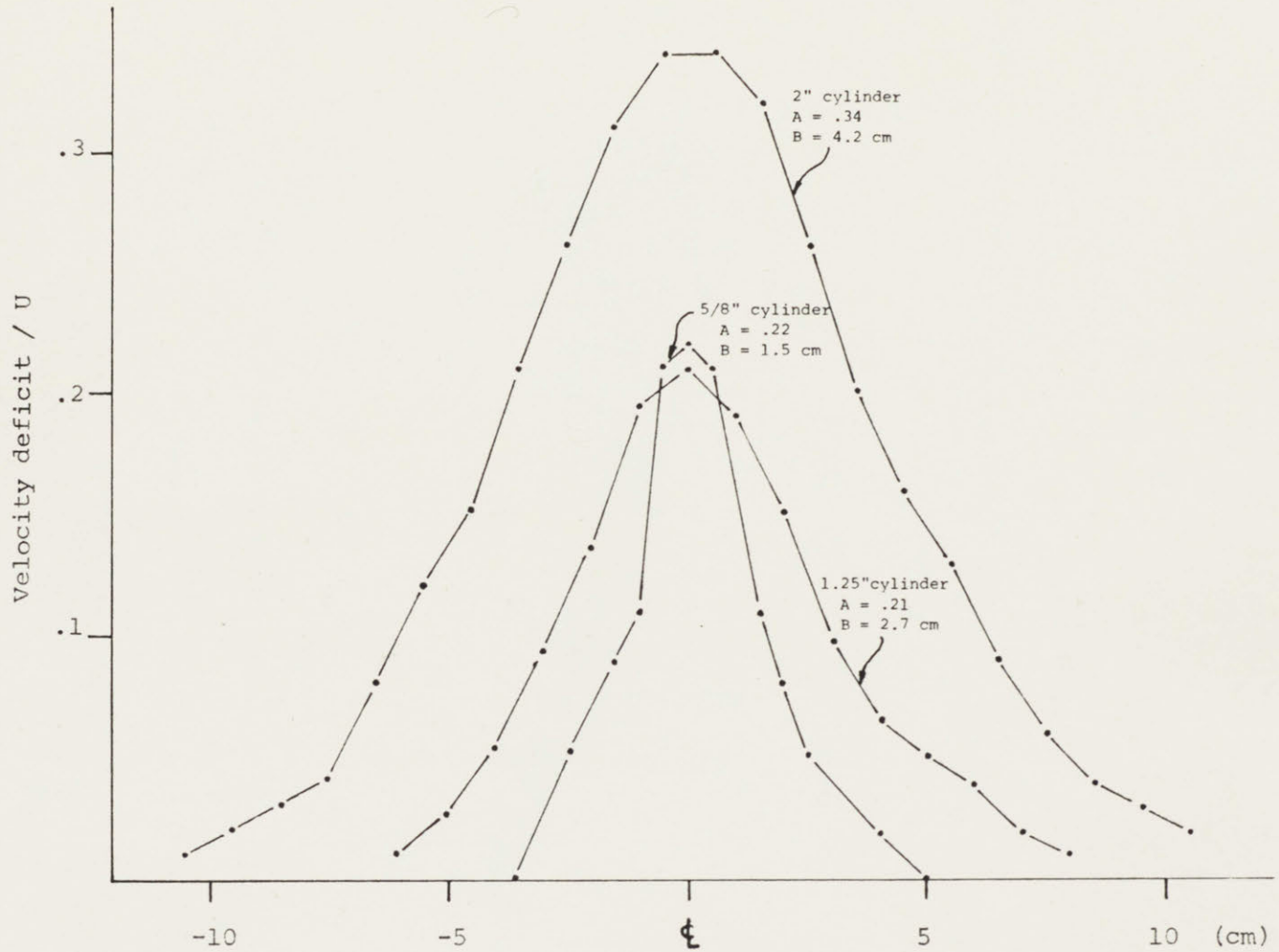

Fig 4.12 Wake Profile 15 Diameters Downstream of a 5/8",1.25", and 2" Cylinder

2 blades

1740 RPM

U = 22.5 MPH

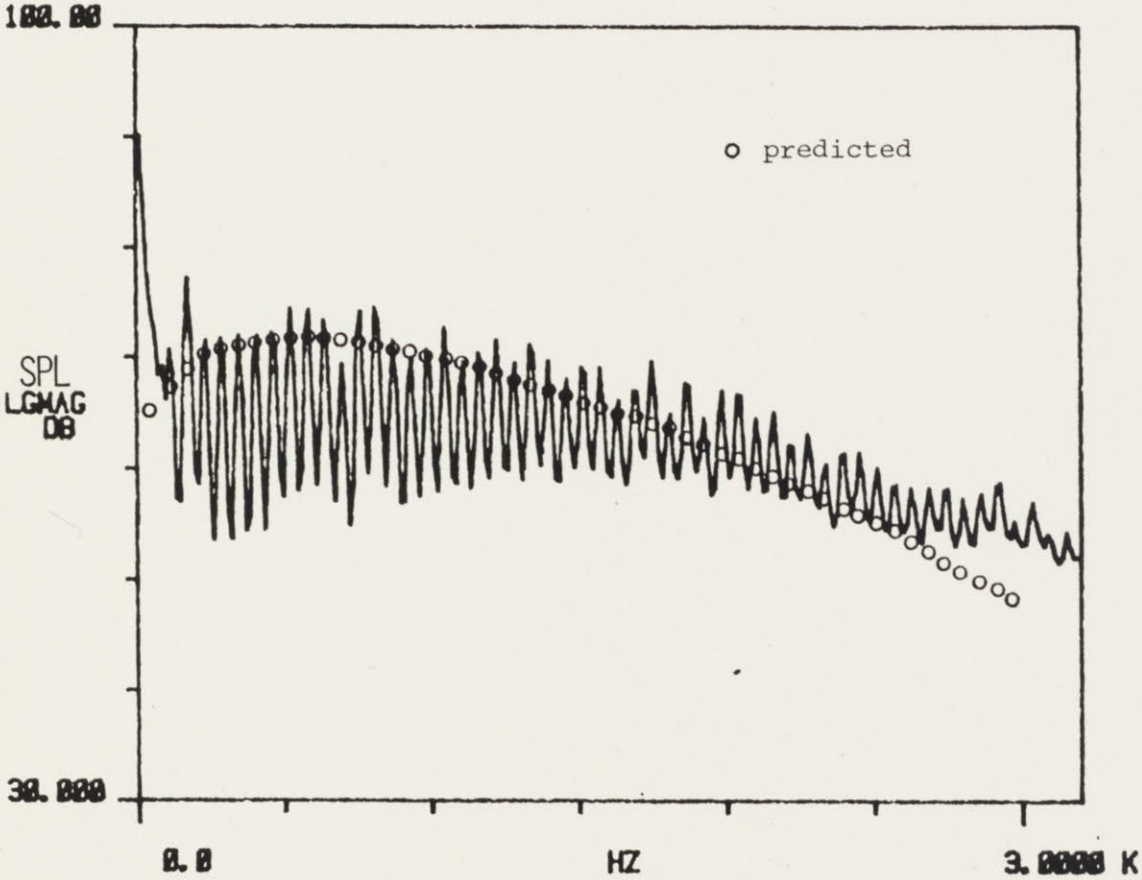

Fig 4.13 Comparison of Measured and Predicted Harmonic Levels for Windturbine Operation in the Wake of a 5/8" Cylinder (On Axis Microphone)

2 blades

1740 RPM

U = 22.5 MPH

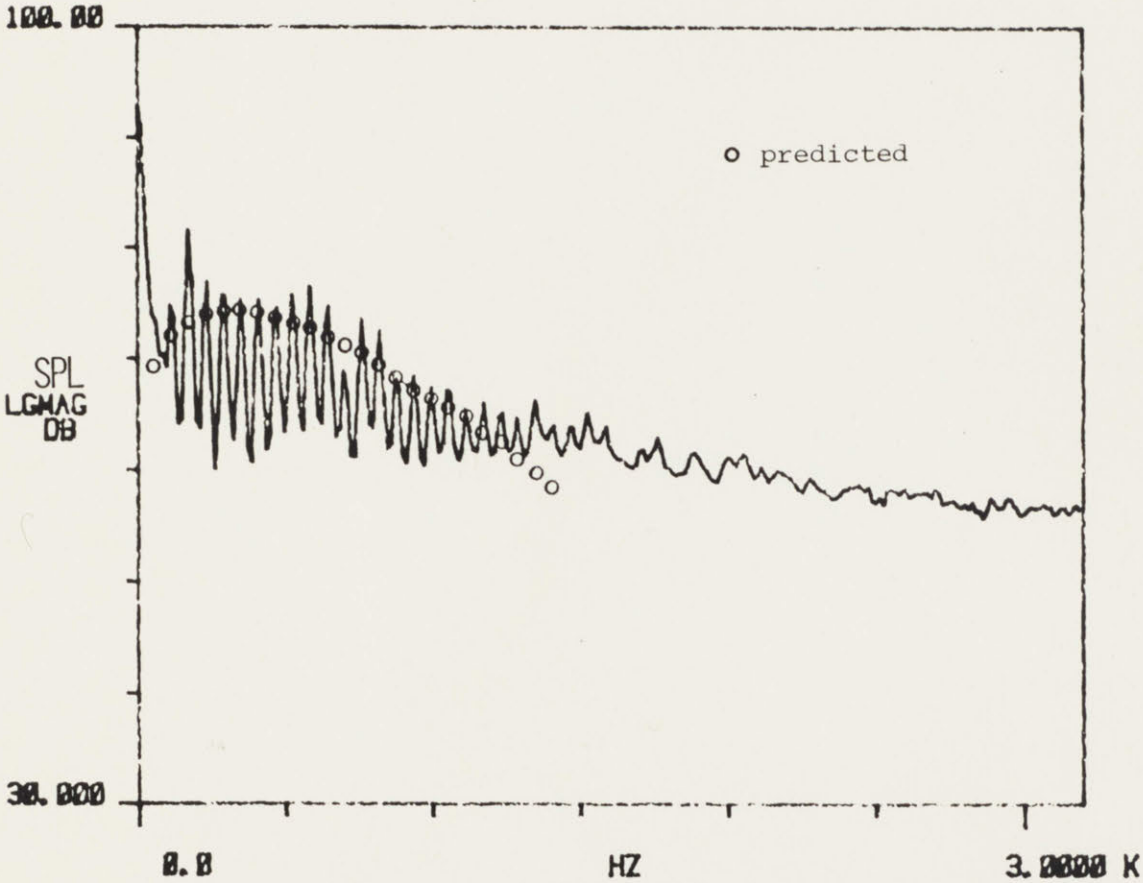

Fig 4.14 Comparison of Measured and Predicted Harmonic Levels for Windturbine Operation in the Wake of a 1.25" Cylinder (On Axis Microphone)

2 blades

1740 RPM

U = 22.5 MPH

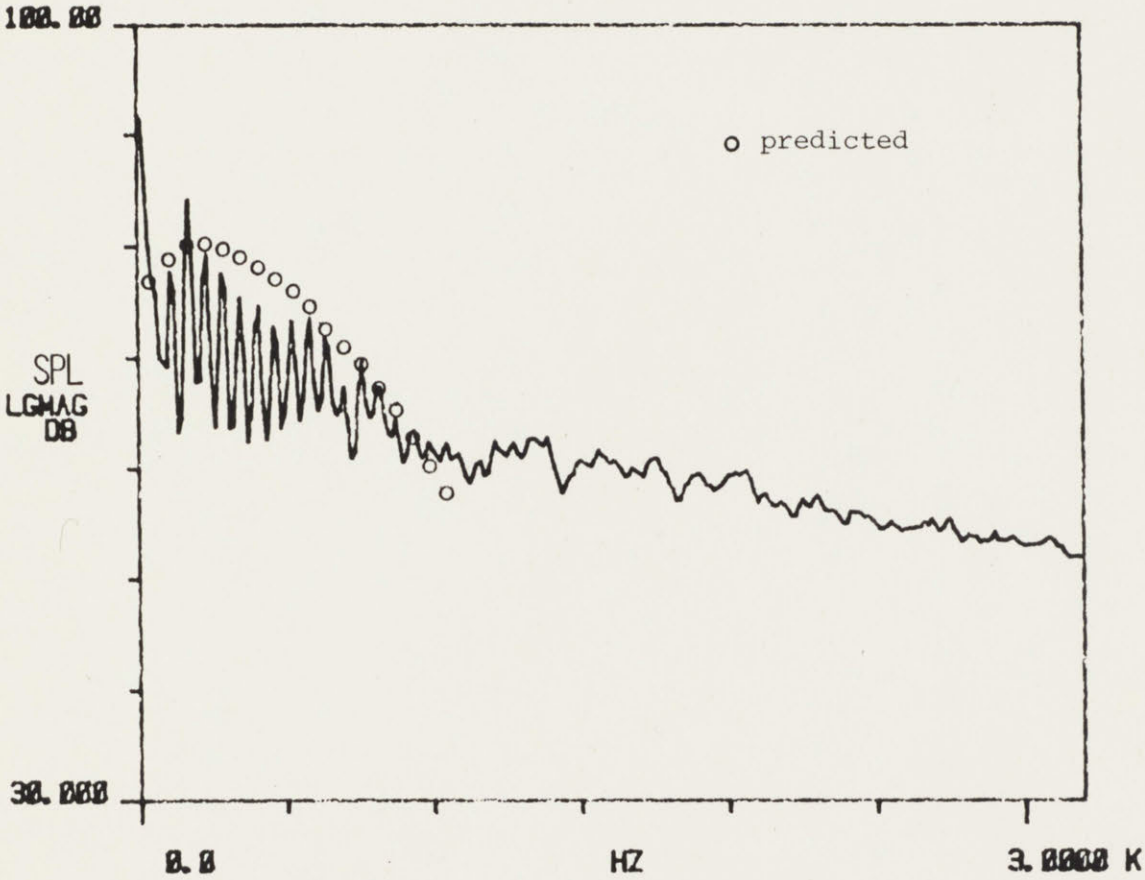

Fig 4.15 Comparison of Measured and Predicted Harmonic Levels for Windturbine Operation in the Wake of a 2" Cylinder (On Axis Microphone)

Fig 4.16 Tower Wake Profile

2 blades

1710 RPM

U = 22.5 MPH

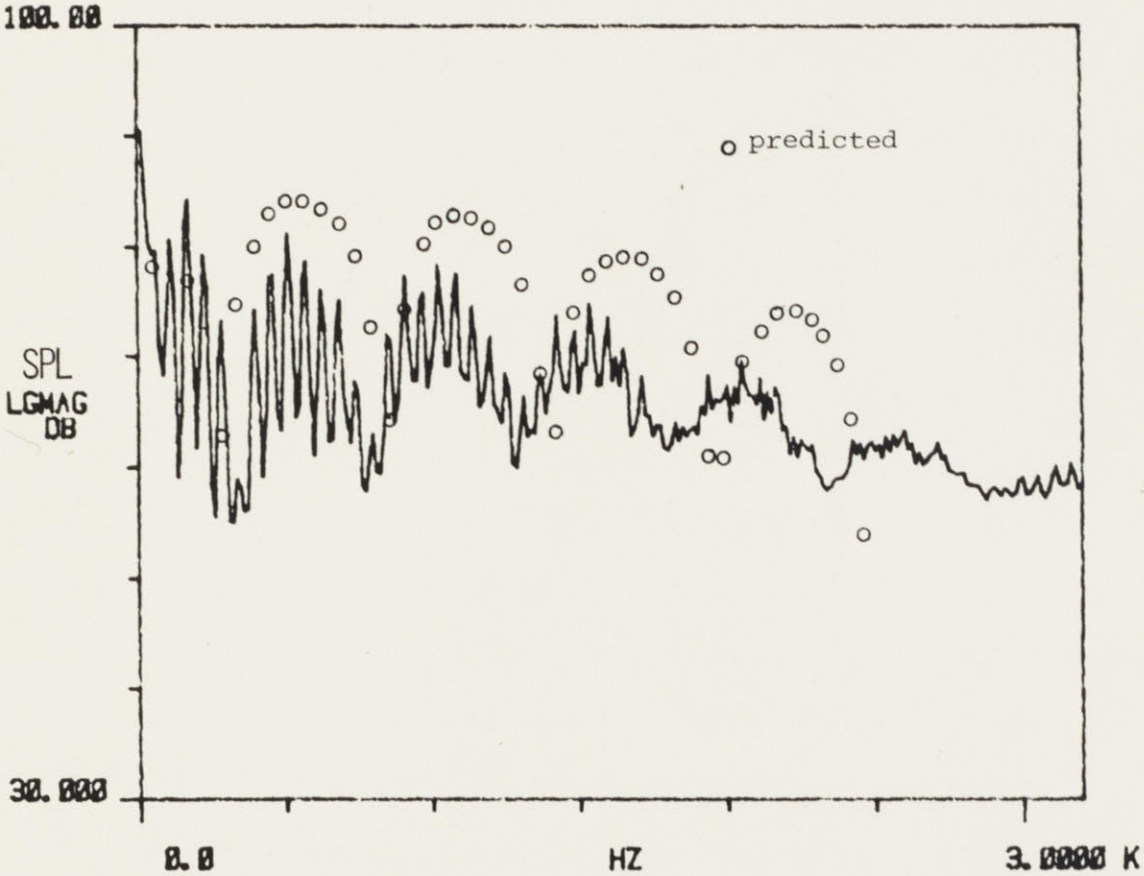

Fig 4.17 Comparison of Measured and Predicted Harmonic Levels for Windturbine Operation in the Tower Wake (On Axis Microphone)

4.6 LOADING TESTS

The scale windturbine was "loaded" by means of a torque applied to the turbine shaft. Conversely, if the shaft torque is released, the windturbine is labeled here as "free spinning".

Figure 4.18 compares on axis acoustic measurements for both the loaded and free spinning windturbine. Both these measurements were made with the windturbine in a downwind configuration, and the windturbine was made to operate at approximately the same RPM. This means that, for the free spinning measurements, the blades had to be stalled in order to slow the windturbine down. Figure 4.18 shows that steady loading has no influence on the harmonic noise of blade tower wake interaction. At low frequencies, the on axis measurements show identical harmonic levels. The loaded windturbine has slightly reduced levels at the higher frequencies, but this reduction is believed to result from a wider wake produced by various wires which were lead to the generator and taped to the legs of the windturbine tower. For the free spinning tests, these wires were disconnected.

The off axis measurements of the loaded and free spinning windturbine can be compared in figure 4.19 where it appears that the lowest blade passage harmonics exhibit a slight two decibel increase with the blade loading. If these are the Gutin harmonics, then this is a result which is to be expected. Unfortunately, for a given size windturbine, it is very difficult to sweep the load over a wide enough range to

significantly influence the acoustics of Gutin noise. Experimental conclusions concerning the influence of blade loading on Gutin noise should probably be obtained on comparison of data between windturbines of different size.

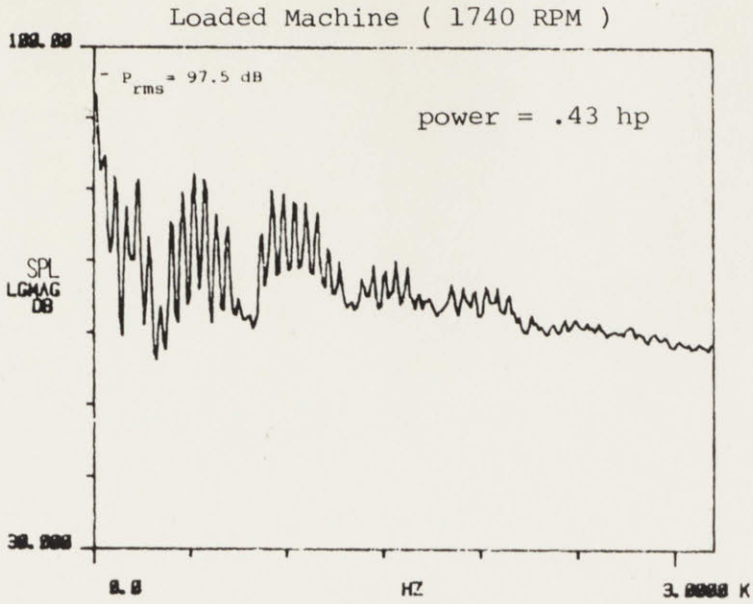

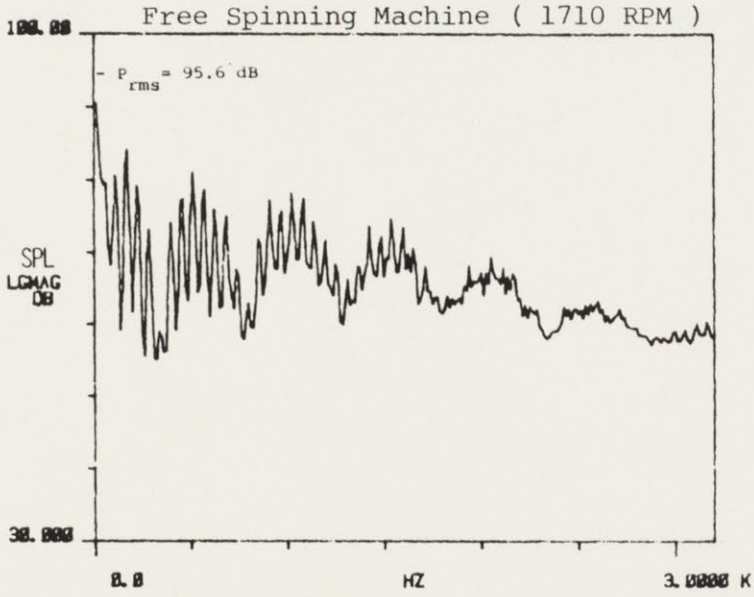

Fig 4.18 On Axis Microphone Comparison for a Loaded and Free Spinning Windturbine

2 blades
U = 22.5 MPH

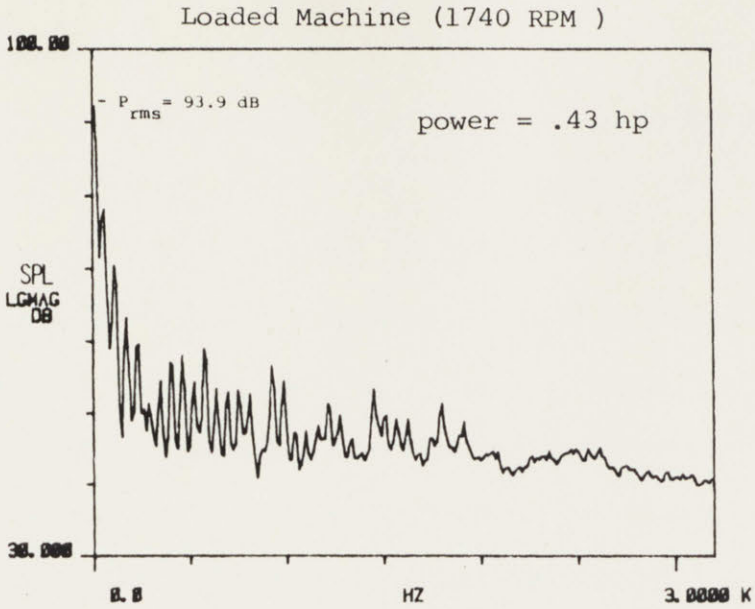

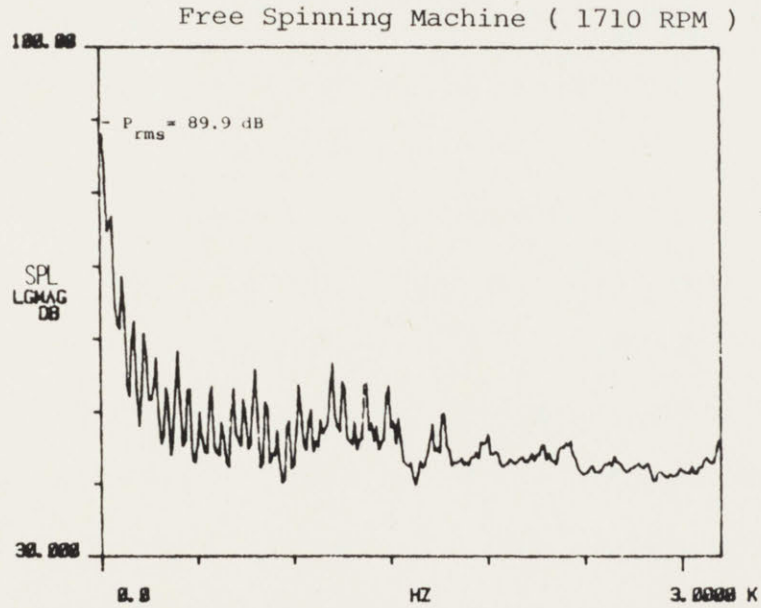

Fig 4.19 Off Axis Microphone Comparison for a Loaded and Free Spinning Windturbine

2 blades
U = 22.5 MPH

4.7 TURBULENT BOUNDARY LAYER AND BLADE VORTEX INTERACTION TESTS

An interesting example of blade interaction with unsteady flow can be seen in figure 4.20 which shows the acoustic spectrum of a windturbine rotating through the vortex street of a two inch cylinder. This spectrum features both the usual peaks at the blade passage harmonics (these peaks are due to blade passage through the mean wake of the cylinder), and pairs of peaks which are found between the blade passage harmonics. In the context of the broadband theory of Chapter 2, these latter peaks are predicted to arise from modulation at the unsteady frequencies of the flowfield. Indeed each one of the "sideband" peaks of figure 4.20 can be associated with a blade passage harmonic which is 40 hz away. This is encouraging because 40 hz was the measured shedding frequency of the cylinder.

As a further test on broadband noise due to blade interaction with incident turbulence, two spires were constructed to create boundary layers with different velocity gradients and turbulent intensities. These spires were, one at a time, placed two meters upstream of the upwind facing scale model. Subsequently, an acoustic spectrum was measured for windturbine operation in each of the boundary layers.

The boundary layer spire shapes are shown in figure 4.21. Figure 4.22 shows the mean velocity profile of each boundary layer. At a height of 14" in the profiles, a hotwire was placed and used to measure fluctuating velocities in axial

direction. The spectral distribution of these hotwire measurements appear in figures 4.23 and 4.24, and, unfortunately, these measurements were made without the windturbine in operation. Shown alongside these turbulent spectra are values of the turbulent scale which can be calculated from the asymptotic behavior of the spectrum (ref. 16).

Acoustic measurements for the windturbine operating in both boundary layer environments can be compared in figures 4.25 and 4.26. The spectra can be compared at high frequencies, where the levels are approximately equal, and low frequencies, where boundary layer #1 has more intense broadband levels. This low frequency result is to be expected because the turbulent velocities of boundary layer #1 are more intense than those of boundary layer #2.

It is unfortunate that the high frequency acoustic levels appear uninfluenced by the particular spires of this experiment. Probably, the high frequency broadband noise which was recorded here is produced by small scale inflow turbulence of the quickly spinning rotor, and, as was mentioned before, this turbulence was not measured. In a future test it would seem appropriate to simultaneously record both the hotwire and acoustic signals.

Alongside the acoustic measurements of figures 4.25 and 4.26 are shown the broadband levels which are predicted from the input of the turbulent scale and rms velocity into equation 2.19. Comparison with measurements show the

predictions to have good agreement at frequencies above 1 khz but, below this frequency the broadband levels are over-estimated. In fact, the high frequency agreement is not a sign of great success because these frequencies are believed to be generated by the small scale inflow turbulence which was not measured. In general, all the calculations for broadband noise are believed to be overestimated. This result follows from the hotwire measurements which were made deep in the boundary layer and probably overestimated rms velocities seen through the rotor plane. This problem is believed to be more acute for boundary layer #1 where low frequency predictions exceed the measurements by ten to fifteen decibels.

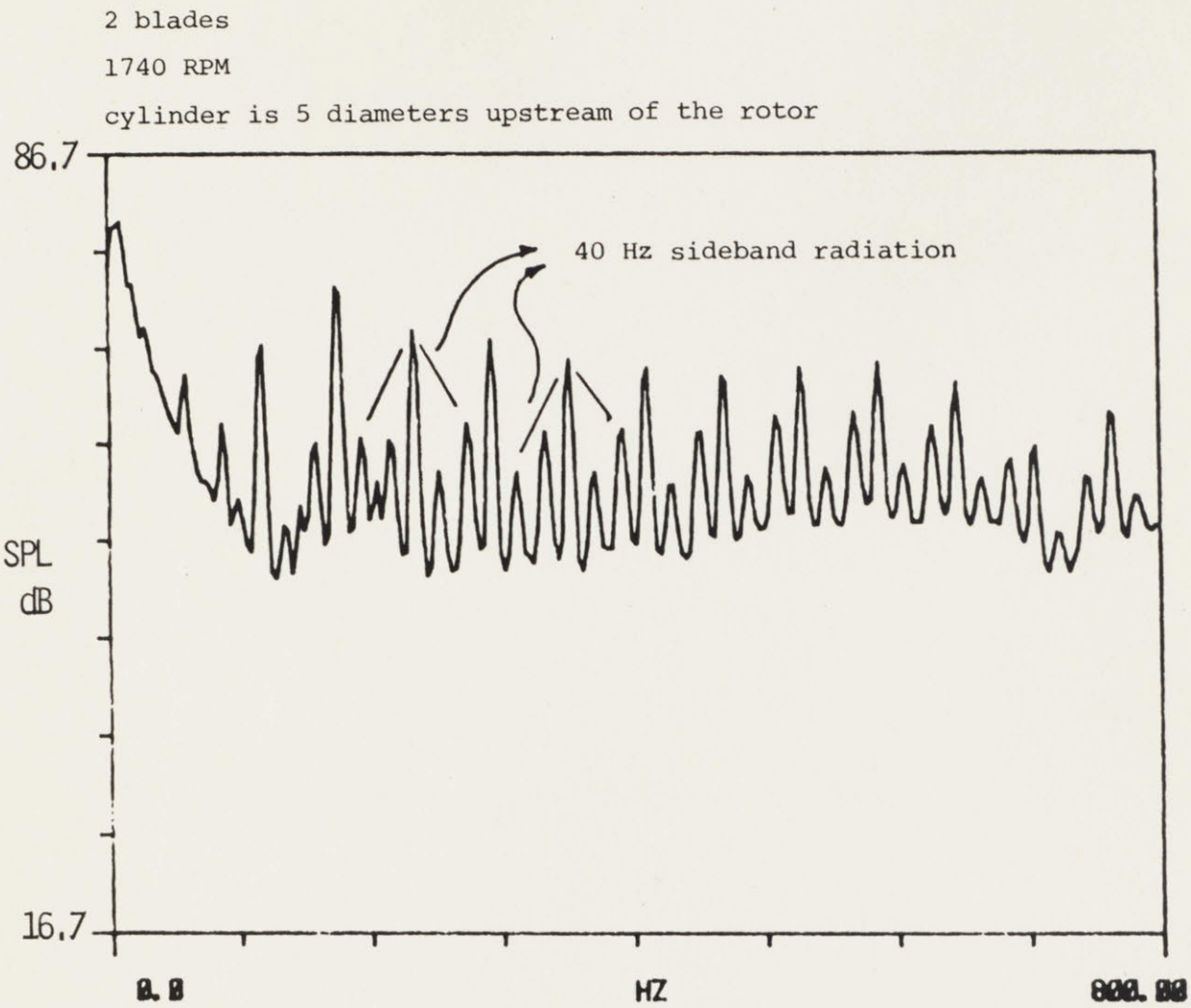

Fig 4.20 Modulation of the Blade Passage Harmonics for Windturbine Operation in the Vortex Street of a 2" Cylinder (On Axis Microphone)

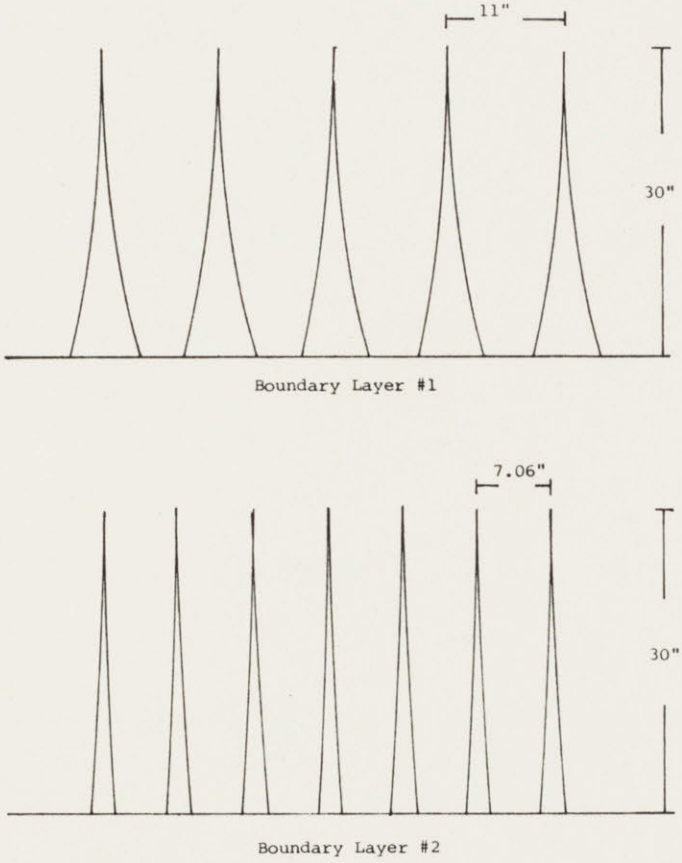

Fig 4.21 Shape of the Boundary Layer Spires

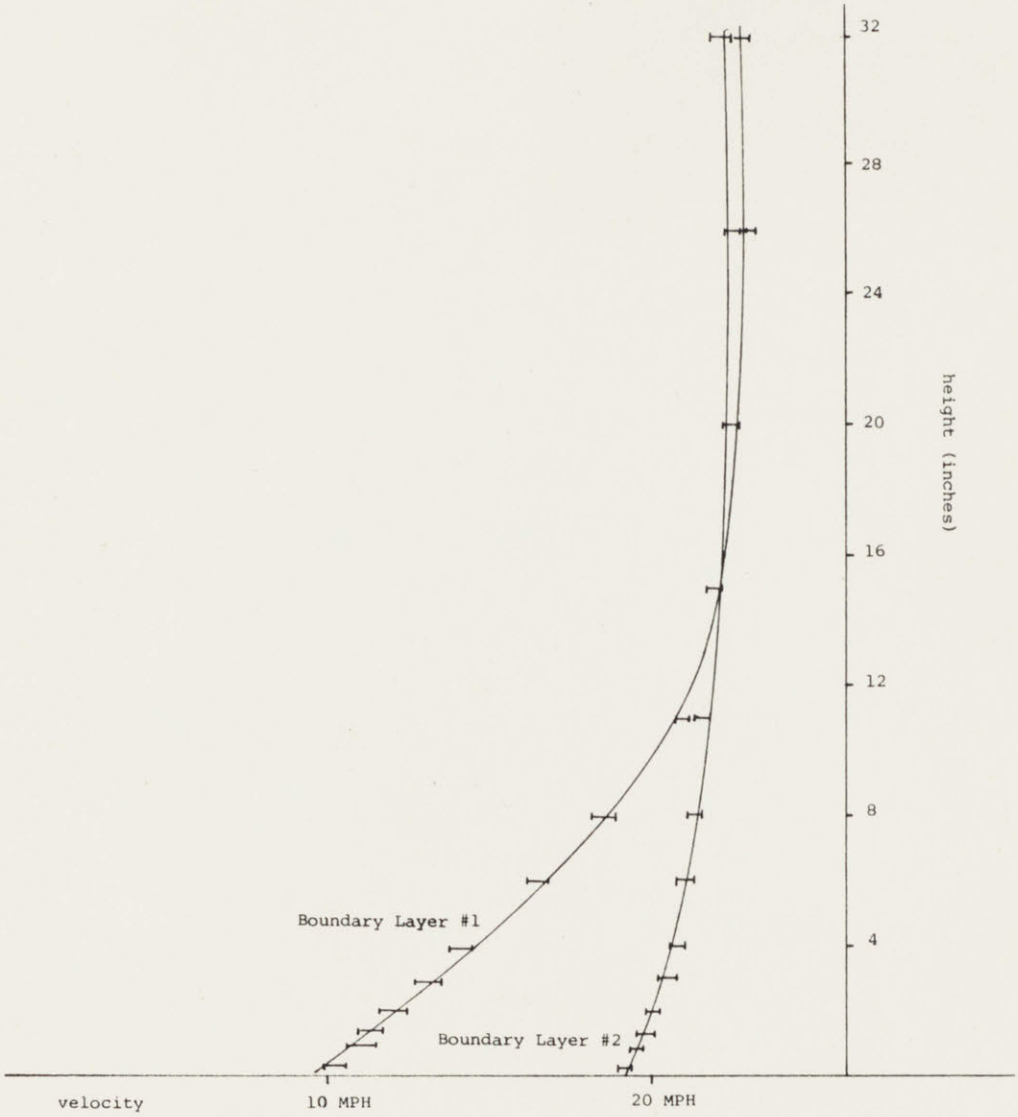

Fig 4.22 Boundary Layer Profiles

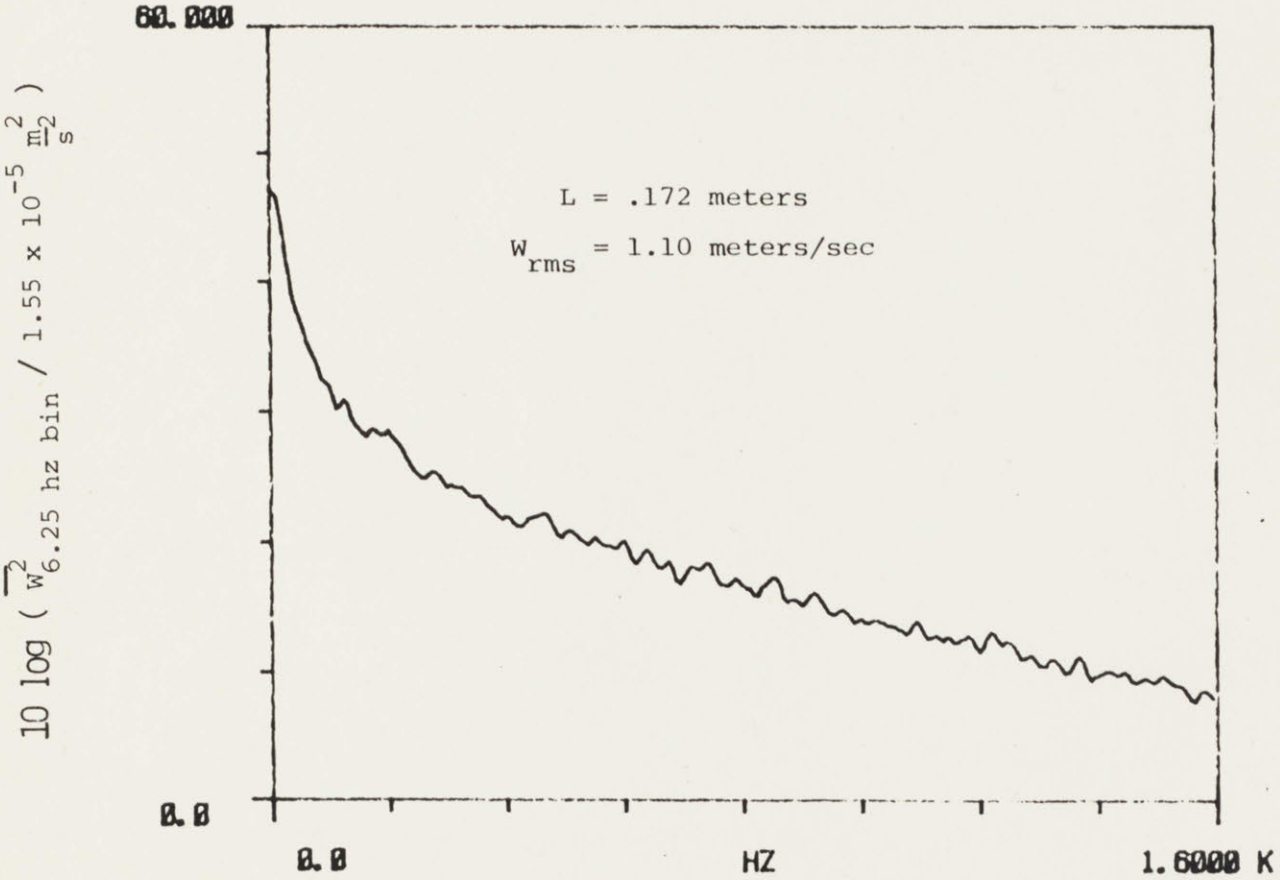

Fig 4.23 Spectral Distribution of the Axial Turbulence Behind Boundary Layer #1 *

* Spectral density is integrated over each 6.25 hz bin of the analyzer.

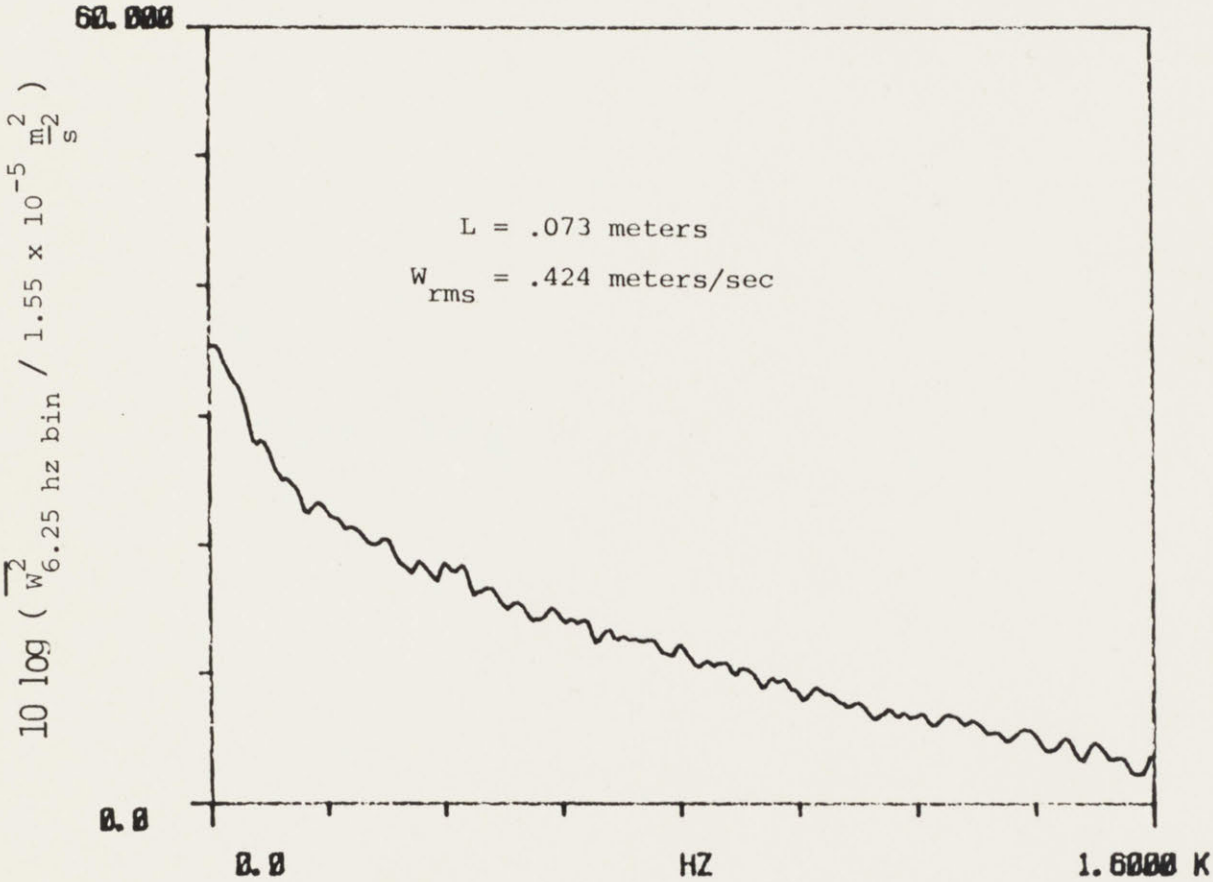

Fig 4.24 Spectral Distribution of the Axial Turbulence Behind Boundary Layer #2 *

* Spectral density is integrated over each 6.25 hz bin of the analyzer.

2 blades

1990 RPM

U = 22.5 MPH

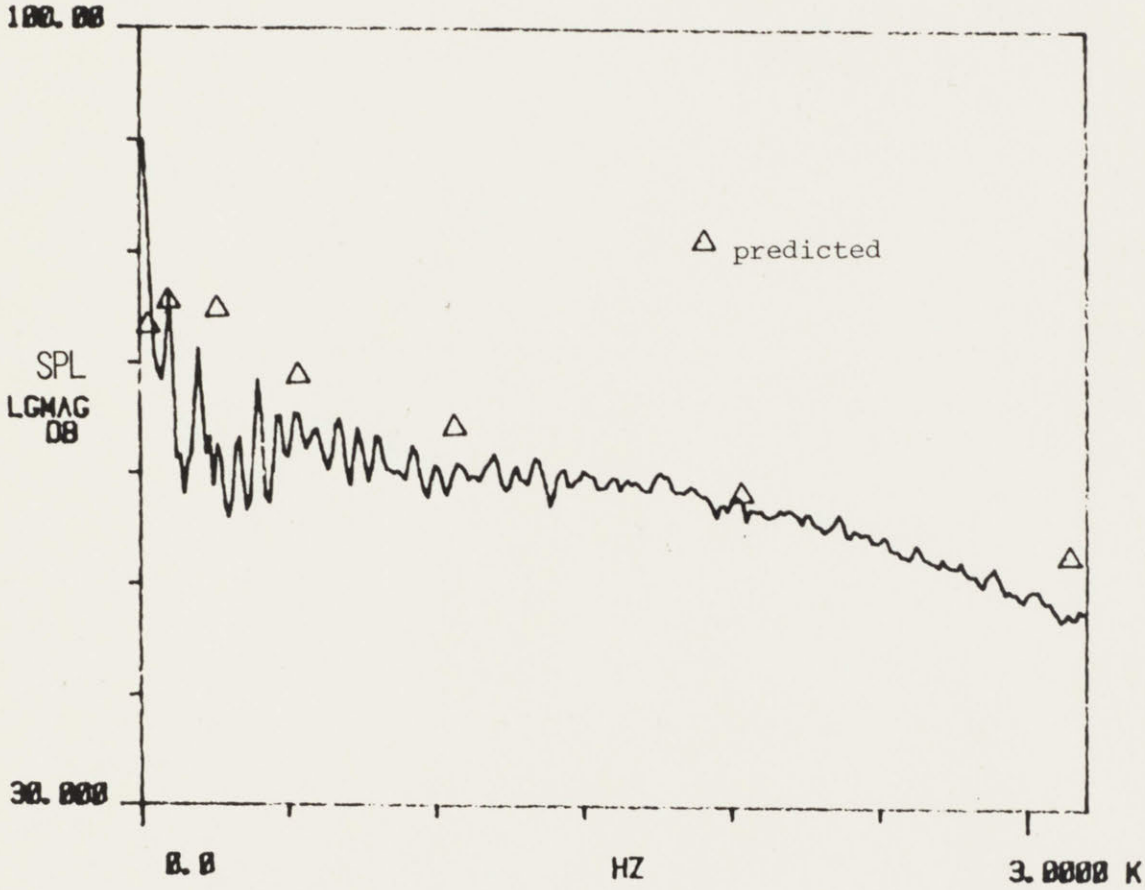

Fig 4.25 Comparison of Measured and Predicted Broadband Levels for Windturbine Operation in Boundary Layer #1 (On Axis Microphone)

2 blades

1990 RPM

U = 22.5 MPH

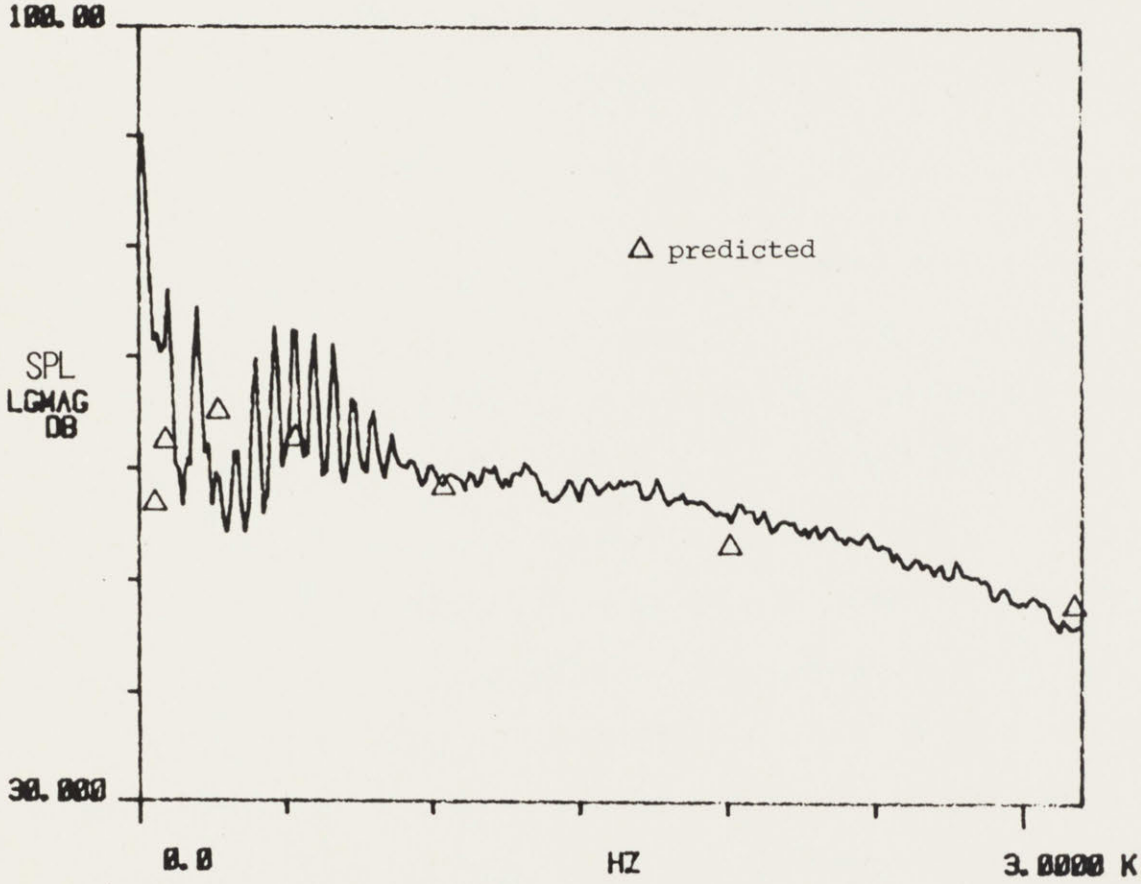

Fig 4.26 Comparison of Measured and Predicted Broadband Levels for Windturbine Operation in Boundary Layer #2 (On Axis Microphone)

CHAPTER 5

CONCLUSIONS AND RECOMMENDATIONS

Combining the experimental and theoretical results of this thesis, the following list of conclusions and suggestions is given.

1) An upwind facing windturbine will produce far less blade tower wake interaction noise than its downwind counterpart.

2) The noise of blade tower wake interaction is found to have a strong on axis directionality. The intensity of this noise is measured to increase with the fourth power of the rotation speed. In light of the agreement between predicted and measured spectra, the intensity is also predicted to increase with the second power of the tower drag coefficient. Significant improvements in the noise of blade tower wake interaction may then be realized in two steps. First, if possible, it is advantageous to reduce the turbine RPM. A second suggestion is to reduce the tower drag by means of aerodynamic fairings which are attached to the tower legs, and which rotate with shifting direction of the wind.

3) Gutin noise harmonics can be found in the off axis direction of both an upwind and downwind machine. For the

experiments conducted here, the Gutin harmonics are the major source of noise for an upwind machine. For a downwind machine, the noise of blade tower wake interaction dominates the noise of Gutin harmonics.

4) Broadband noise is predicted to increase with both the fourth power of the R.P.M. and with the kinetic energy of incident turbulence. At frequencies above the first blade passage harmonics, broadband noise is expected to increase with the ratio of the span to the turbulent scale. In view of the computed results of figure 2.1, it is this author's opinion that the broadband "humps" observed for MOD-1 are not the result of atmospheric turbulence, but rather, they are the consequence of smaller scale turbulence within the tower wake.

5) The acoustic influence of multiple blades is to increase the power found at or between the blade passage harmonics. As the number of blades increases, the frequency difference between these harmonics also increases, and so the power is spread over a wider range of frequency. The combined effects of increased interharmonic power and frequency stretching tend to compensate one another, and integration of the power spectral density yields overall acoustic levels which are roughly independent of blade number.

A number of researchers have analyzed the noise of blade tower wake interaction and, with convincing success, matched calculations to noise measurements which are made in the field. It is fair to say that the problem of blade tower wake interaction noise is therefore well understood. Reduction of this kind of noise may be realized by improved aerodynamic tower design, and by a slowing down of the rotor.

The advent of very large windturbines such as MOD-1 and MOD-2 create the need for further study on problems of broadband noise. This is especially true in light of the results from Chapter 2 where broadband noise is found to increase with the ratio of the span to the turbulent scale. Regarding future work on broadband noise, it first seems appropriate to develop an inexpensive method for computing the integrals of equation (2.19). One possible technique is to expand this integral about its point of stationary phase. In any case, once this computation is completed and can handle a wide range of the parameter Λ , the severity of broadband levels may be predicted for a full scale windturbine. Then, if these predictions describe high levels of broadband noise which are encountered in the field, an experimental program of scale model design solutions could be initiated. This model testing would be sophisticated. It would have to simulate both the ratio of the span to the turbulent scale, and the ratio of the rotation speed to the free stream convected frequencies of the turbulence.

REFERENCES

1) DOE Energy Information Report to Congress, Third Quarter, Dec. 1981.

2) Gutin, L.Y., On the Sound Field of a Rotating Propeller, NACA TM 1195, 1948.

3) Homicz, G.F. and George, A.R., Broadband and Discrete Frequency Radiation from Subsonic Rotors, J. of Sound and Vibration, Vol 36, 1974, pp. 151-177.

4) Ffowcs Williams, J.E. and Hawkings, D.L., Theory Relating to the Noise of Rotating Machinery, J. of Sound and Vibration, Vol. 10, 1969, pp.10-21.

5) Morfey, C.L, and Tanna, H.K., Sound Radiated from a Point Force in Circular Motion, J. of Sound and Vibration, Vol. 15, 1971, pp. 325-351.

6) Amiet, R.K., Acoustic Radiation From an Airfoil in a Turbulent Stream, J. of Sound and Vibration, Vol. 41, No. 4, 1975, pp. 407-420.

7) Amiet, R.K., Noise Produced by Turbulent Flow into a Propeller or Helicopter Rotor, AIAA paper 76-560, 1976.

8) Sears, W.R., Some Aspects of Non Stationary Airfoil Theory and its Practical Application, J. Aero. Sci. Vol. 8, No. 3, 1941.

9) Martinez, R., Widnall, S.E., and Harris, W.L., Prediction of Low Frequency and Inpulsive Sound Radiation From Horizontal Axis Windturbines, SERI Report, 1981.

10) Tocci, G.C. and Marcus, E.N., A Parametric Evaluation of Windturbine Noise, Eleventh International Conference on Noise Control Engineering, San Francisco, Ca., 1982.

11) Humbad, N.G., Effect of Tip Geometry on Model Helicopter Rotor Broadband Noise, PhD Thesis, M.I.T., 1981.

12) Viterna, L.A., Method for Predicting Impulsive Noise Generated by Windturbine Rotors, Eleventh International Conference on Noise Control Engineering, San Francisco, Ca., 1982

13) Harris, W.L., Windtunnel Measurements and Predicted Noise from a Downwind Rotor Horizontal Axis Windturbine, Eleventh International Conference of Noise Control, San Francisco, Ca., 1982.

14) Brower, M., Tower Noise in the MOD-1 Windturbine: An Experimental Study, S.B. Thesis, MIT, 1981.

15) Liepmann, H.W., Extension of the Statistical Approach to Buffeting and Gust Response of Wings of Finite Span, J. of Aero. Sci., Vol. 22, pp. 197-200.

16) Houbolt, J.C., Steiner, R., and Pratt, K.G., Dynamic Response of Airplanes to Atmospheric Turbulence Including Flight Data on Input and Response, NASA TR R-199, 1964.

17) Kelley, N.D., Noise Measurements and Wecs, Seri Task 3532.55, 1980.

18) Hubbard, H.H., Shepherd, K.P., and Grosveld, F.W., Broadband Sound From Windturbine Generators, NASA Contractor Report 165810.

19) Hubbard, H.H. and Shepherd, K.P., Sound Measurements and Observations of the MOD-OA Windturbine Generator, NASA Contractor Report 165856.

20) Lipstein, N.J., MOD-1 Windturbine Generator Aeroacoustics, G.E. Company Report, 1980.

21) Stephens, D.G., Shepherd, K.P., Hubbard, H.H., and Grosveld, F.W., Guide to the Evaluation of Human Exposure to Noise from Large Windturbines, NASA Technical Memorandum 83288.

22) Durgin, F.H., An Improved Method for the Design of Windtunnel Velocity Profile Grids, Lincoln Laboratory Technical Note, 1970.

23) Wells, R.J., Prediction of Windturbine Sound with Specific Application to the Proposed MOD - 5A, G.E. Company Report, 1981.

24) Watson, G.N., Theory of Bessel Functions, Cambridge University Press, Cambridge, 1952.

25) Morse, P.M. and Ingard, K.U., Theoretical Acoustics, McGraw-Hill, New York, 1968.

26) Thomson, D.W., Noise Propagation in the Atmosphere's Surface and Planetary Boundary Layers, Eleventh International Conference on Noise Control Engineering, San Francisco, Ca., 1982.

27) Park, C., Effects of Turbulent Wakes on Windturbine Noise, S.M. Thesis, MIT, 1981.

28) Personal Communication, U.S. Windpower Corp., 1982.

29) Sforza, P.M., Sheerin, P., and Smorto, M., Three Dimensional Wakes of Simulated Wind Turbines, AIAA Journal, Vol. 19, No. 9, 1981, pp. 1101-1107.

APPENDIX A

Calculation of $\langle \tilde{W}(K_x,K_y,K_z)\ \tilde{W}^*(K'_x,K'_y,K'_z)\rangle$

Writing the definition of the wavenumber density,

$$\tilde{W}(K_x, K_Y, K_Z) = \frac{1}{(2\pi)^3} \iiint_{-\infty}^{\infty} W(X,Y,Z)\, e^{-i(K_X X + K_Y Y + K_Z Z)}\, dX\, dY\, dZ$$

the ensemble averaged product becomes

$$\langle \tilde{W}(K_X, K_Y, K_Z)\, \tilde{W}^*(K_X', K_Y', K_Z')\rangle = \frac{1}{(2\pi)^6} \iiiint\!\!\iint_{-\infty}^{\infty} dX\, dY\, dZ\, dX'\, dY'\, dZ'$$

$$\langle W(X,Y,Z)\, W(X',Y',Z')\rangle\, e^{i(K_X' X' + K_Y' Y' + K_Z' Z')}\, e^{-i(K_X X + K_Y Y + K_Z Z)}$$

Letting $x' = x - \Delta x$, this integral may be written,

$$\langle \tilde{W}(K_X, K_Y, K_Z)\, \tilde{W}^*(K_X', K_Y', K_Z')\rangle = \frac{1}{(2\pi)^3} \iiint_{-\infty}^{\infty} dX\, dY\, dZ\, e^{i\{(K_X'-K_X)X + (K_Y'-K_Y)Y + (K_Z'-K_Z)Z\}}$$

$$\left[\frac{1}{(2\pi)^3} \iiint_{-\infty}^{\infty} \langle W(X,Y,Z)\, W(X+\Delta X, Y+\Delta Y, Z+\Delta Z)\rangle\, e^{-i(K_X'\Delta X + K_Y'\Delta Y + K_Z'\Delta Z)}\, d\Delta X\, d\Delta Y\, d\Delta Z\right]$$

The quantity in square brackets will be recognized as the Fourier transform of the correlation function R_{ww}. If the turbulence is homogeneous, the correlation function and its Fourier transform are independent of position. The quantity in square brackets then becomes, by definition, the power spectral density $\Phi_{ww}(K_x, K_y, K_z)$ of the turbulence. The ensemble averaged product of the wavenumber distributions can then be written,

$$\langle W(K_x, K_y, K_z)\, W^*(K_x', K_y', K_z') \rangle =$$

$$\Phi_{ww}(K_x', K_y', K_z') \frac{1}{(2\pi)^3} \iiint_{-\infty}^{\infty} e^{i\{(K_x'-K_x)x + (K_y'-K_y)y + (K_z'-K_z)z\}} dx\,dy\,dz$$

$$= \Phi_{ww}(K_x', K_y', K_z')\ \delta(K_x - K_x')\ \delta(K_y - K_y')\ \delta(K_z - K_z')$$

APPENDIX B
Listing of the Computer Programs

BLADE TOWER WAKE INTERACTION NOISE PREDICTION PROGRAM

```
      dimension spl(6Ø),a(2),b(2),theta(2)
      common a,b,c,co,omega,pi,x2,yo,f,psum,m,n,g,theta,span
      open (unit=6,file='cyl.dat',status='new')
c
c     ******************************************************
c
c     WINDTURBINE HARMONIC NOISE PREDICTION PROGRAM
c
c     This program calculates the noise produced by periodic
c     windturbine blade passage through two Gaussian wakes.
c     The first sixty harmonics of the acoustic field are
c     calculated.
c
c     ******************************************************
c
c     If one wishes to do the calculation for a single wake
c     instead of two wakes, then, when the user is prompted
c     for the dimensions of the second wake,simply enter
c     a(2)=Ø, b(2)=Ø, theta(2)=Ø .
c
c     ******************************************************
c
c     Program written by James Wang and Edward Marcus in the
c     spring of 1982. Thesis supervisor is Prof. Wesley Harris.
c
c     ******************************************************
c
c     This work is supported by the Solar Energy Research Inst.
c
c     ******************************************************
c
c     define variables   units(meters,kg,sec)
c
c     variable                    description
c
c     a                      wake depth (nondimensional)
c     b                      wake width
c     c                      blade chord
c     co                     sound speed
c     omega                  rotation speed
c     pi                     3.1416
c     row                    air density
c     U                      free stream
c     x2                     observer / blade distance
```

```
c       yo                      observer to hub height
c       m                       number of blades
c       span                    rotor span
c       theta                   angular position of the wake
c
c
c
        data c/.Ø53/,co/344.Ø/,pi/3.1416/,row/1.29/,span/.6/
c
c      ********************************************************
c       This segment of the program prompts the user for input
c
        print*,' please enter the number of blades.'
        read(5,*)m
        m = float(m)
        print*,' enter the free stream velocity (m/s)'
        read(5,*)u
        print*,' enter the rotation speed (rad/s)'
        read(5,*)omega
        print*,' enter observer/rotor plane distance (meters)'
        read(5,*)x2
        print*,' enter observer distance below the hub (meters)'
        read(5,*)yo
        print*,' enter wake depth a(1)'
        read(5,*)a(1)
        print*,' enter wake width b(1) (meters)'
        read(5,*)b(1)
        print*,' enter wake angle theta(1) (radians)'
        read(5,*)theta(1)
        print*,' enter second wake depth a(2)'
        read(5,*)a(2)
        print*,' enter  second wake width b(2) (meters)'
        read(5,*)b(2)
        print*,' enter second wake angle theta(2) (radians)'
        read(5,*)theta(2)
c
        write(6,2Ø) m,u,omega,x2,yo,a(1),b(1),theta(1),
      1 a(2),b(2),theta(2)
2Ø      format(1x,'number of blades = ',I2/
      1 1x,'free stream velocity= ',f8.4,' meters/sec'/
      1 1x,'rotation speed =',f1Ø.4,' radians/sec'/
      1 1x,'observers horizontal distance = ',f8.4,' meters'/
      1 1x,'observer height to hub height = ',f8.4,' meters'/
      1 1x,'first wake depth = ',f8.4/
      1 1x,'first wake width = ',f8.4,' meters'/
      1 1x,'first wake angle = ',f8.4,' radians'/
      1 1x,'second wake depth = ',f8.4/
      1 1x,'second wake width = ',f8.4,' meters'/
      1 1x,'second wake angle = ',f8.4,' radians'///
      1 1Øx,'harmonic',1Øx,'spl (dB)'/)
c
```

```
c       ********************************************
        sum =0.0
c
c       Calculate the SPL from the sixty harmonics
c
        do 100 n=1,60
c       Load factor
        g = 2. * ((pi*log(2.))**(.5))
        f = 2.*pi*n*(m**2.)*row*omega*c*U/g
c       go and integrate the phase along the blade
        call blade
        spl(n) = 20. * alog10( psum / .00002 )
        write(6,50)n,spl(n)
  50    format(10x,I2,10x,f10.2)
        sum = 10.**(spl(n)/10.) + sum
        continue
c
c       Find the total sound pressure level
        spltot = 10.*alog10(sum)
        write (6,150) spltot
  150   format (1x,'total SPL',3x, f 6.2,' dB')
        close ( unit = 6)
c
        end
c
c
c      ********************************************
        subroutine blade
        common a,b,c,co,omega,pi,x2,yo,f,psum,m,n,g,theta,span
        dimension a(2),b(2),theta(2)
c
c       Blade Integration
        cosum = 0.0
        sisum = 0.0
        do 150 i = 5,60
c       add the contributions from both wakes
        do 100 k=1,2
        y = float(i) * span/60.0
c
c       Find the Gaussian envelope of this wakes spectrum
        w = a(k) * b(k) *exp( -((n*m*b(k)/(g*y))**2.)*pi)
c
c       Sear's function magnitude
        sig = n*m*c/(2. * abs(y))
        s = ( 1. + ( 2. * pi * sig))**(-.5)
c
c       Sear's function phase lead
        sphase = sig * (1 -(pi*pi/(2. + 4.*pi*sig)))
c
c       Green's function phase lag
        r = ( (x2)**2. + (y - yo)**2.)**(.5)
        gphase =  n * m * omega * r / co
```

```
c
c       Total phase
        phase = sphase - gphase -n*m*theta(k)
c
c       Find the pressure at the observation point
        p = f * s * w * (span/60.) * omega/(4.*pi*co*r)
c
c       Cosine sum
        cosum =  p * (cos(phase) + sin(phase)/gphase)+ cosum
c       Sine sum
        sisum =  p * (sin(phase) - cos(phase)/gphase)+ sisum
c
 100    continue
 150    continue
c
        psum = (.5* ( cosum**2. + sisum**2. ))**(.5)
        return
        end
```

BROADBAND NOISE PREDICTION PROGRAM

```
      dimension spl(100),ifreq(100)
      real   L ,Lambda,kap,kapmax
      open (unit=6,file='turb.dat',status='new')
c
c     ****************************************************
c     Broadband Noise Prediction Program
c
c     This program calculates the broadband noise
c     produced by a windturbine in a turbulent atmosphere.
c     The total observed acoustic intensity is calculated
c     for a frequency window the width of the blade passage
c     frequency. This intensity is then divided by the
c     width of the window (delhz), and a spectral density
c     is then obtained.
c
c     ****************************************************
c
c     The required input into this program includes
c     the mean square axial velocity fluctuations of
c     the atmospheric turbulence. Also required is the
c     integral scale of the turbulence,
c
c     ****************************************************
c
c     The wave number distribution is integrated out
c     to the maximum nondimensional wavenumber kapmax.
c     As the frequency increases, the range of wavenumber
c     integration is slightly focused towards the higher
c     wavenumbers. During previous calculations it was
c     found that low wavenumbers do not contribute
c     to the integration of higher order Bessel functions.
c
c     ****************************************************
c
c     Program written by Edward N. Marcus in the Summer
c     of 1982. Thesis supervisor is Prof. Wesley Harris.
c
c     ****************************************************
c
c     This work is supported by the Solar Energy Research Inst.
c
c     *****************************************************
c
c     define variables   units(meters,kg,sec)
c
c     variable                 description
c
c     abw              bandwidth of the acoustic spectrum
c     c                blade chord
c     co               sound speed
```

```
c       delhz           BPF (spectral resolution)
c       omega           rotation speed
c       phi             wavenumber probability distribution
c       pi              3.1416
c       row             air density
c       U               free stream
c       b               number of blades
c       span            rotor span
c       r               radial position/span
c       dis             far field observation distance
c       wrms            rms longitudinal velocity fluctuations
c       L               integral scale of the turbulence
c       Lambda          span/L
c       Kap             transverse wavenumber nondimensionalized
c                         by the integral scale
c       Kapmax          upper limit of the wavenumber integration
c
        data c/.Ø53/,co/344.Ø/,pi/3.1416/,row/1.29/,span/.6/
     1 ,U/1Ø.Ø6/,abw/32ØØ./,b/2./,dis/1.5/
c
c     ********************************************************
c       This segment of the program prompts the user for input
c
        print*,' enter the rotation speed (rad/sec)'
        read(5,*)omega
        print*,'enter wrms (meters/sec)'
        read(5,*)wrms
        print*,'enter the integral turbulent scale (meters)'
        read(5,*) L
c
c       calculate the maximum harmonic
        mmax = abw *2.Ø * pi / (b * omega)
c       calculate the frequency resolution of the spectrum
        delhz  = b*omega/(2.Ø * pi)
c       calculate the ratio of span to turbulent scale
        lambda = span / L
c
        write(6,2Ø) b,U,omega,dis,wrms,L
2Ø      format(1x,'number of blades = ',f8.4/
     1 1x,'free stream velocity= ',f8.4,' meters/sec'/
     1 1x,'rotation speed =',f1Ø.4,' hZ'/
     1 1x,'observers  distance = ',f8.4,' meters'/
     1 1x,'wrms = ',f8.4,' meters/sec'/
     1 1x,'integral scale = ',f8.4,' meters'///
     1 1Øx,'frequency (hz)',1Øx,'spl/hz (dB)'/)
c
c     ********************************************************
c
c       CALCULATE THE CHARACTERISTIC PRESSURE INTENSITY
        p = (row*c*b*b*omega*omega*span*span*wrms/(co * dis))**2
c
c       SET THE WAVENUMBER INCREMENT
```

```
      delkap = b/lambda
c
c     UPPER LIMIT OF WAVENUMBER INTEGRATION
      kapmax = (float(mmax) + 10) * delkap
c
c     SET THE ACCURACY OF THE BESSEL FUNCTION CALCULATION
      d    = .0001
c
c     START ITERATING THROUGH THE HARMONICS(geometrically)
      do 300 k = 0,mmax
      m      = 2**k
      if (m .ge. mmax) m = mmax
      mb     = m * b
      nmax   = (mmax + 10) - m/2 - 1
      sum    = 0.0
c
c     INTEGRATE THE WAVENUMBER DISTRIBUTION
      do 200 n = 0,nmax
      kap  =  kapmax -  (float(n) * delkap)
      phi  = (kap**3)/((1.0 + kap**2)**2.5)
      delr = delkap/kap
      if ( delr .gt. .2) delr = 1.0/5.0
      imax = int(1.0/delr)
      imin = imax/2
      bsum = 0.0
c
c     INTEGRATE ALONG THE SPAN (outer half)
      do 100 i = imin,imax
      r    = float(i) * delr
      x    = kap * lambda * r
      call besj ( x,mb,BJ,d,ier)
      bsum = (bj * r * delr )  + bsum
100   continue
c
      sum =  (bsum * bsum * phi * delkap) + sum
200   continue
c
c     SEAR'S FUNCTION CORRECTION (75% span)
      sig      = m * b * c / (2.0 * .75 * span)
      sears    = 1.0 / (1.0 + (2.0 * pi * sig))
c
      psqr     = p * sum *m * m * 3.0/32.0 * sears
      ifreq(m) = int(m * delhz)
      spl (m)  = 20.0 * alog10 ( sqrt(psqr/delhz)/.00002 )
      write(6,250) ifreq(m),spl(m)
250   format(10x,I4,10x,f10.2)
      if ( m .ge. mmax ) go to 400
300   continue
400   end
```

APPENDIX C

Catalog of the Acoustic Data

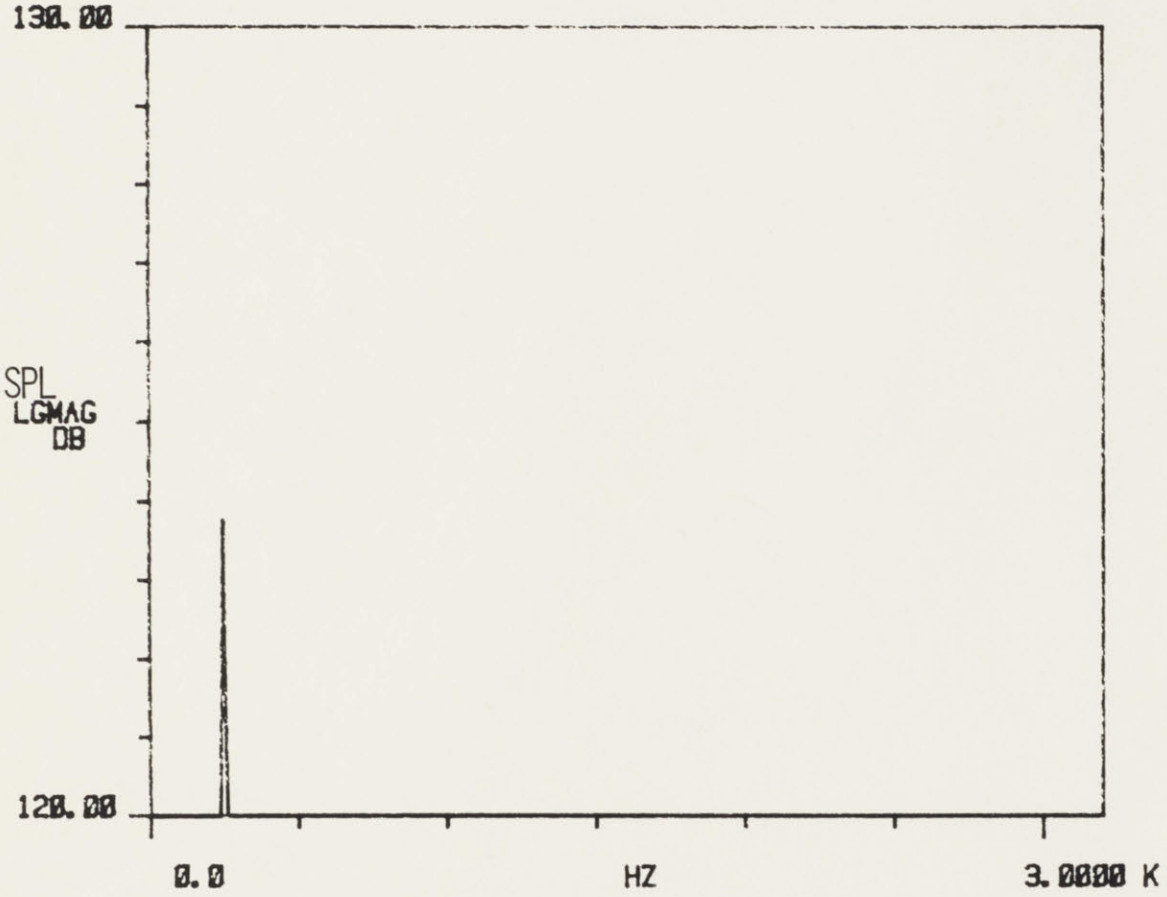

Fig C.1 124 Decibel Caltone , 250 Hz

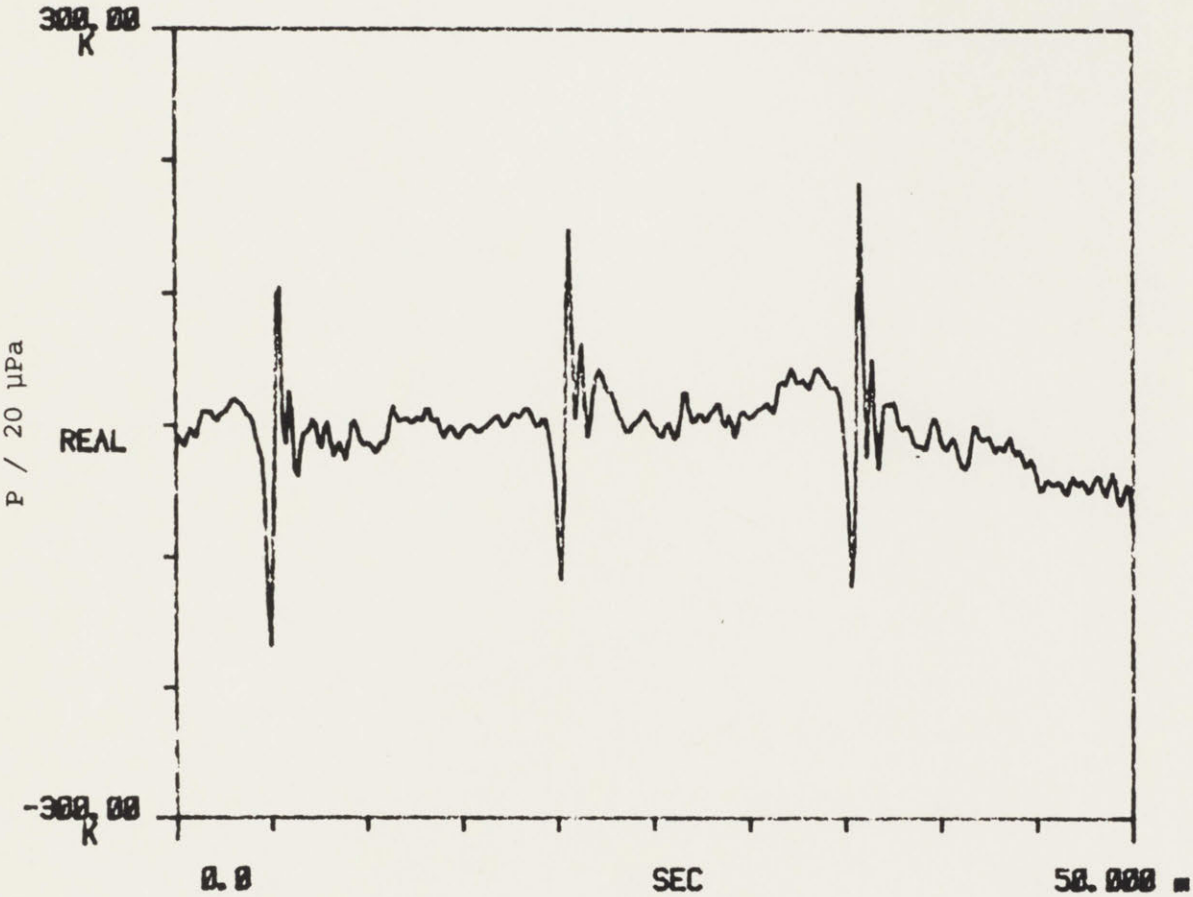

Fig C.2 Acoustic Signature for Blade Passage Through the Wake of a 5/8" Cylinder

Tower Wake Test

Tape 2 Counter 823

2 blades 520 RPM

U = 15 MPH

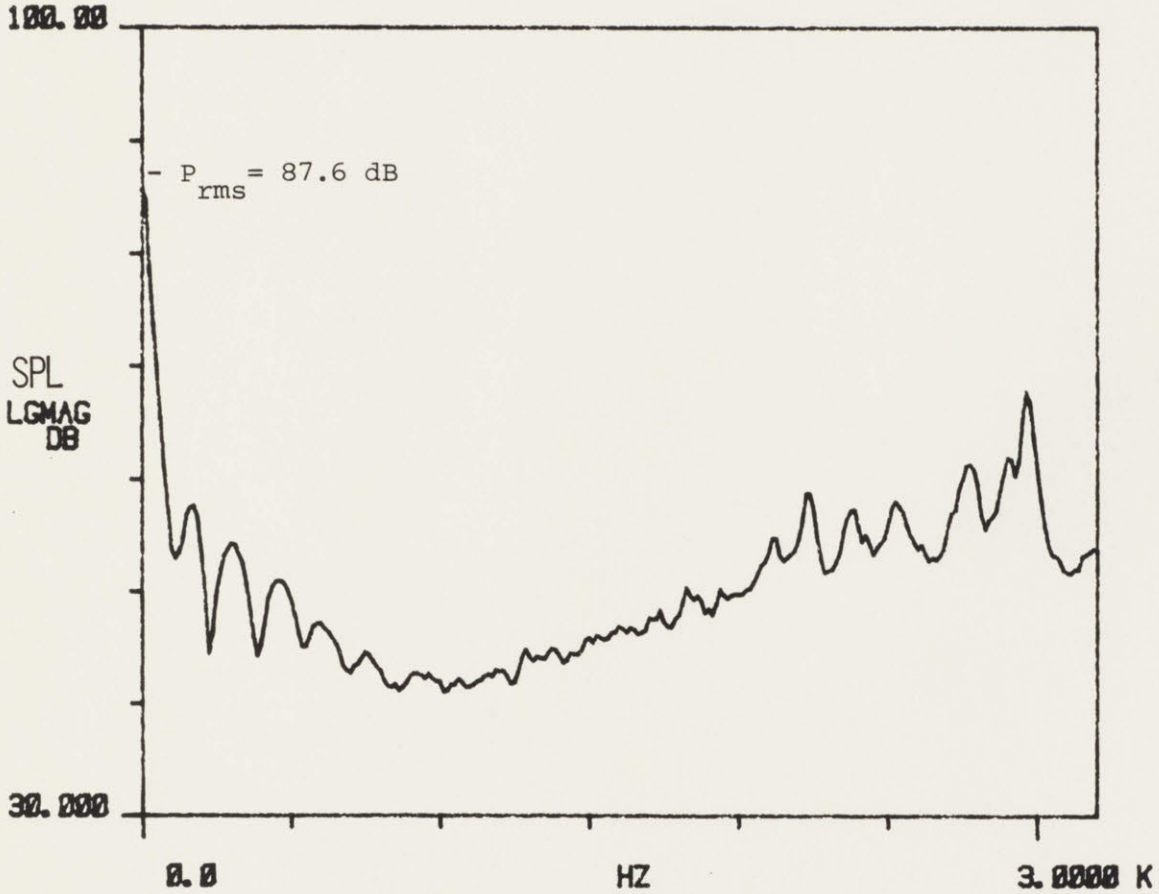

Fig C.3 On Axis Microphone From Tower Wake Test

Tower Wake Test

Tape 2 Counter 823

2 blades 520 RPM

U = 15 MPH

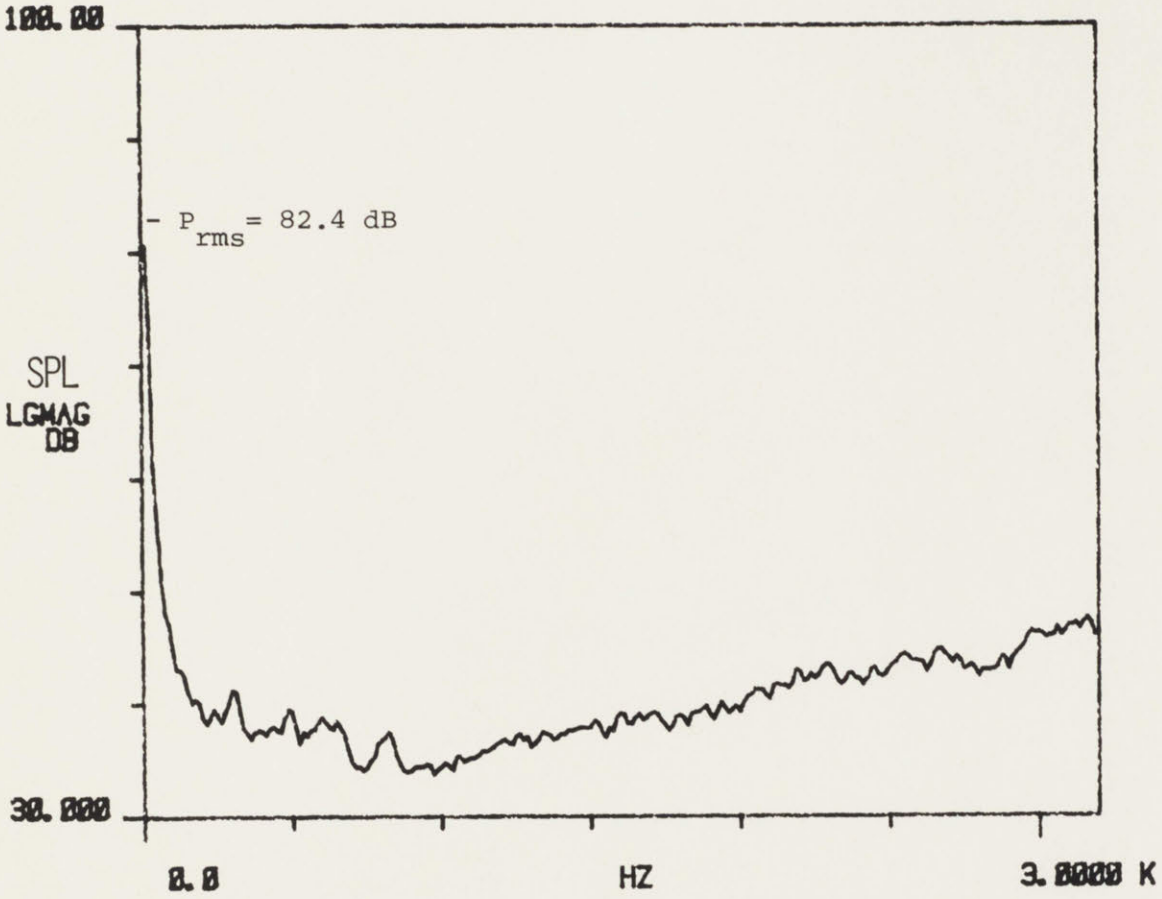

Fig C.4 Off Axis Microphone From Tower Wake Test

Tower Wake Test

Tape 2 Counter 1031

2 blades 710 RPM

U = 20 MPH

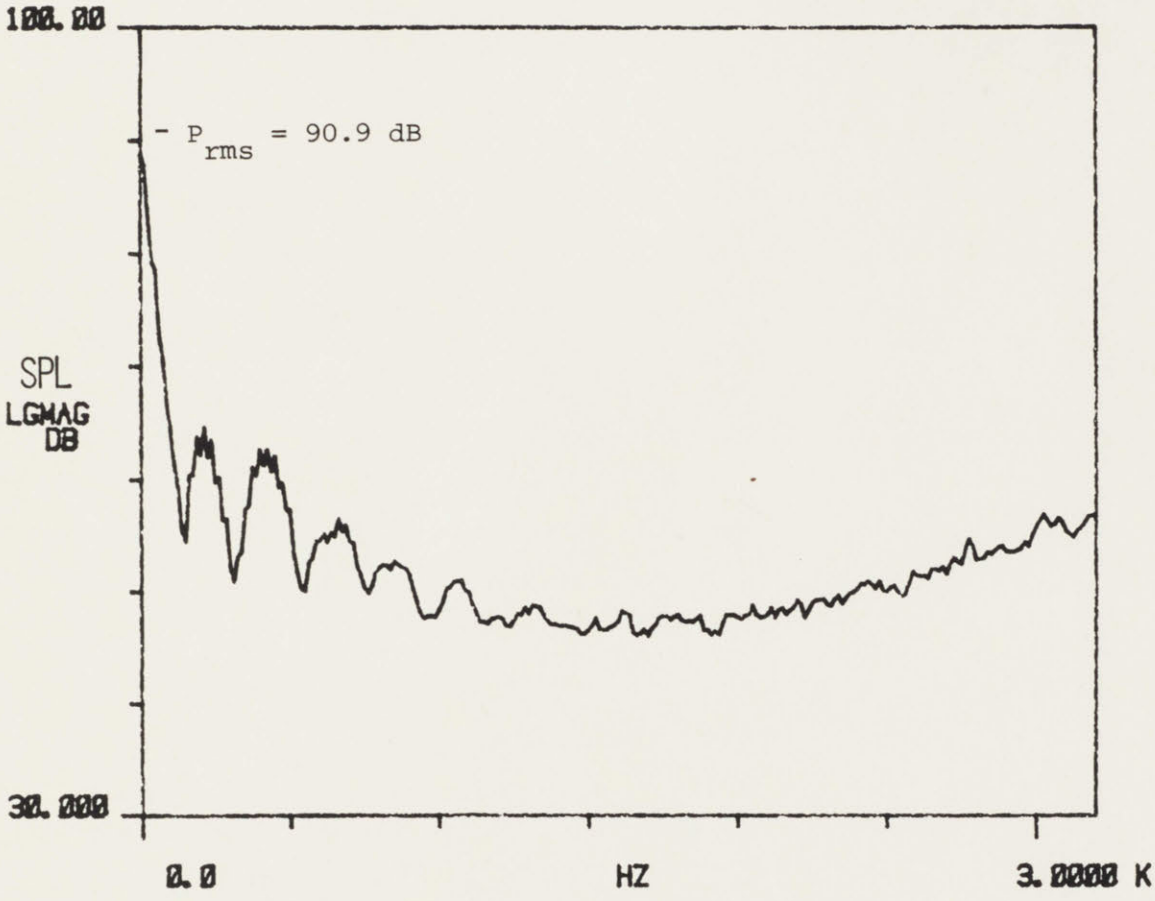

Fig. C.5 On Axis Microphone From Tower Wake Test

Tower Wake Test

Tape 2 Counter 1031

2 blades 710 RPM

U = 20 MPH

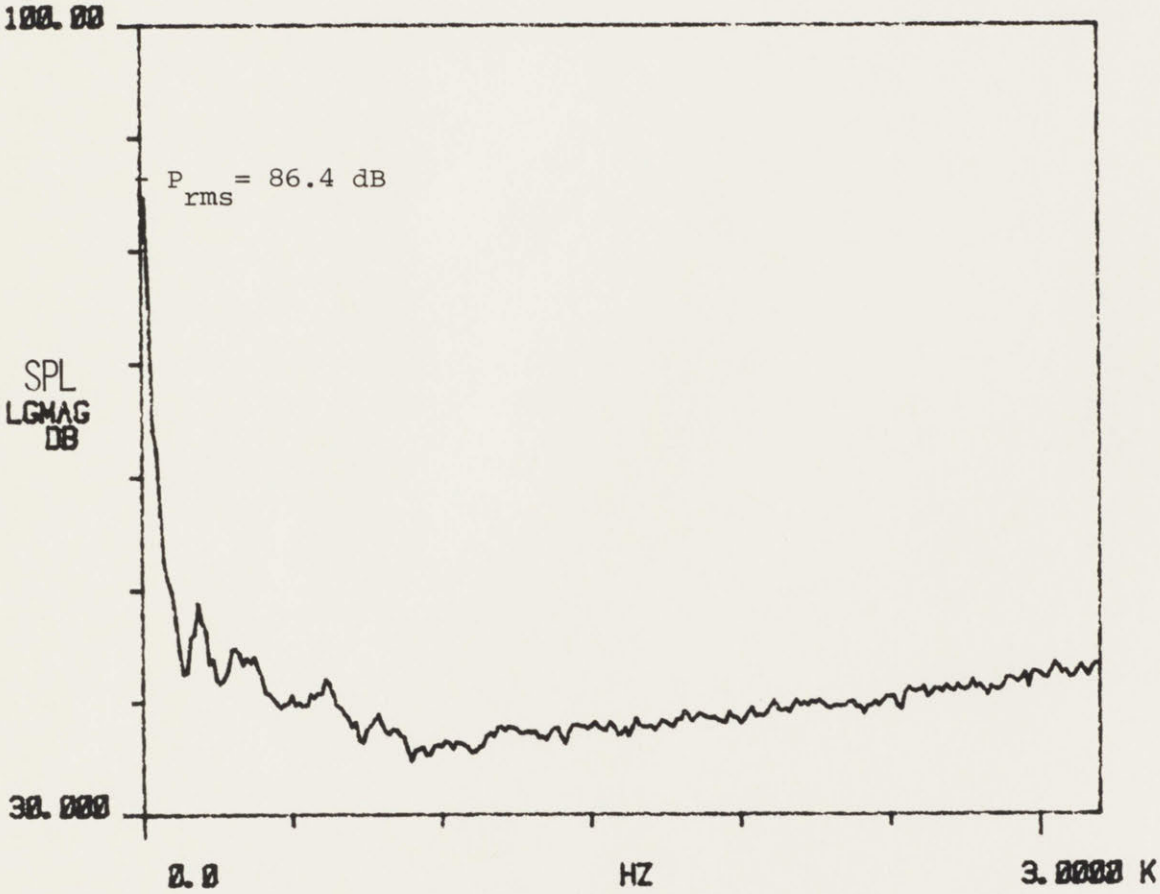

Fig. C.6 Off Axis Microphone From Tower Wake Test

Tower Wake Test

Tape 2 Counter 194

2 blades 760 RPM

U = 15 MPH

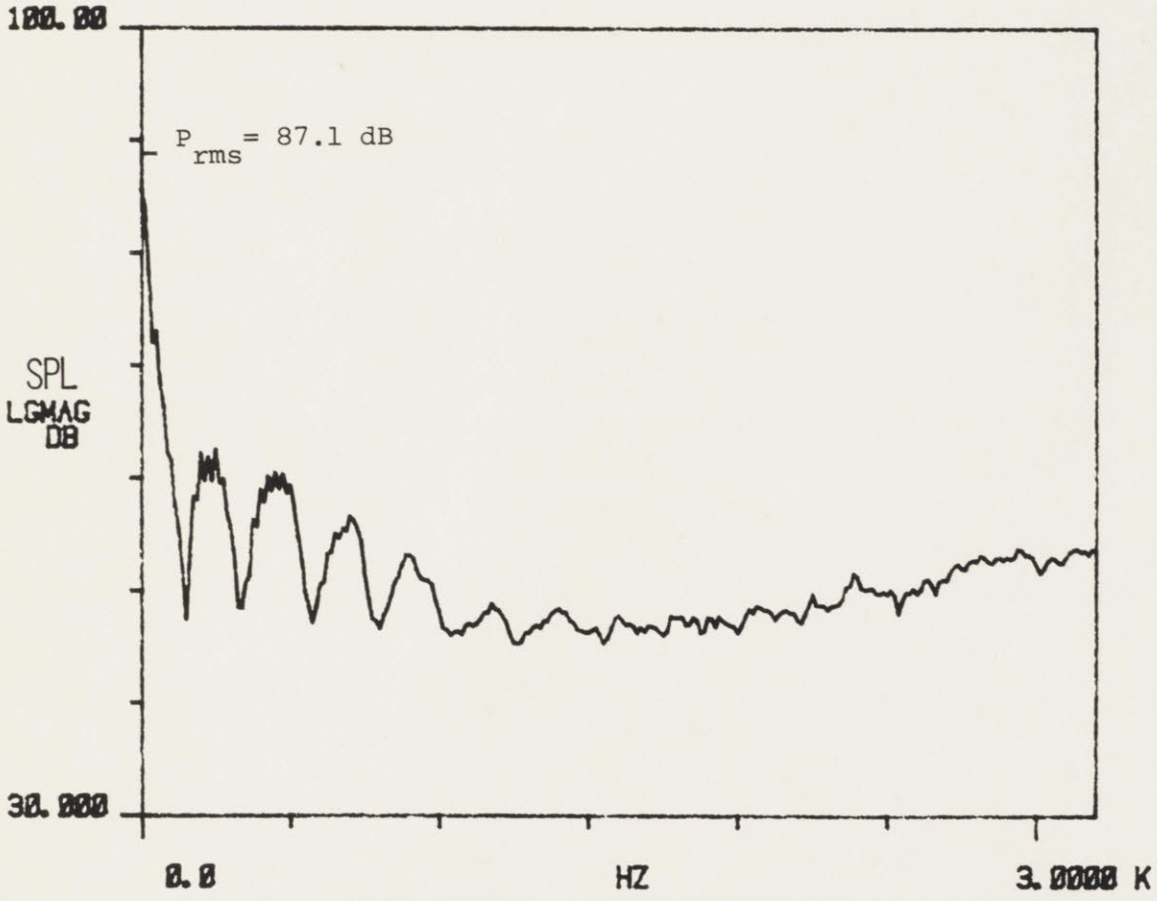

Fig C.7 On Axis Microphone From Tower Wake Test

Tower Wake Test

Tape 2 Counter 194

2 blades 760 RPM

U = 15 MPH

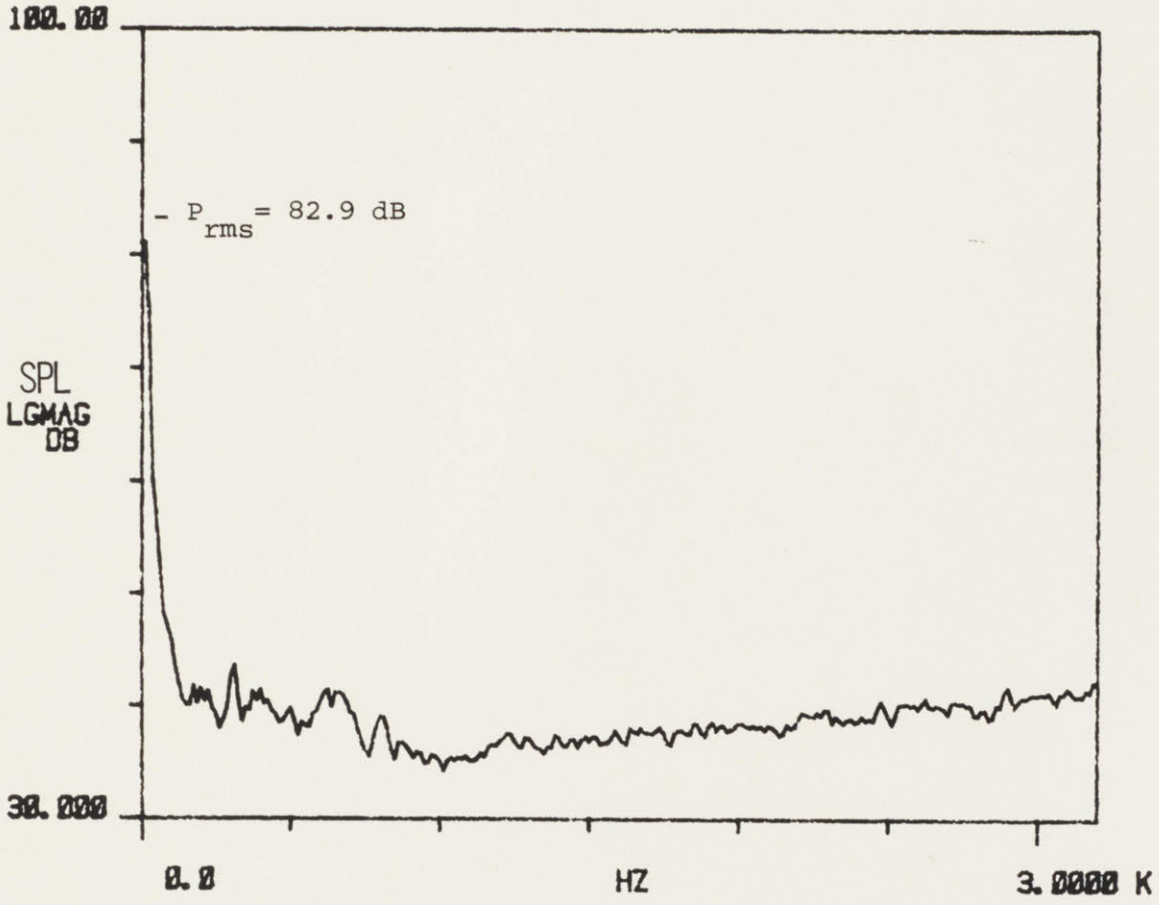

Fig C.8 Off Axis Microphone From Tower Wake Test

Tower Wake Test

Tape 2 Counter 1241

2 blades 810 RPM

U = 22.5 MPH

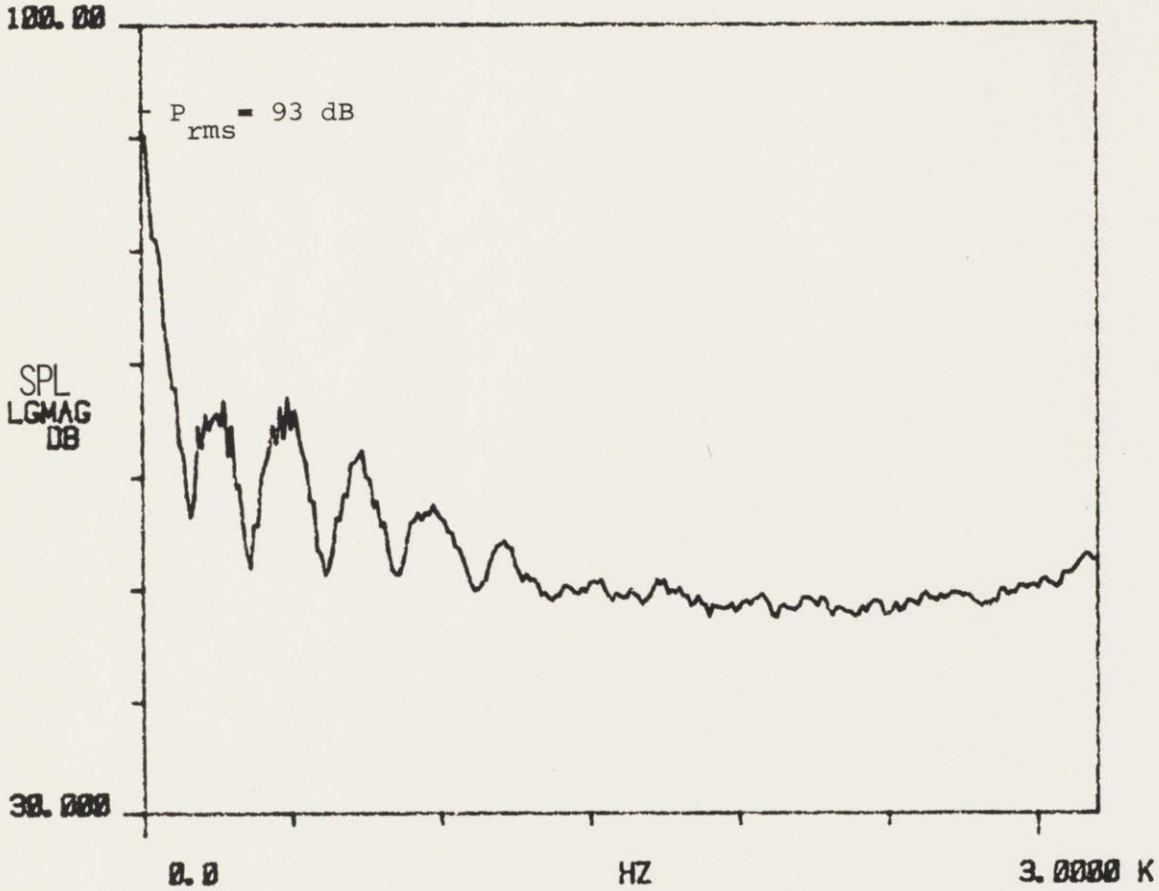

Fig C.9 On Axis Microphone From Tower Wake Test

Tower Wake Test

Tape 2 Counter 1241

2 blades 810 RPM

U = 22.5 MPH

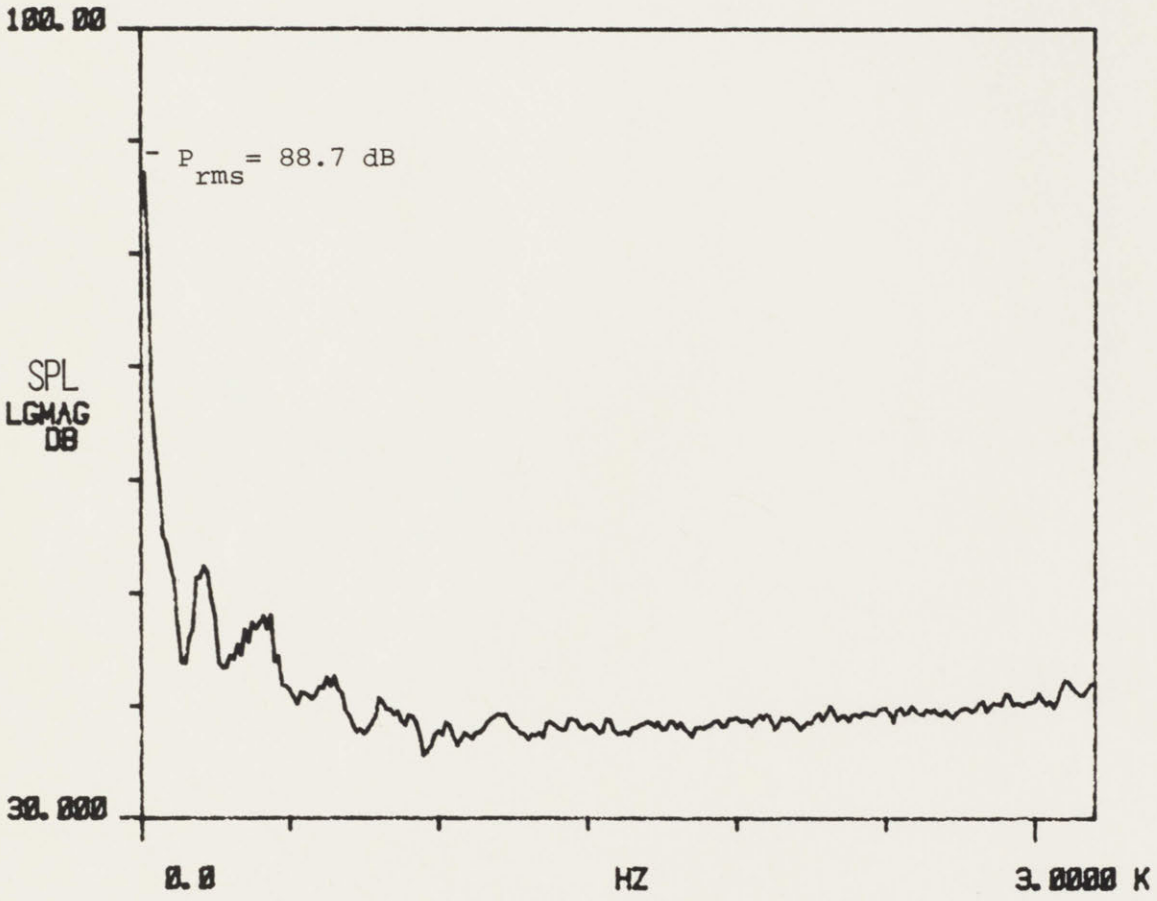

Fig C.10 Off Axis Microphone From Tower Wake Test

Tower Wake Test

Tape 2 Counter 403

2 blades 1020 RPM

U = 20 MPH

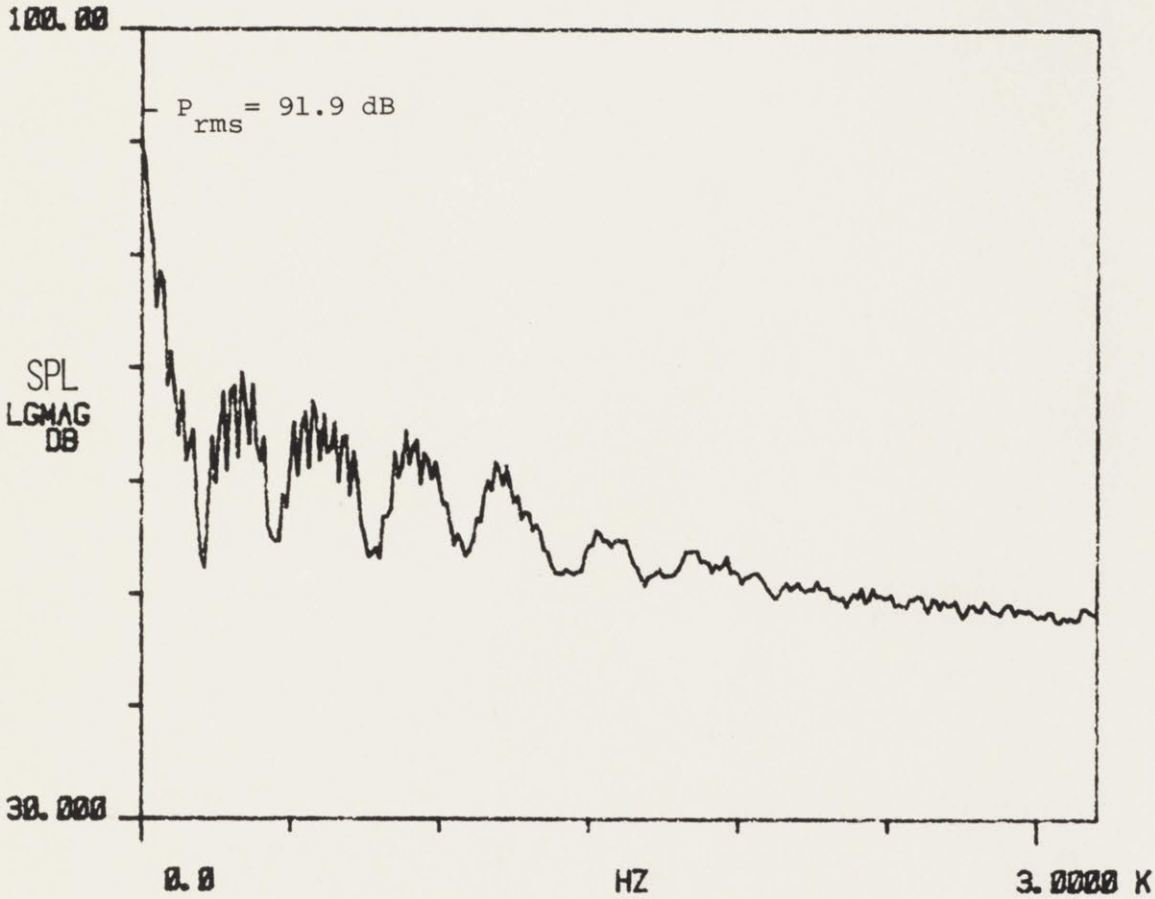

Fig C.11 On Axis Microphone From Tower Wake Test

Tower Wake Test

Tape 2 Counter 403

2 blades 1020 RPM

U = 20 MPH

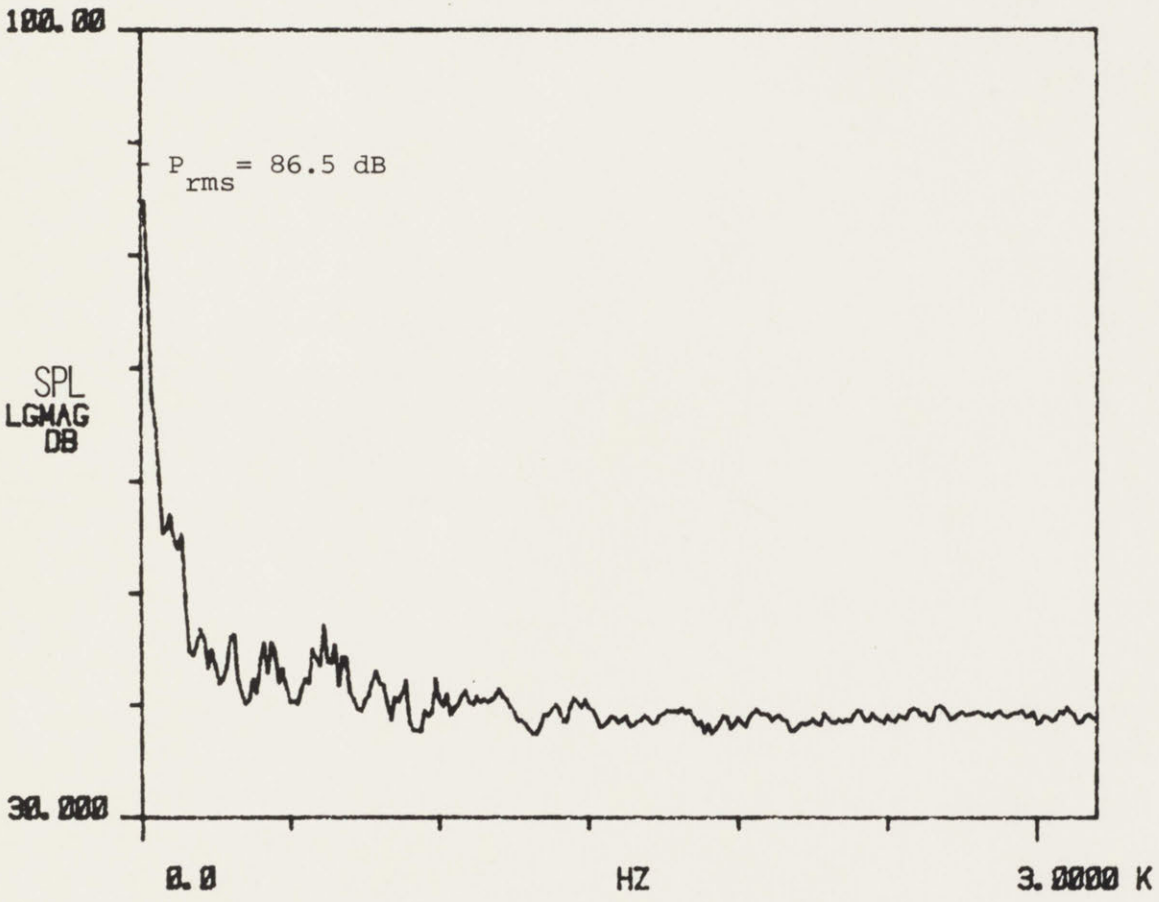

Fig C.12 Off Axis Microphone From Tower Wake Test

Tower Wake Test

Tape 1 Counter 170

2 blades 1110 RPM

U = 15 MPH

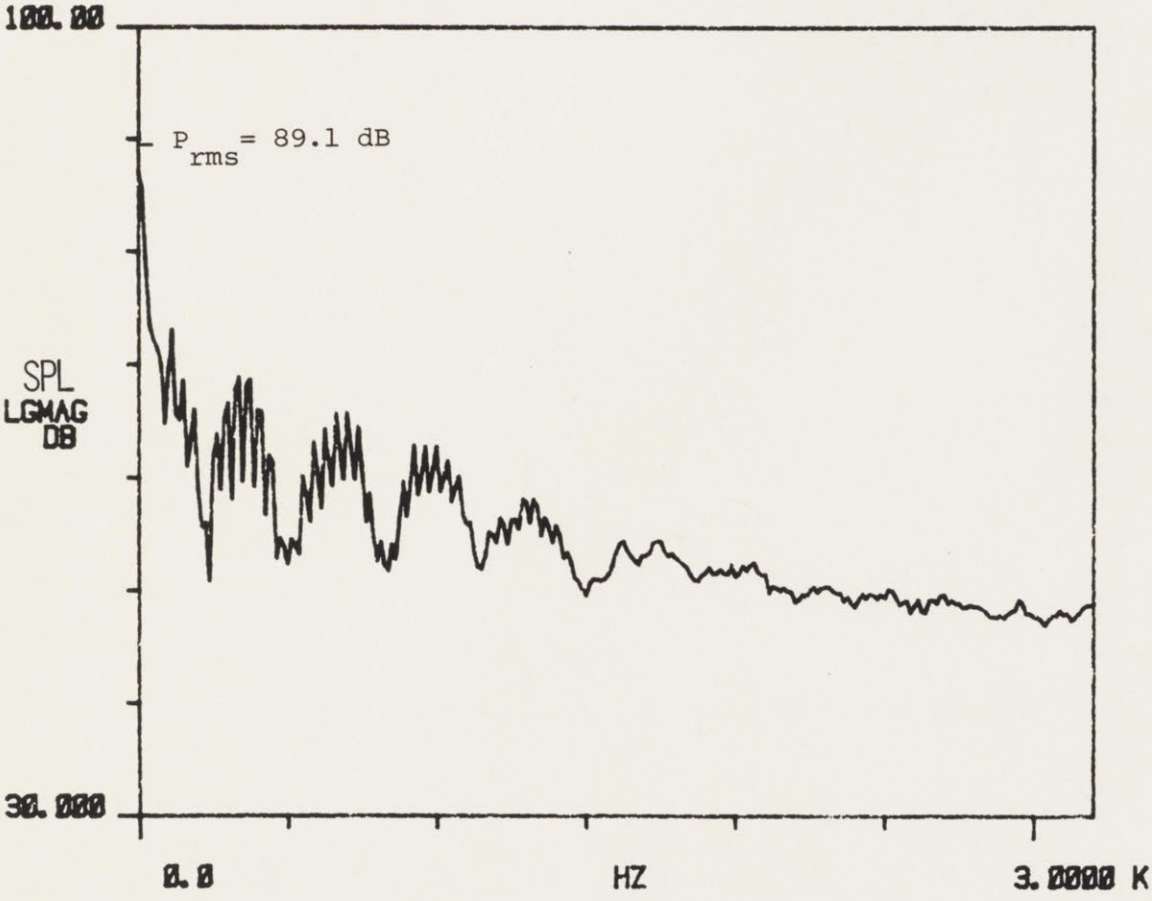

Fig C.13 On Axis Microphone From Tower Wake Test

Tower Wake Test

Tape 1 Counter 170

2 blades 1110 RPM

U = 15 MPH

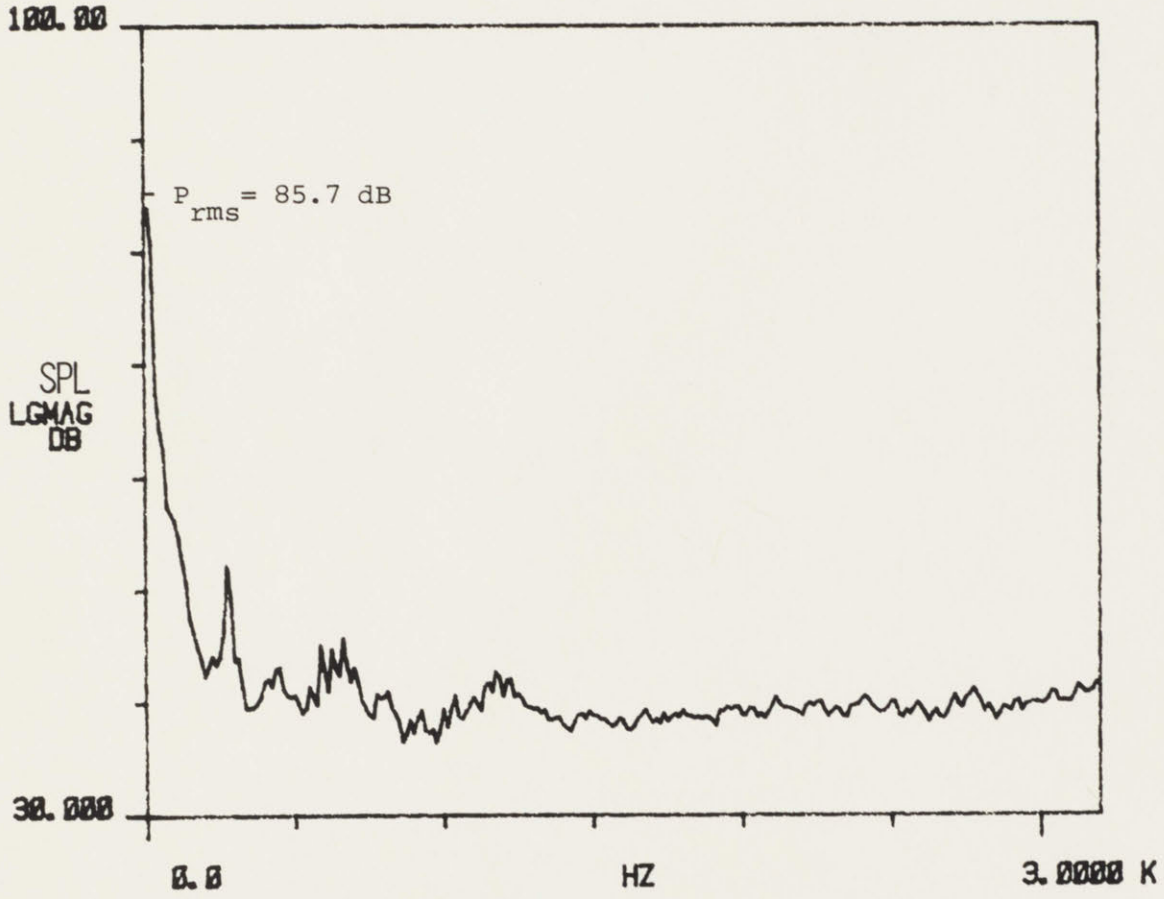

Fig C.14 Off Axis Microphone From Tower Wake Test

Tower Wake Test

Tape 2 Counter 614

2 blades 1160 RPM

U = 22.5 MPH

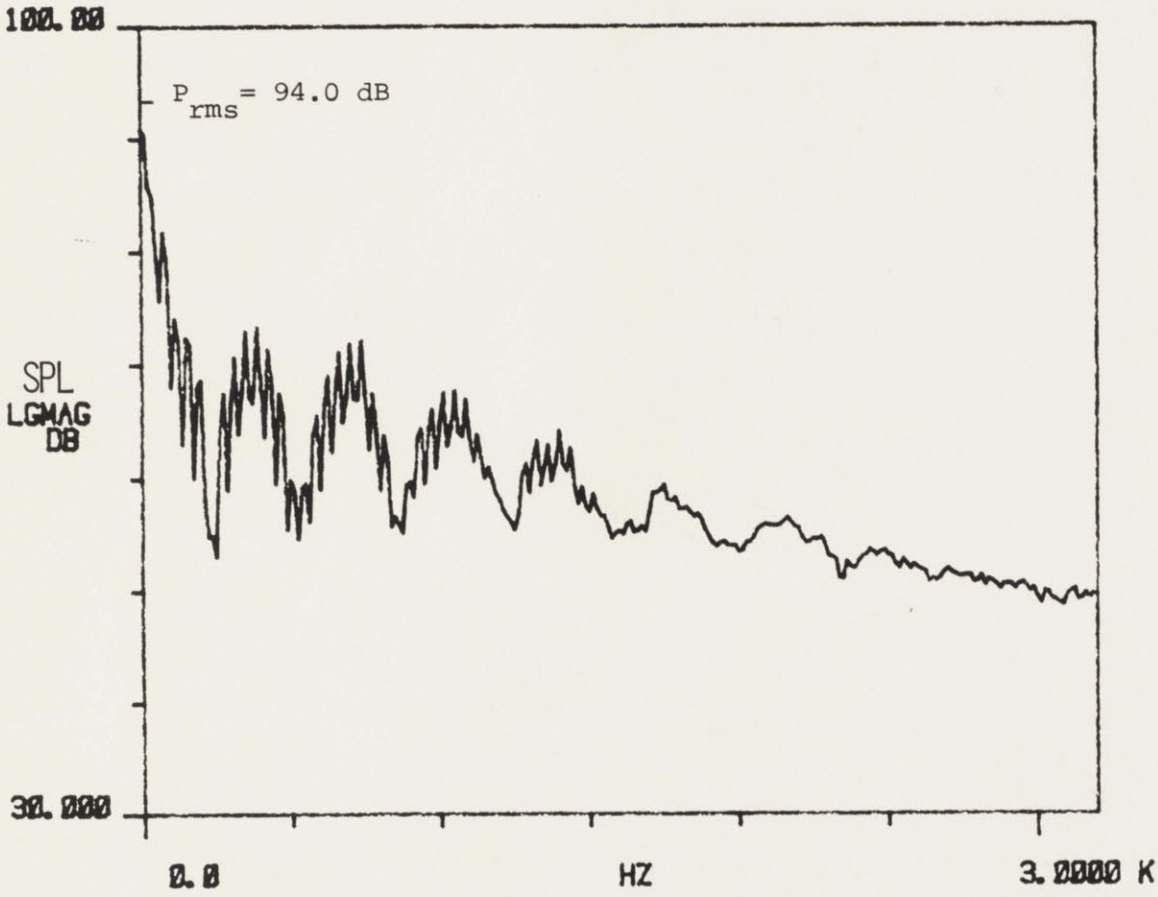

Fig C.15 On Axis Microphone From Tower Wake Test

Tower Wake Test

Tape 2 Counter 614

2 blades 1160 RPM

U = 22.5 MPH

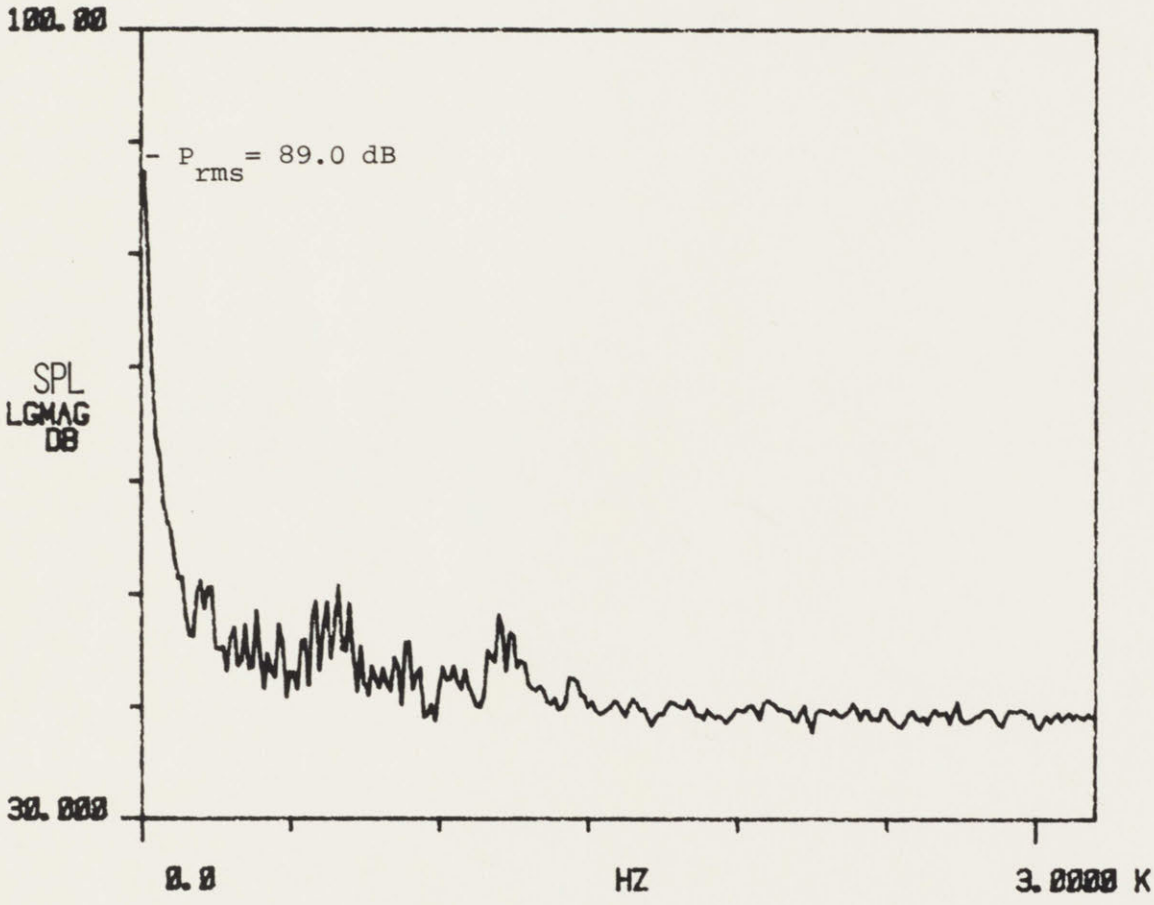

Fig C.16 Off Axis Microphone From Tower Wake Test

Tower Wake Test

Tape 1 Counter 924

2 blades 1520 RPM

U = 20 MPH

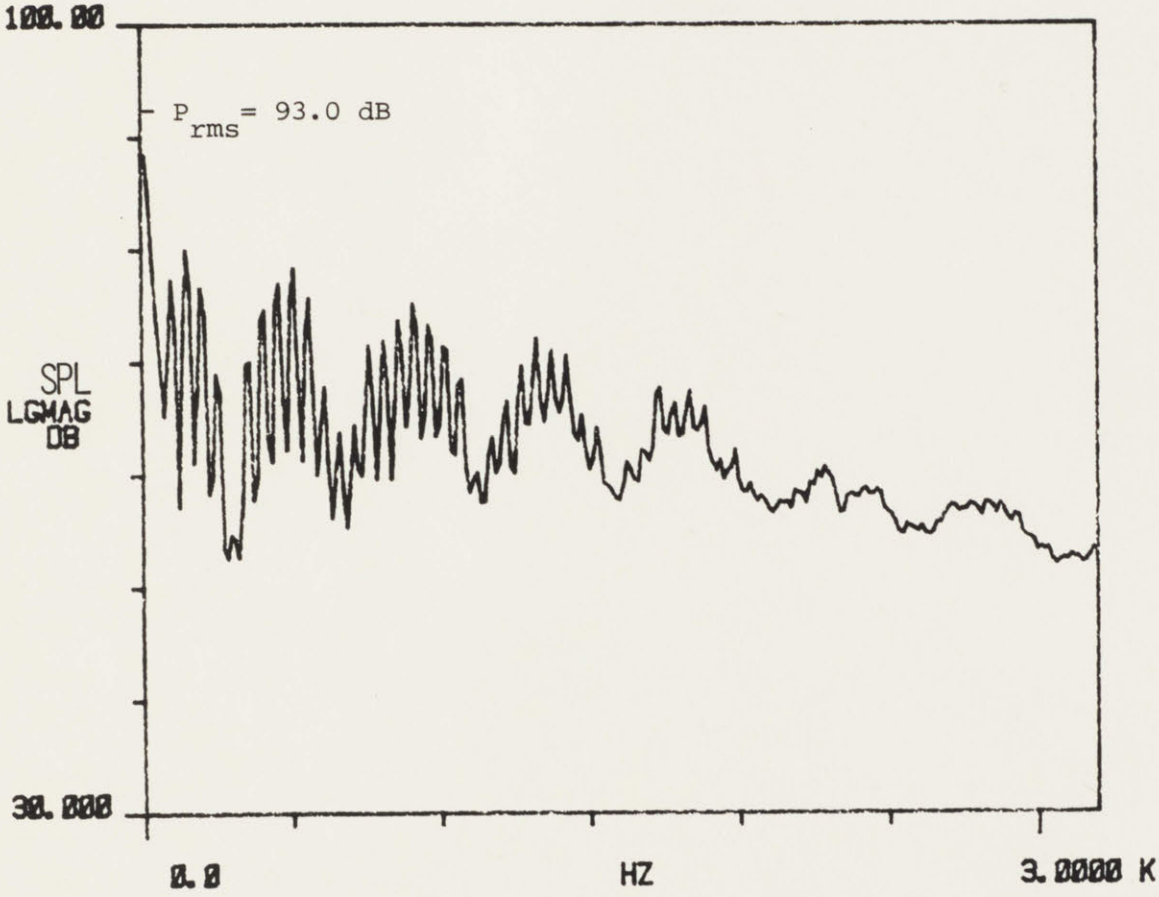

Fig C.17 On Axis Microphone From Tower Wake Test

Tower Wake Test

Tape 1 Counter 924

2 blades 1520 RPM

U = 20 MPH

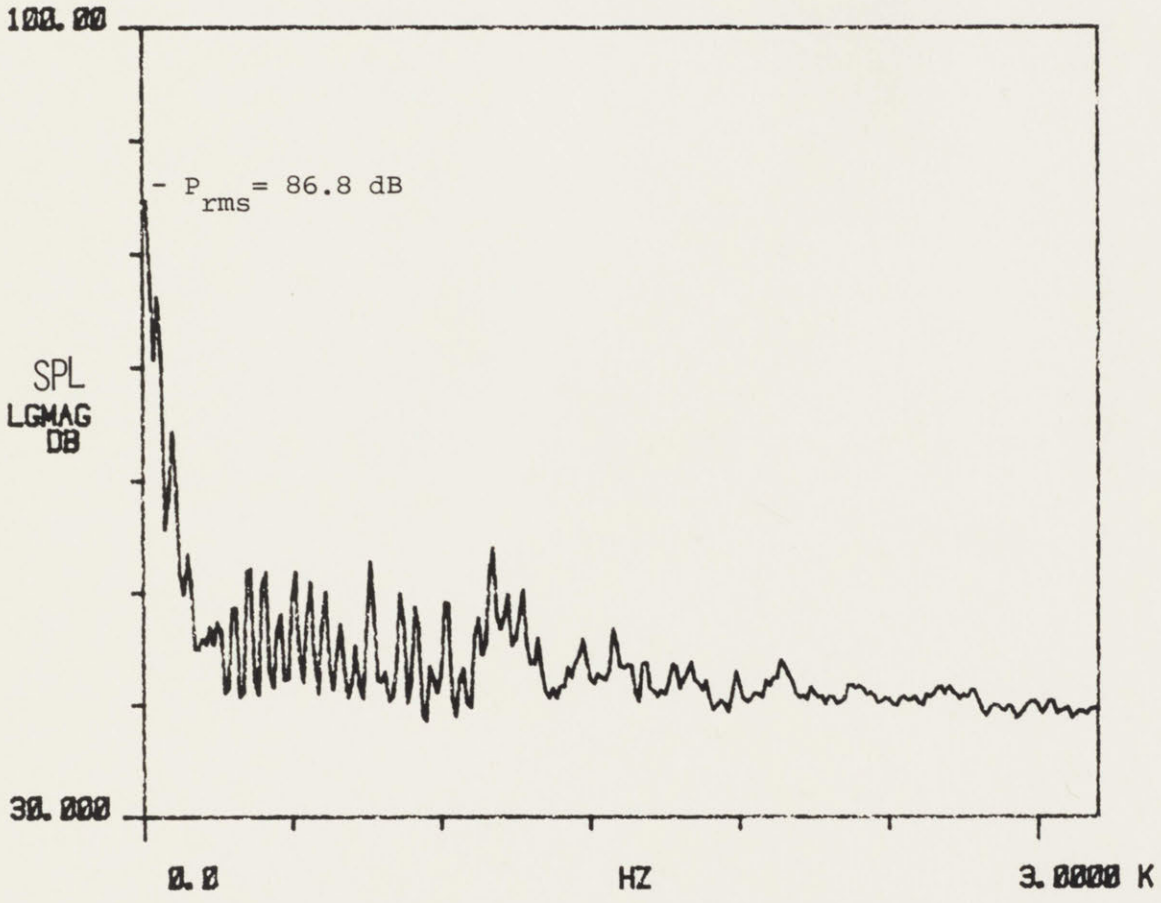

Fig C.18 Off Axis Microphone From Tower Wake Test

Tower Wake Test

Tape 1 Counter 1141

2 blades 1670 RPM

U = 15 MPH

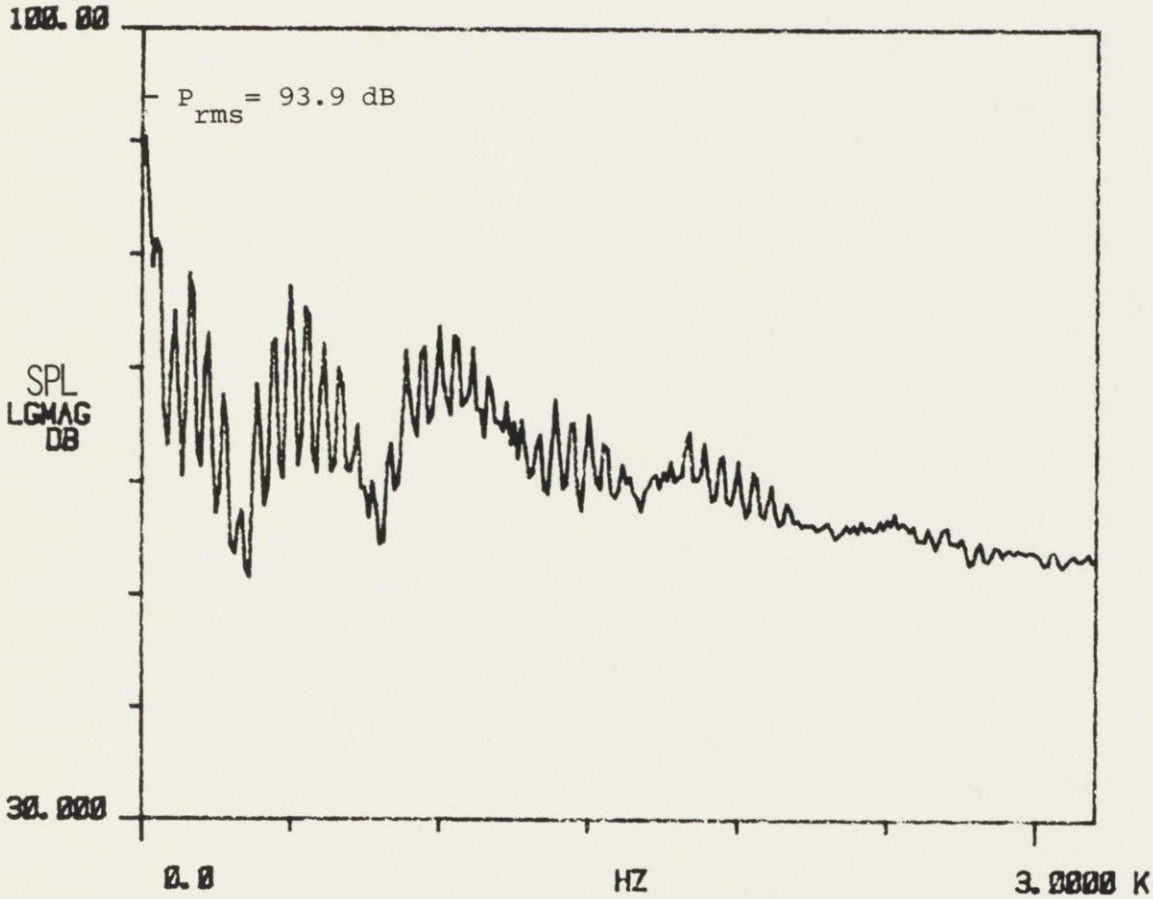

Fig C.19 On Axis Microphone From Tower Wake Test

Tower Wake Test

Tape 1 Counter 1141

2 blades 1670 RPM

U = 15 MPH

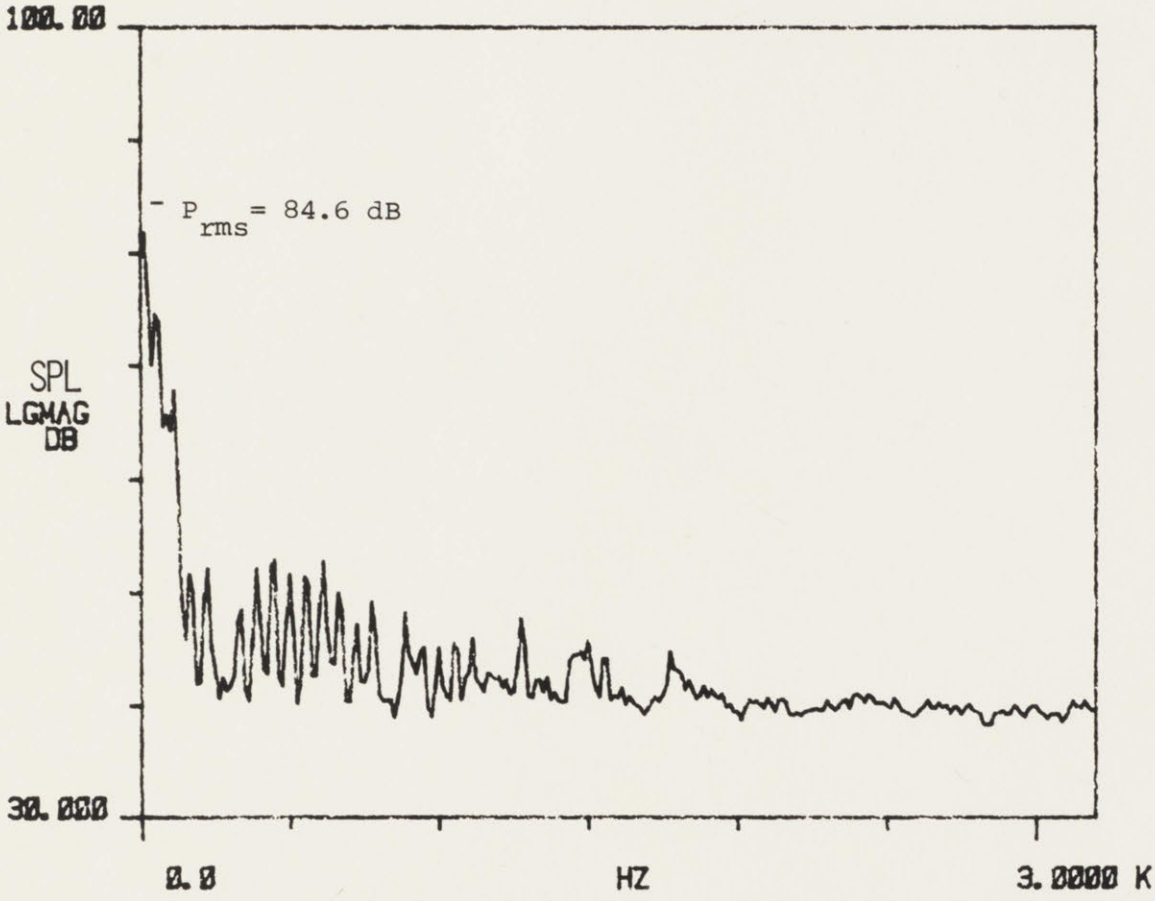

Fig C.20 Off Axis Microphone From Tower Wake Test

Tower Wake Test

Tape 1 Counter 379

2 blades 1710 RPM

U = 22.5 MPH

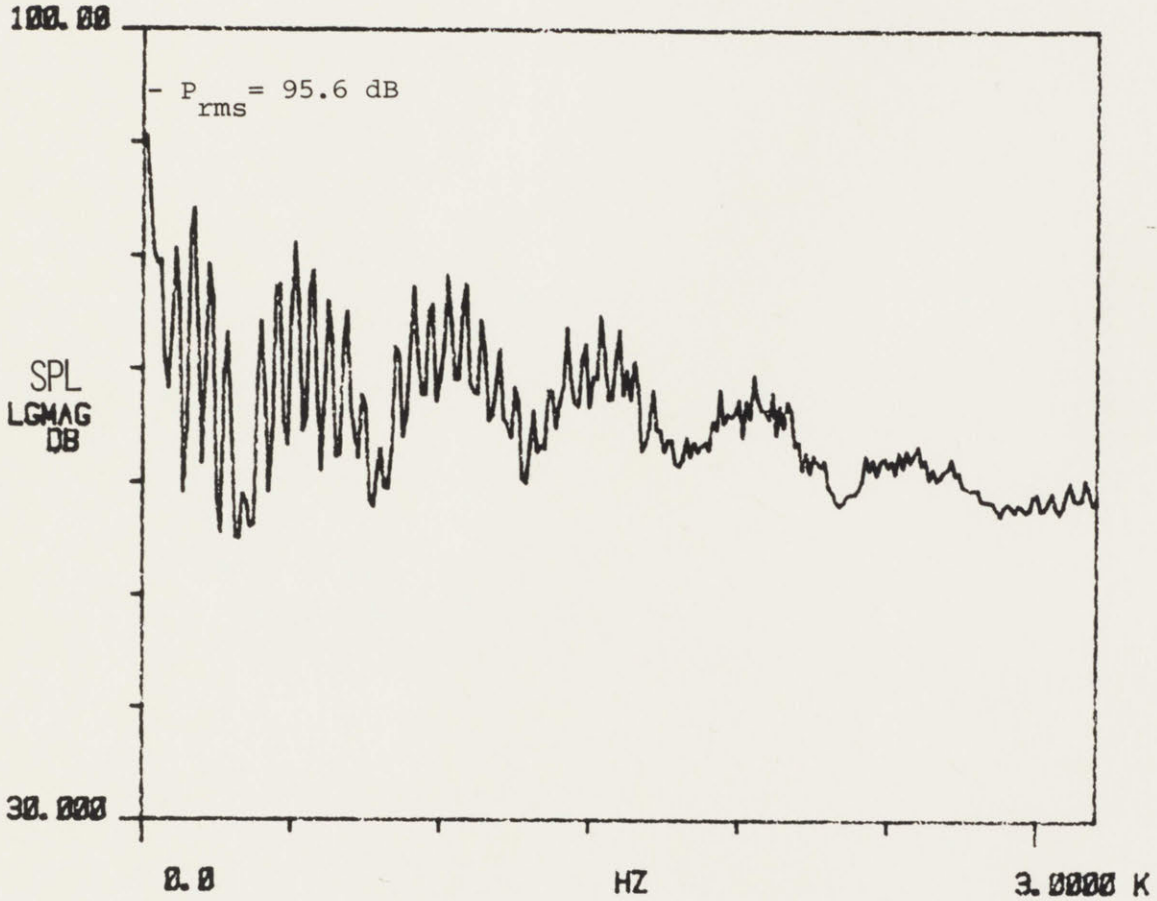

Fig C.21 On Axis Microphone From Tower Wake Test

Tower Wake Test

Tape 1 Counter 379

2 blades 1710 RPM

U = 22.5 MPH

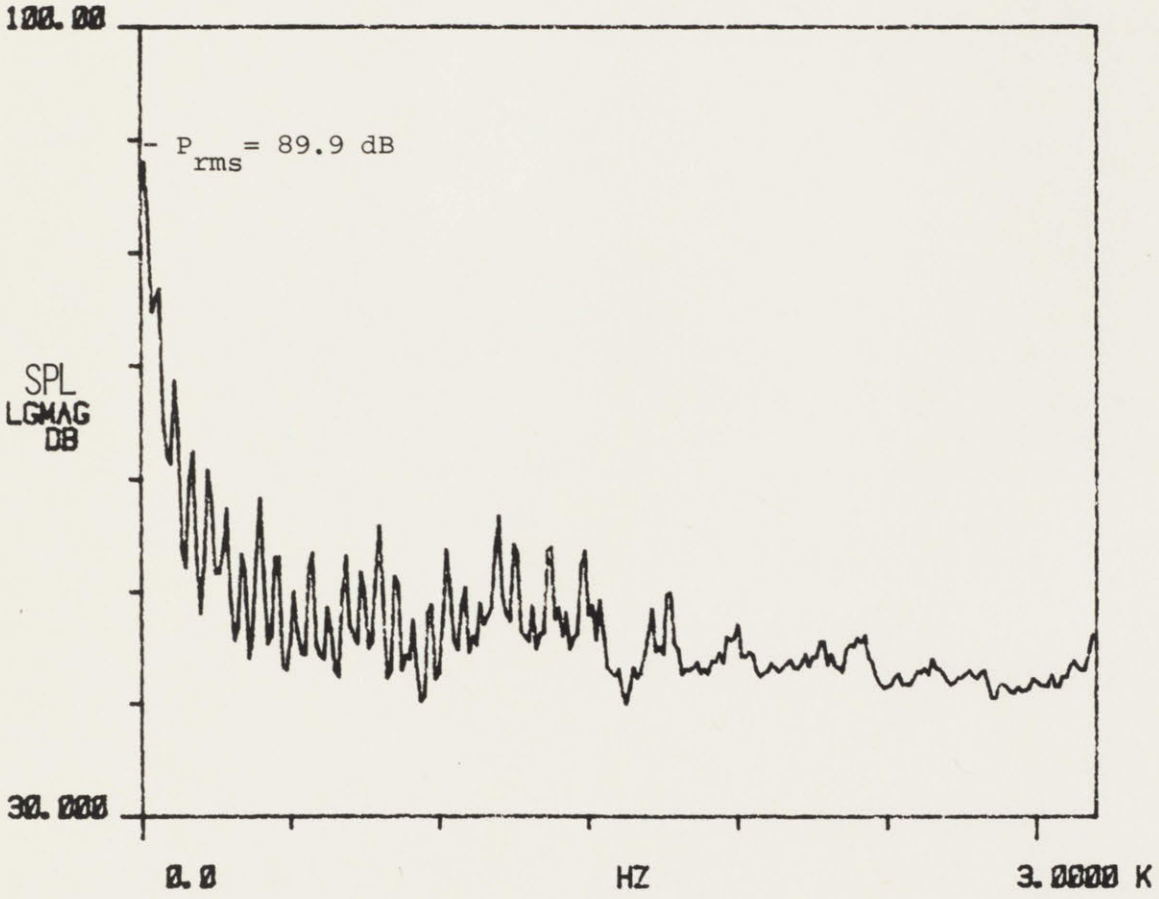

Fig C.22 Off Axis Microphone From Tower Wake Test

Tower Wake Test

Tape 1 Counter 1361

2 blades 2260 RPM

U = 20 MPH

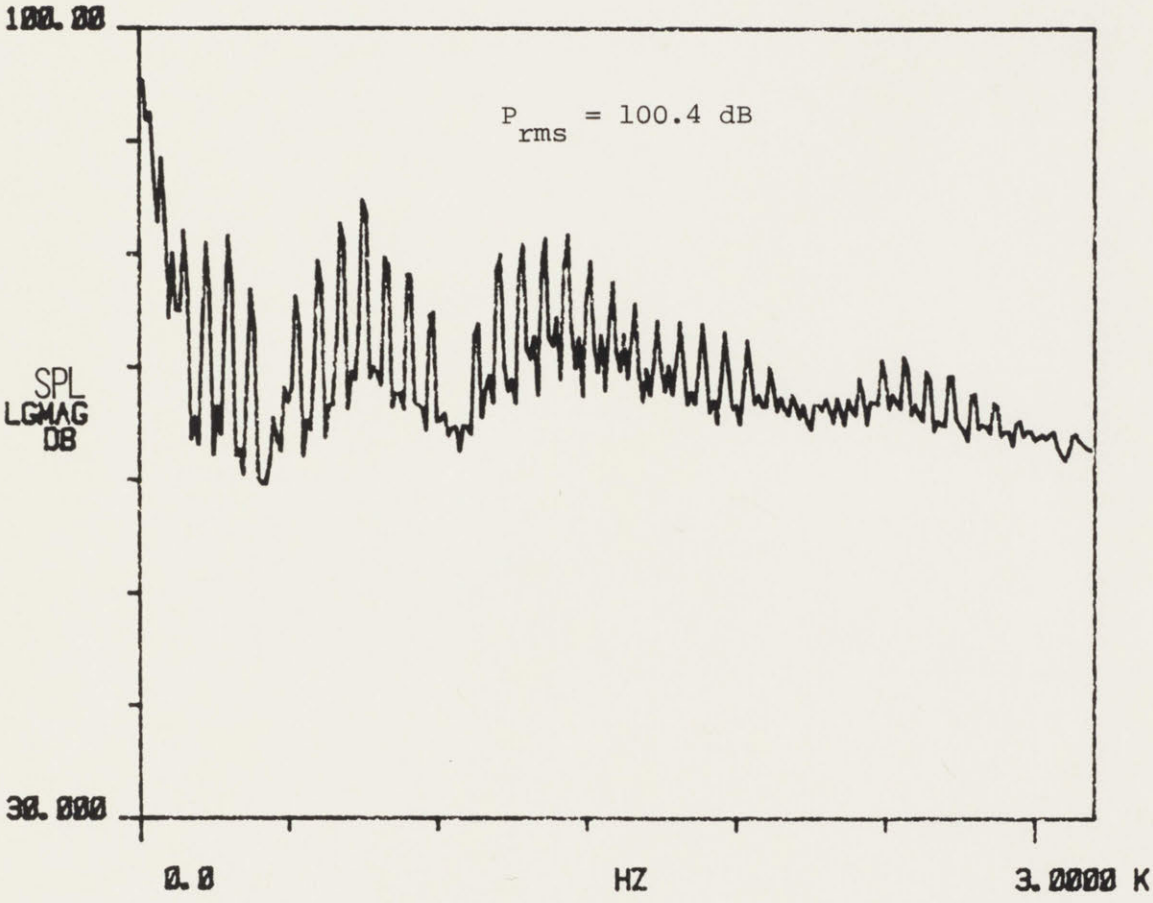

Fig C.23 On Axis Microphone From Tower Wake Test

Tower Wake Test

Tape 1 Counter 1361

2 blades 2260 RPM

U = 20 MPH

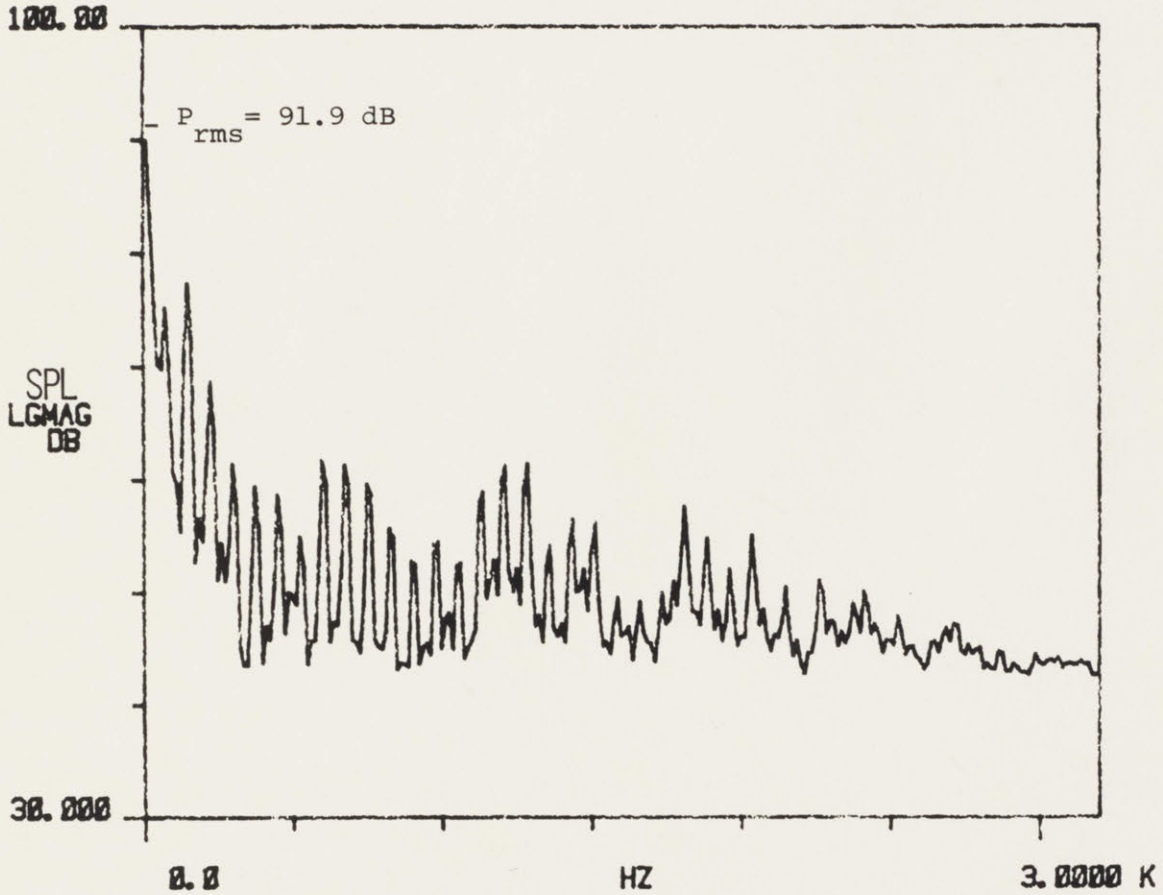

Fig C.24 Off Axis Microphone From Tower Wake Test

Tower Wake Test

Tape 1 Counter 1589

2 blades 2520 RPM

U = 22.5 MPH

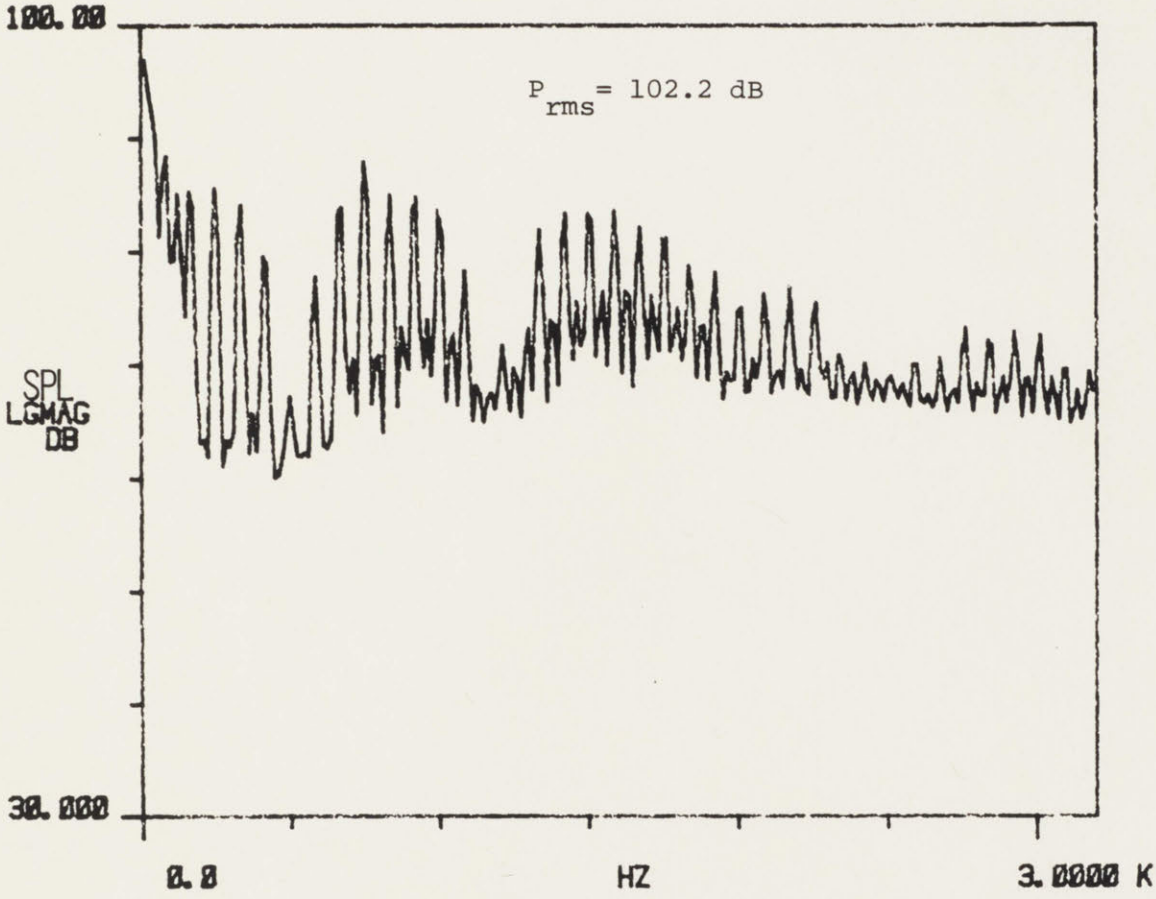

Fig C.25 On Axis Microphone From Tower Wake Test

Tower Wake Test

Tape 1 Counter 1589

2 blades 2520 RPM

U = 22.5 MPH

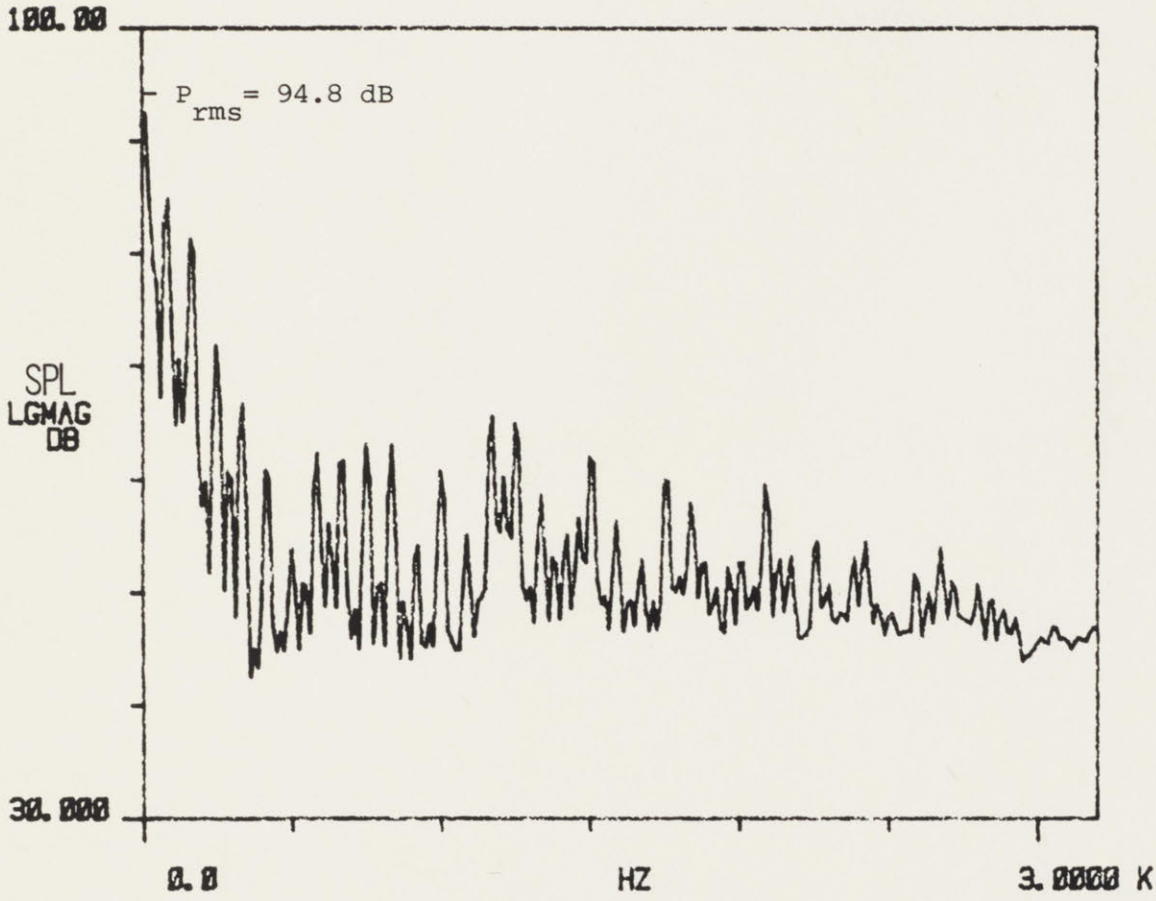

Fig C.26 Off Axis Microphone From Tower Wake Test

Upwind Configuration Test

Tape 3 Counter 1260

2 blades 1720 RPM

U = 22.5 MPH

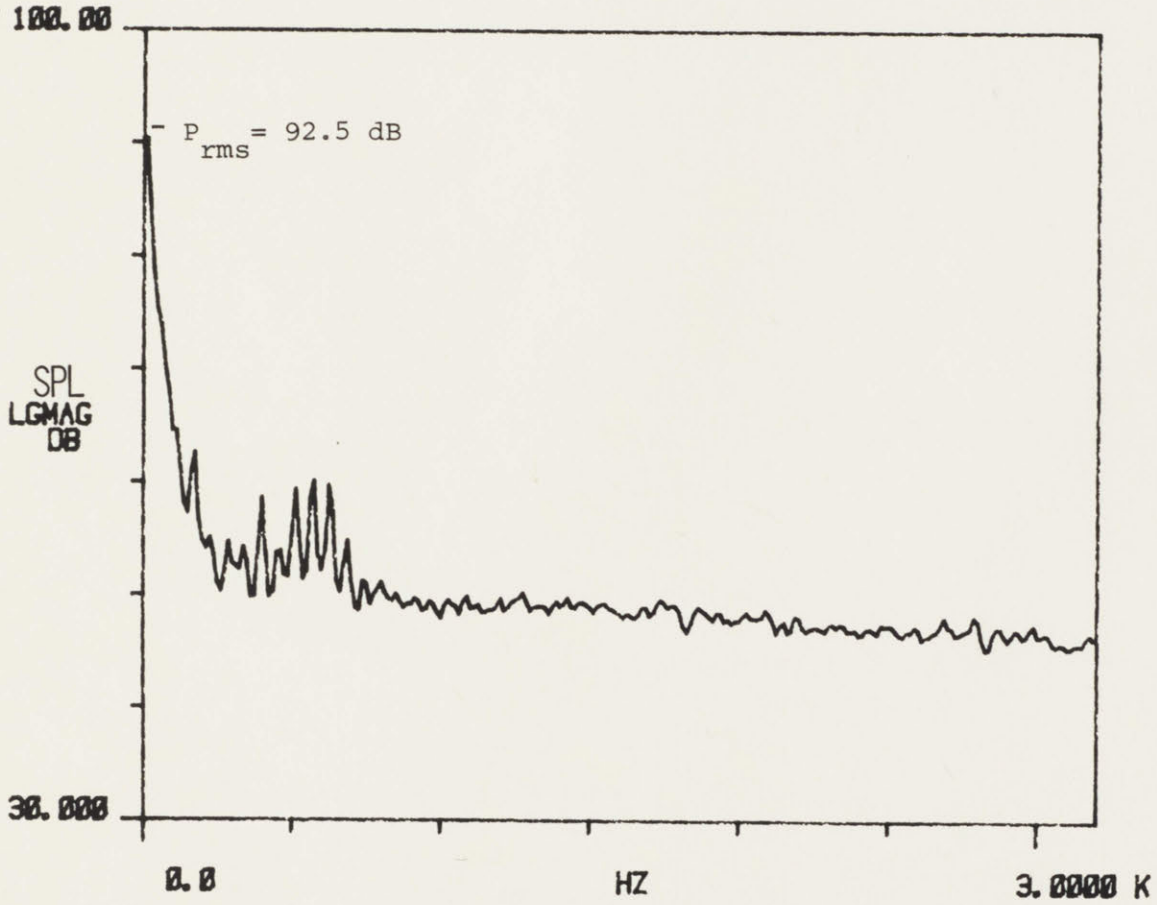

Fig C.27 On Axis Microphone From Upwind Configuration Test

Upwind Configuration Test

Tape 3 Counter 1260

2 blades 1720 RPM

U = 22.5 MPH

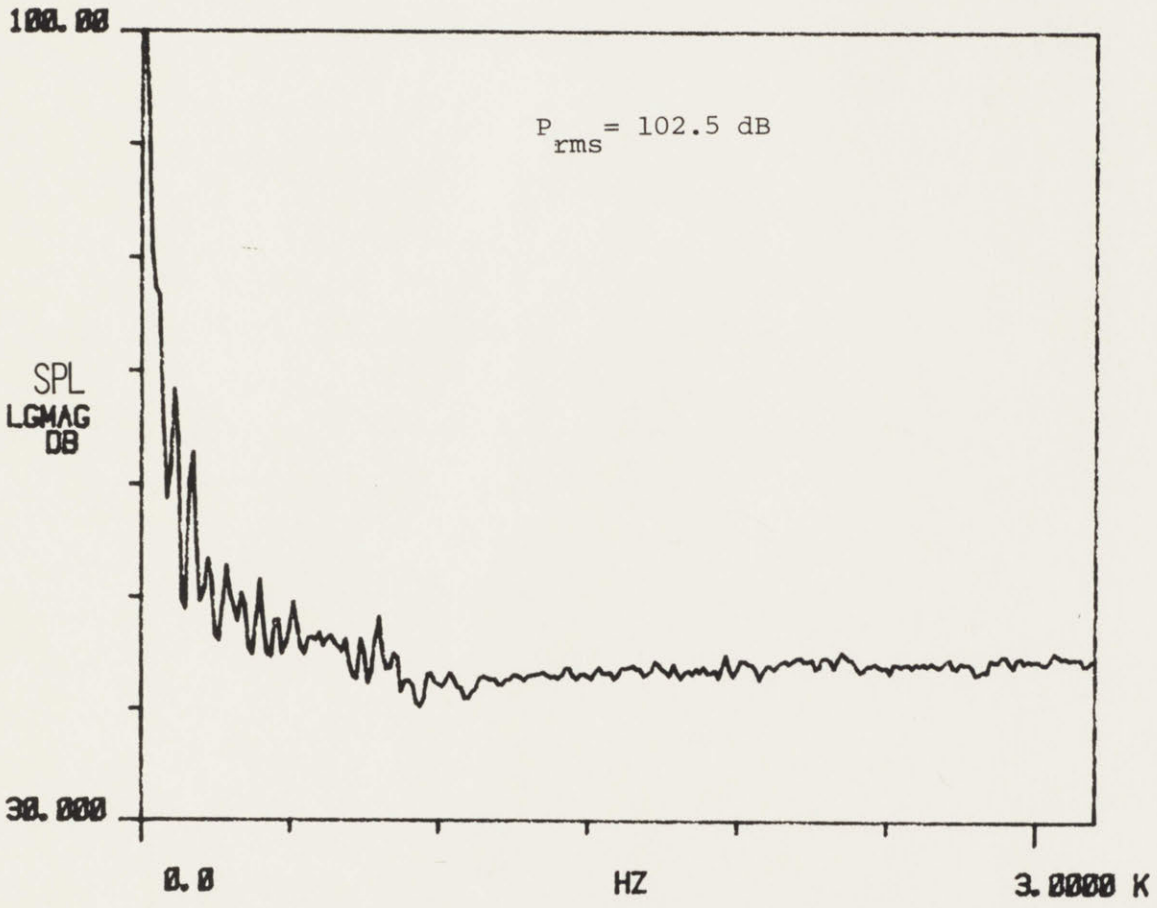

Fig C.28 Off Axis Microphone From Upwind Configuration Test

Upwind Configuration Test

Tape 3 Counter 1647

3 blades 1750 RPM

U = 22.5 MPH

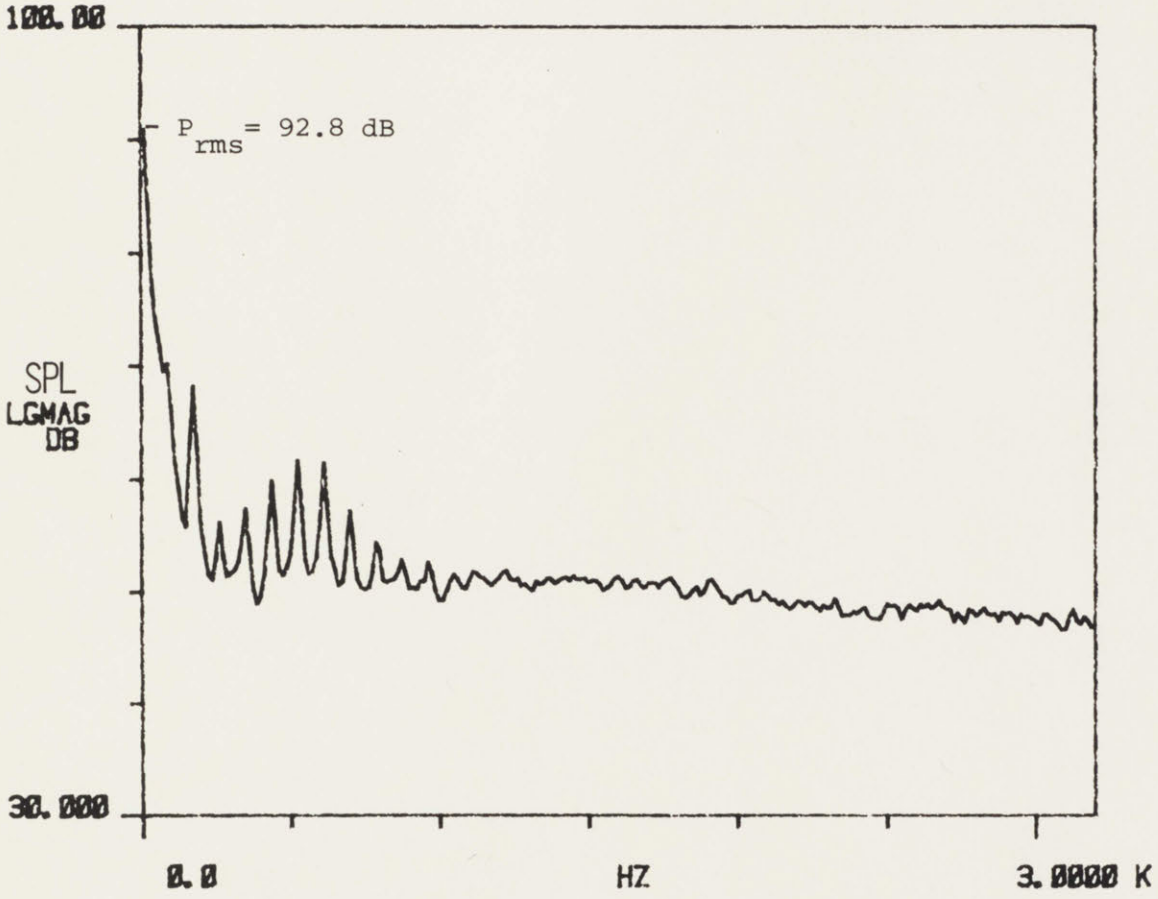

Fig C.29 On Axis Microphone From Upwind Configuration Test

Upwind Configuration Test

Tape 3 Counter 1647

3 blades 1750 RPM

U = 22.5 MPH

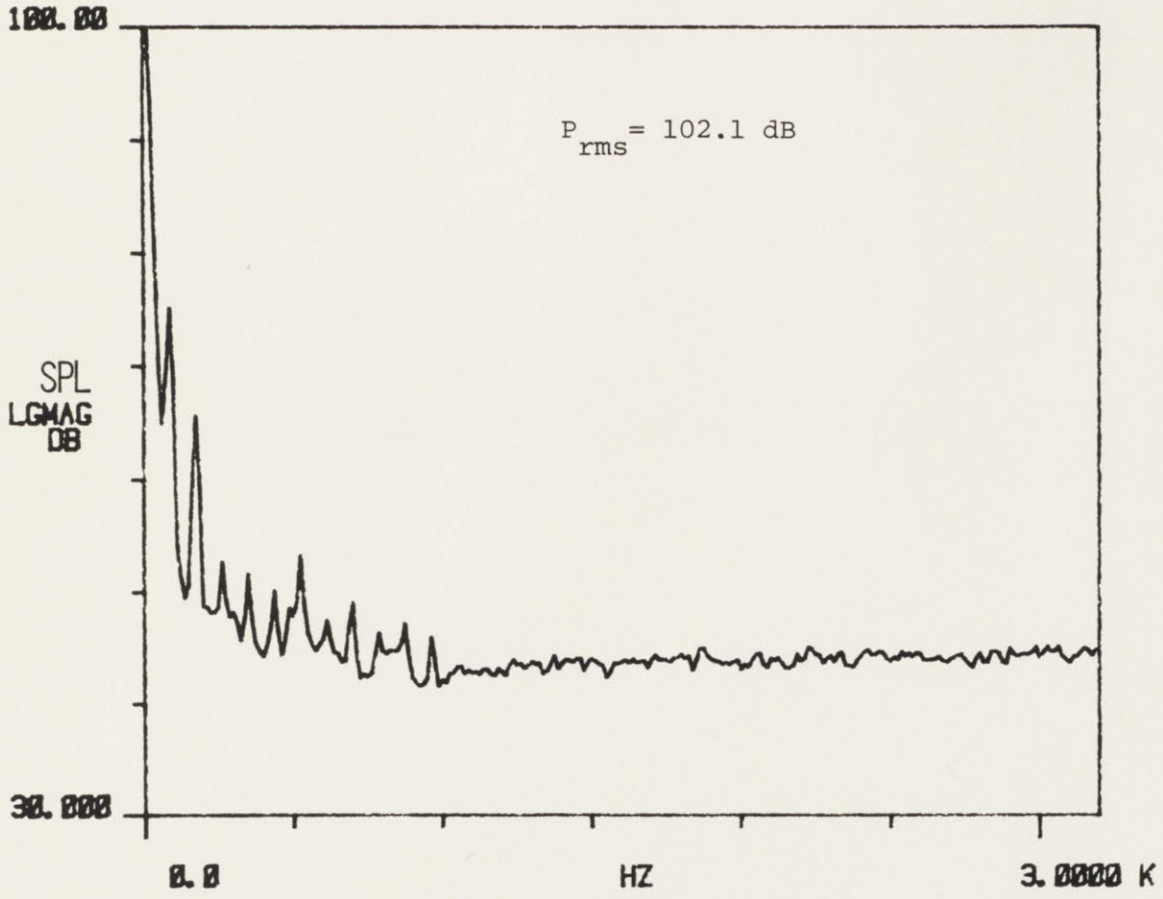

Fig C.30 Off Axis Microphone From Upwind Configuration Test

Multiple Blade Tower Wake Test

Tape 2 Counter 1450

3 blades 1920 RPM

U = 22.5 MPH

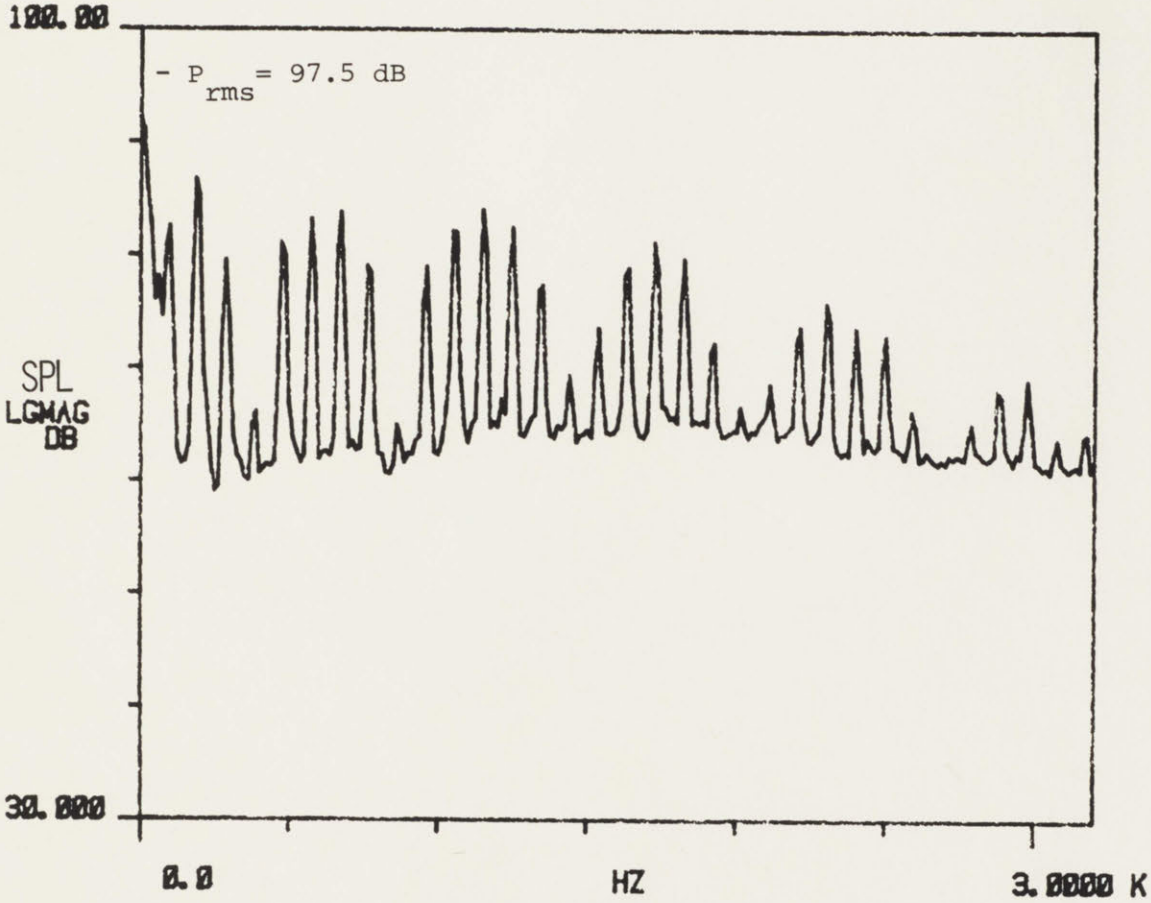

Fig C.31 On Axis Microphone From Multiple Blade Test in the Tower Wake

Multiple Blade Tower Wake Test

Tape 2 Counter 1450

3 blades 1920 RPM

U = 22.5 MPH

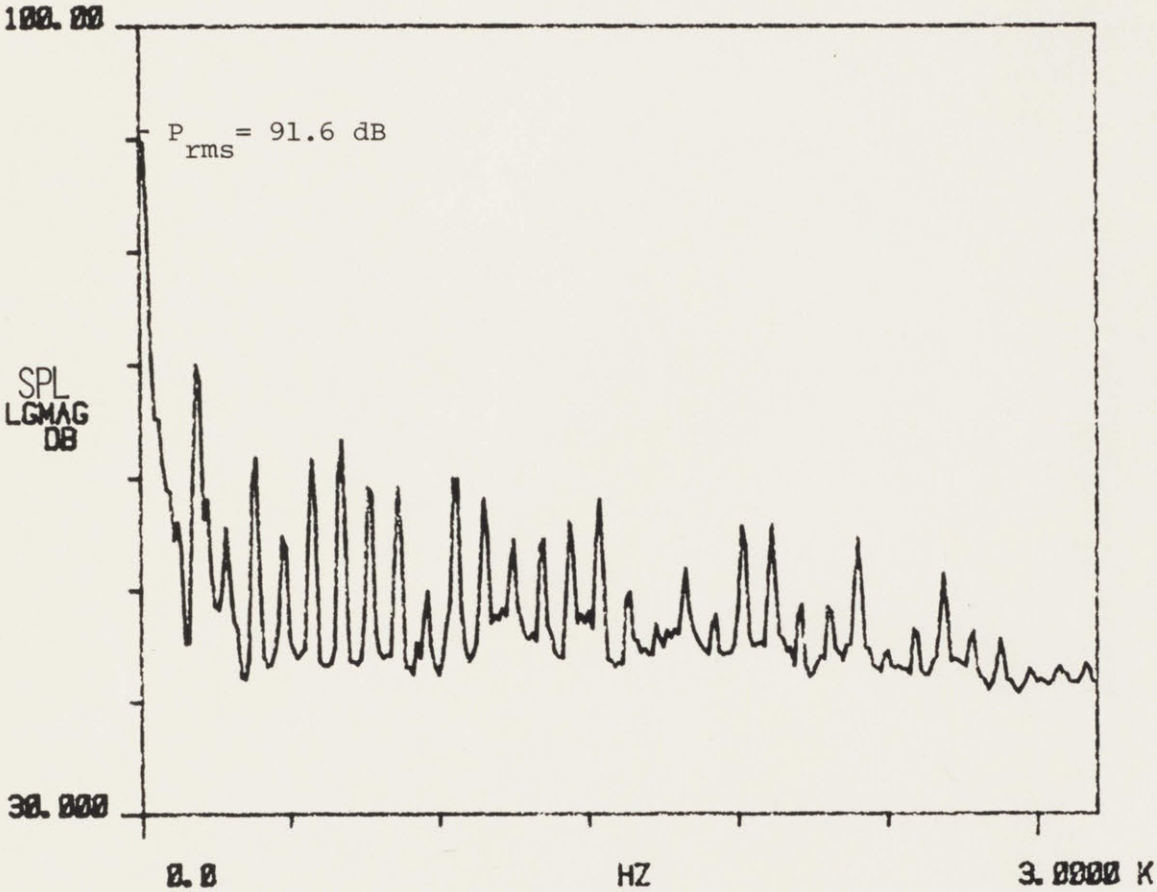

Fig C.32 Off Axis Microphone From Multiple Blade Test in the Tower Wake

Multiple Blade Tower Wake Test

Tape 2 Counter 1584

4 blades 1760 RPM

U = 22.5 MPH

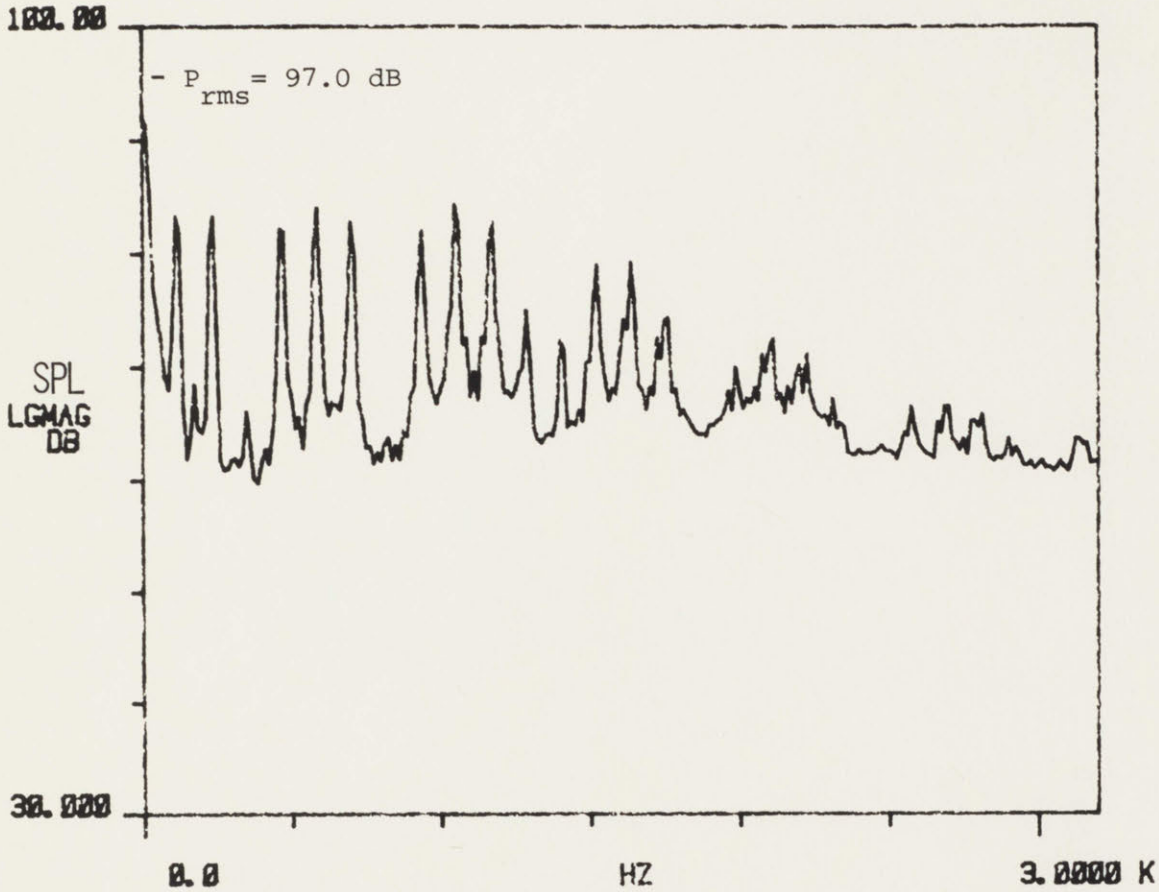

Fig C.33 On Axis Microphone From Multiple Blade Test in the Tower Wake

Multiple Blade Tower Wake Test

Tape 2 Counter 1584

4 blades 1760 RPM

U = 22.5 MPH

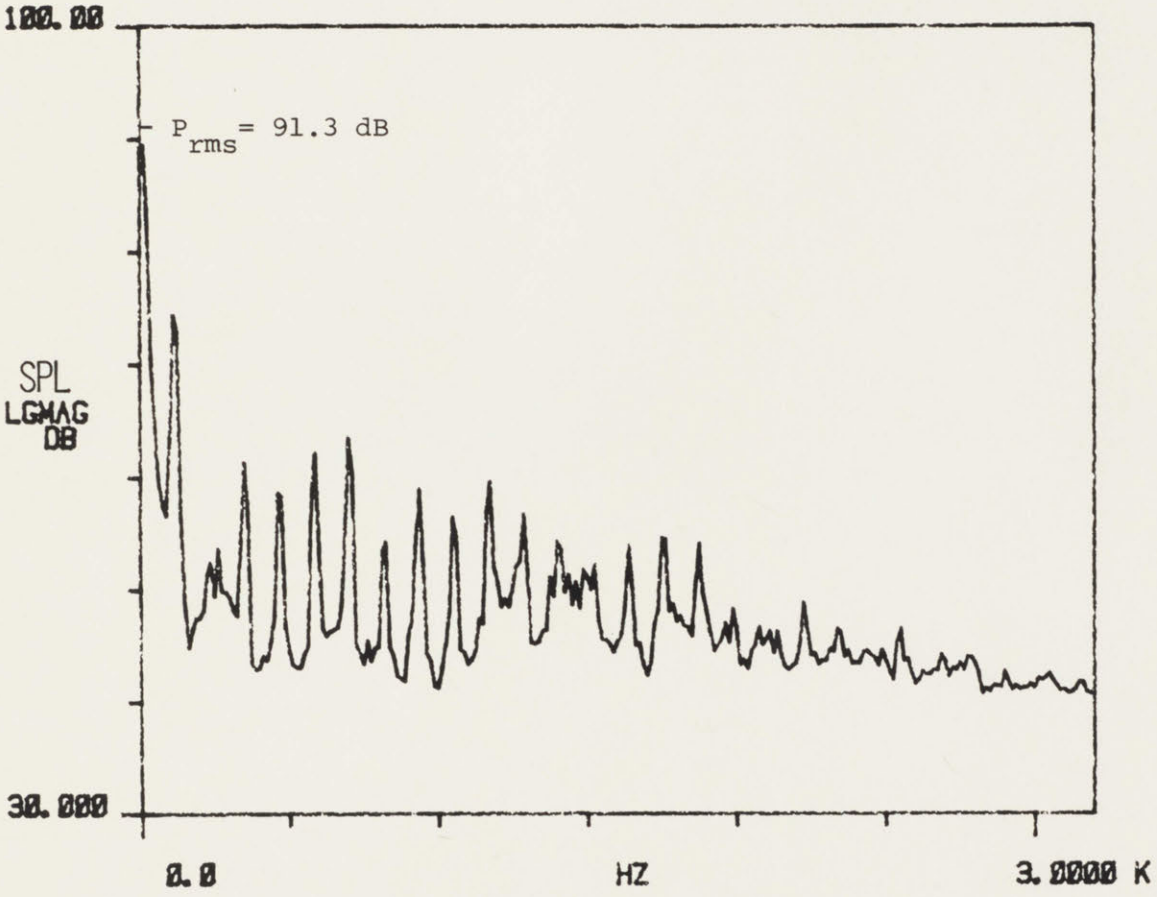

Fig C.34 Off Axis Microphone From Multiple Blade Test in the Tower Wake

Multiple Blade Cylinder Wake Test

Tape 8 Counter 100

2 blades 1990 RPM

U = 22.5 MPH

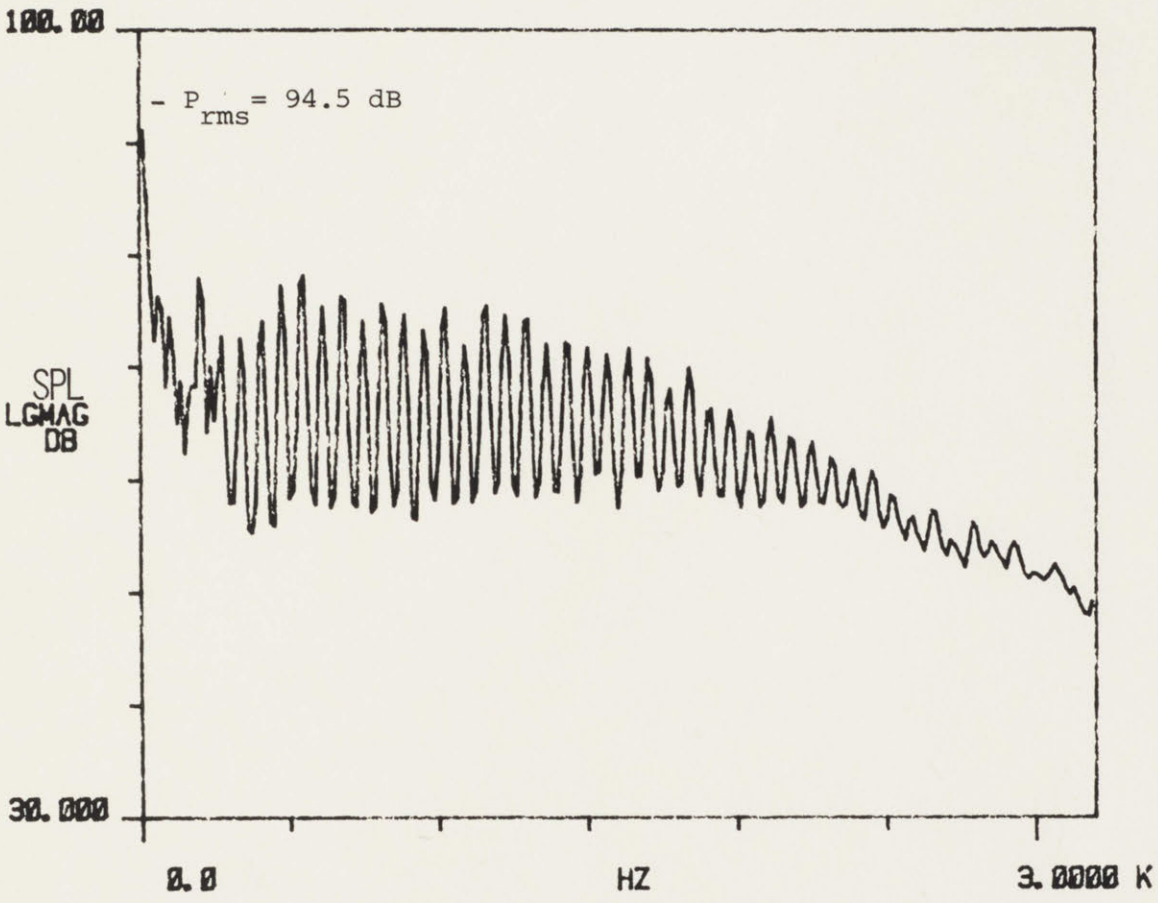

Fig C.35 On Axis Microphone From Multiple Blade Cylinder Wake Test

5/8 " cylinder
15 diameters upstream of the rotor

Multiple Blade Cylinder Wake Test

Tape 8 Counter 240

3 blades 1990 RPM

U = 22.5 MPH

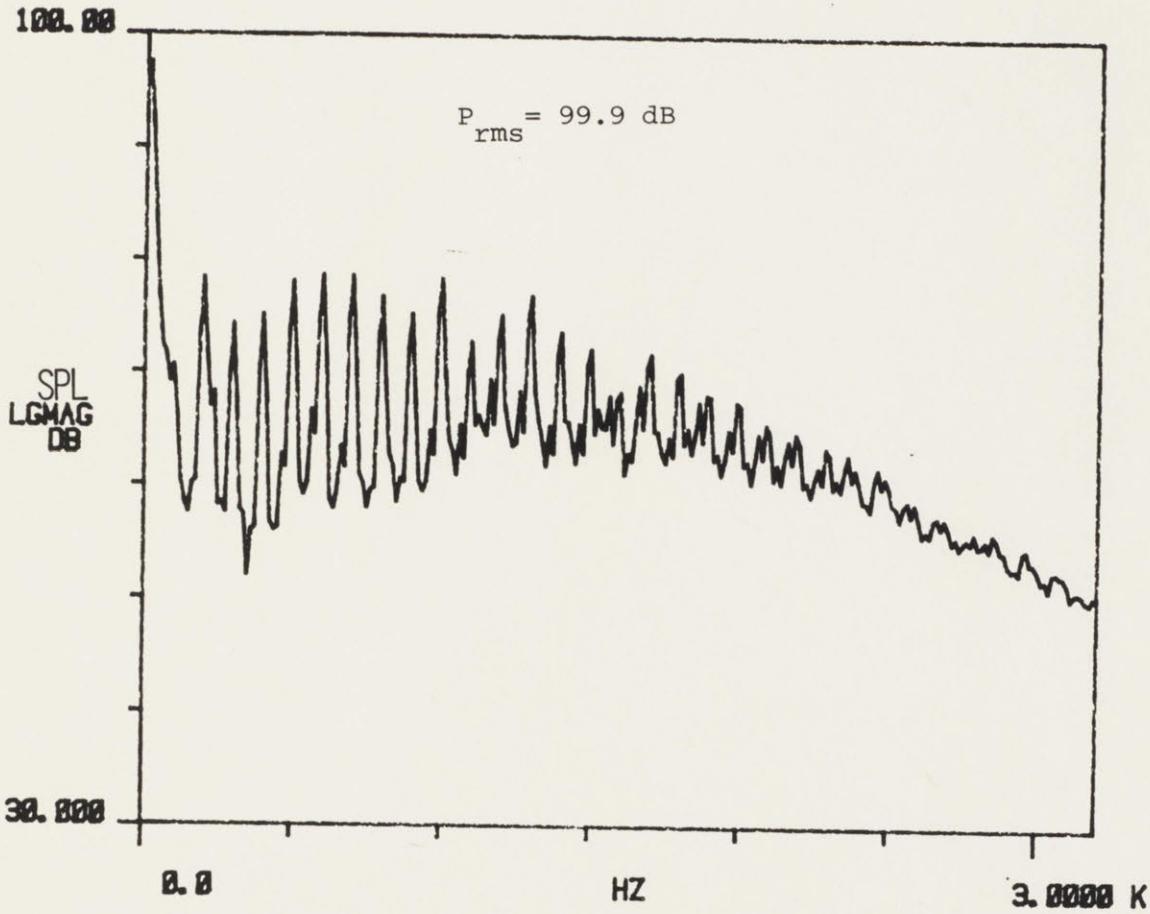

Fig C.36 On Axis Microphone From Multiple Blade Cylinder Wake Test

5/8" cylinder
15 diameters upstream of the rotor

Multiple Blade Cylinder Wake Test

Tape 8 Counter 380

4 blades 1970 RPM

U = 22.5 MPH

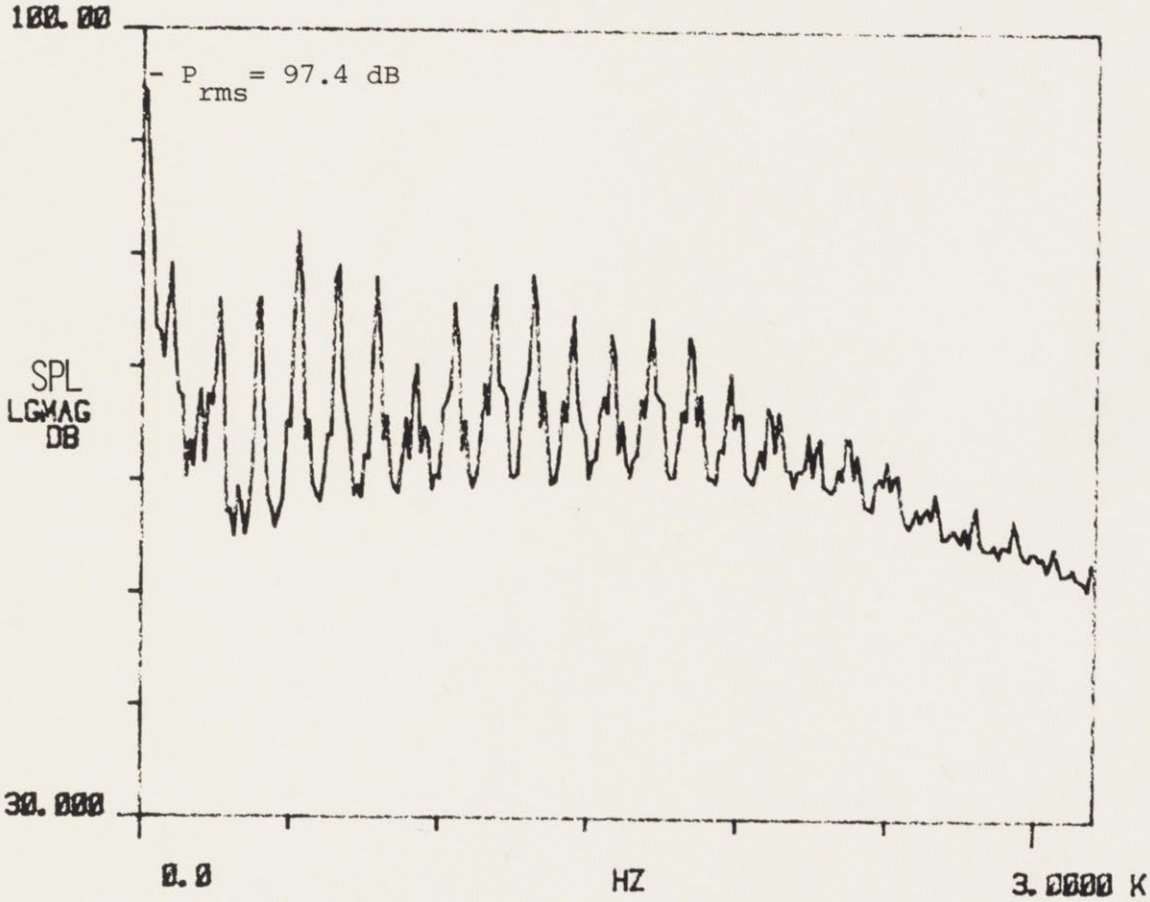

Fig C.37 On Axis Microphone From Multiple Blade Cylinder Wake Test

5/8" cylinder
15 diameters upstream of the rotor

Loading Test

Tape 3 Counter 600

2 blades 1740 RPM

U = 22.5 MPH

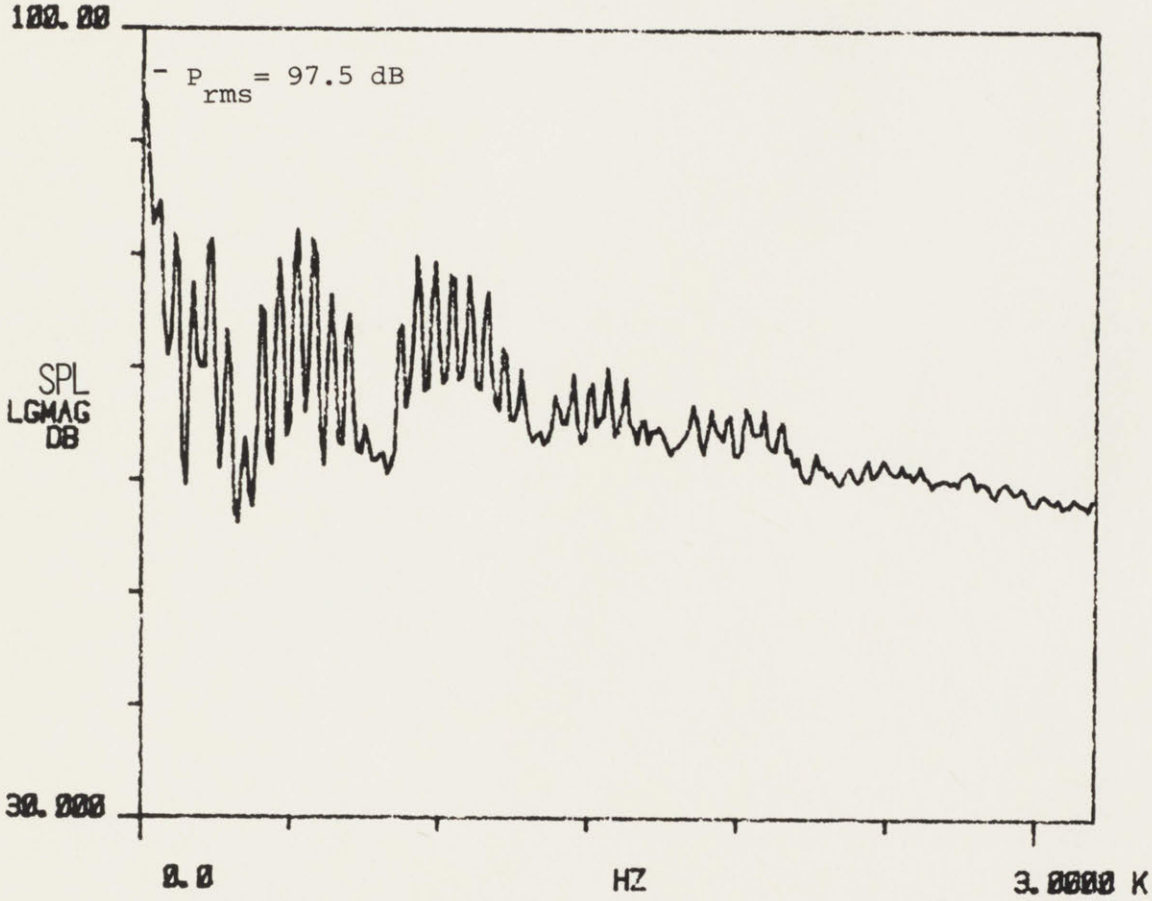

Fig C. 38 On Axis Microphone From Loading Test in the Tower Wake (turbine draws .43 hp)

Loading Test

Tape3 Counter 600

2 blades 1740 RPM

U = 22.5 MPH

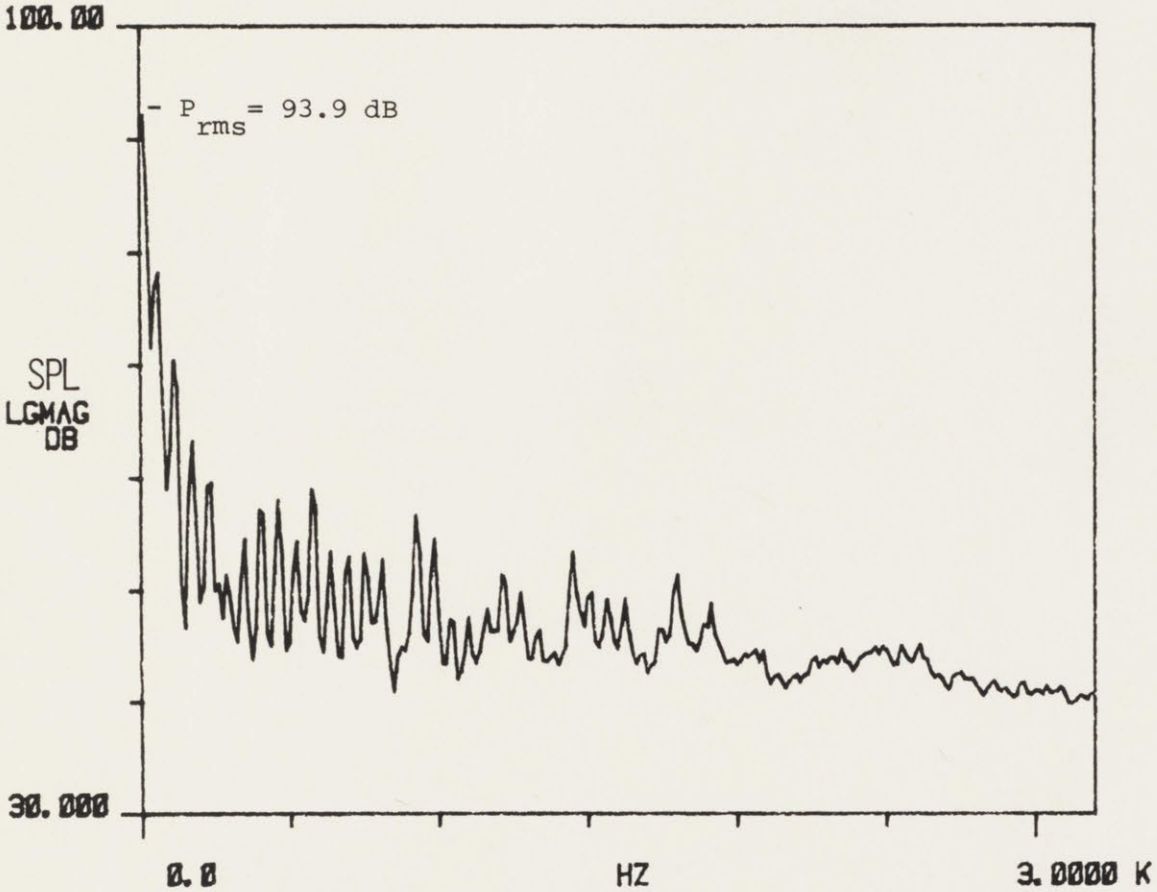

Fig C.39 Off Axis Microphone From Loading Test in the Tower Wake (turbine draws .43 hp)

Loading Test

Tape 3 Counter 820

3 blades 1730 RPM

U = 22.5 MPH

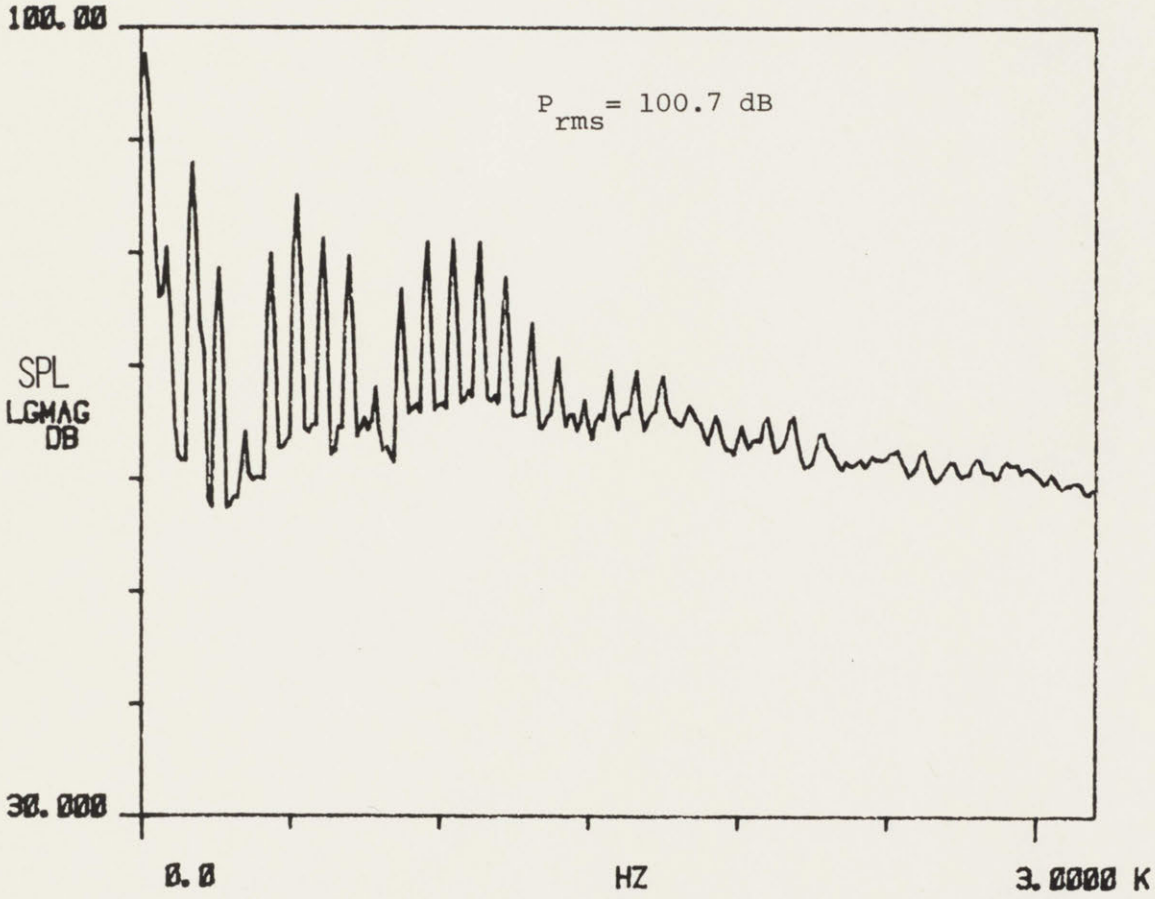

Fig C.40 On Axis Microphone From Loading Test in the Tower Wake (turbine draws .35 hp)

Loading Test

Tape 3 Counter 820

3 blades 1730 RPM

U = 22.5 MPH

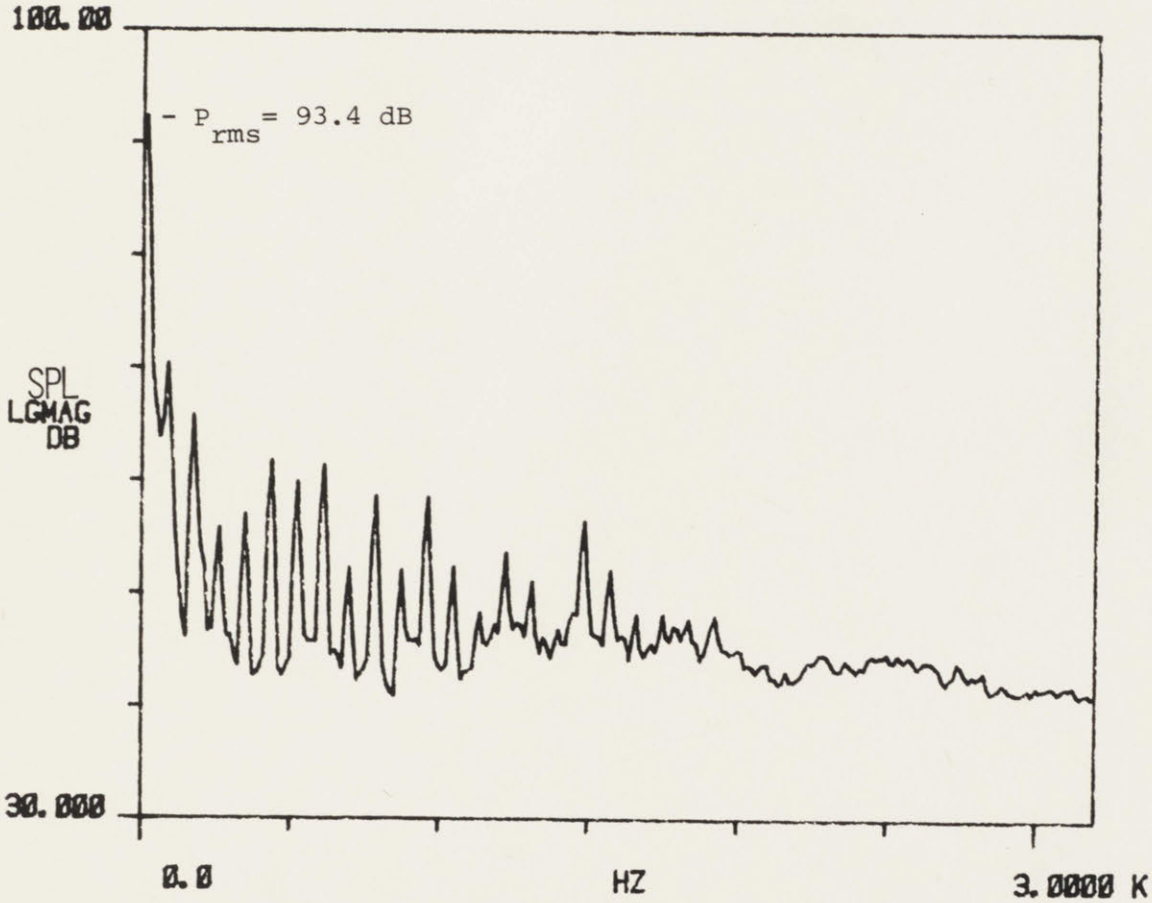

Fig C.41 Off Axis Micrphone From Loading Test in the Tower Wake (turbine draws .35 hp)

Loading Test

Tape 3 Counter 1040

4 blades 1690 RPM

U = 22.5 MPH

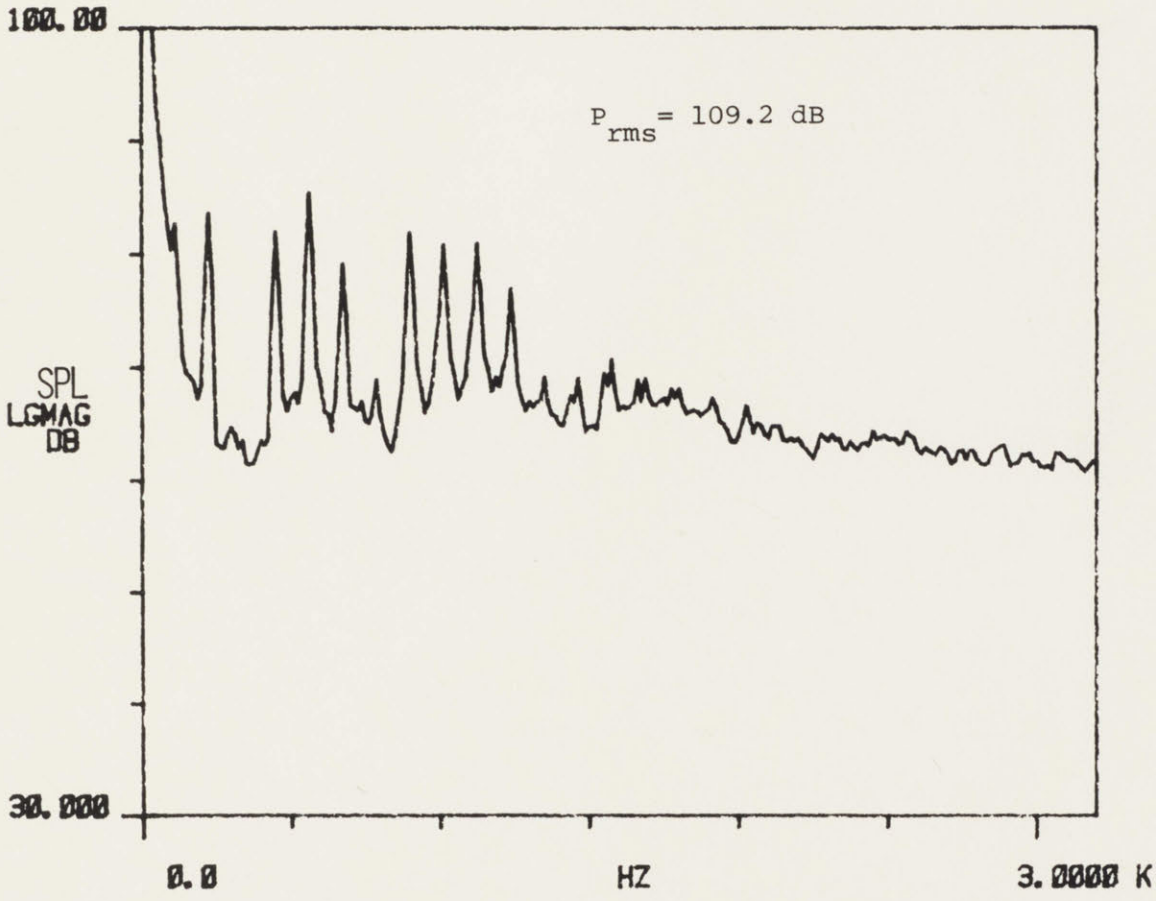

Fig C.42 On Axis Microphone From Loading Test in the Tower Wake (turbine draws .24 hp)

Loading Test

Tape 3 Counter 1040

4 blades 1690 RPM

U = 22.5 MPH

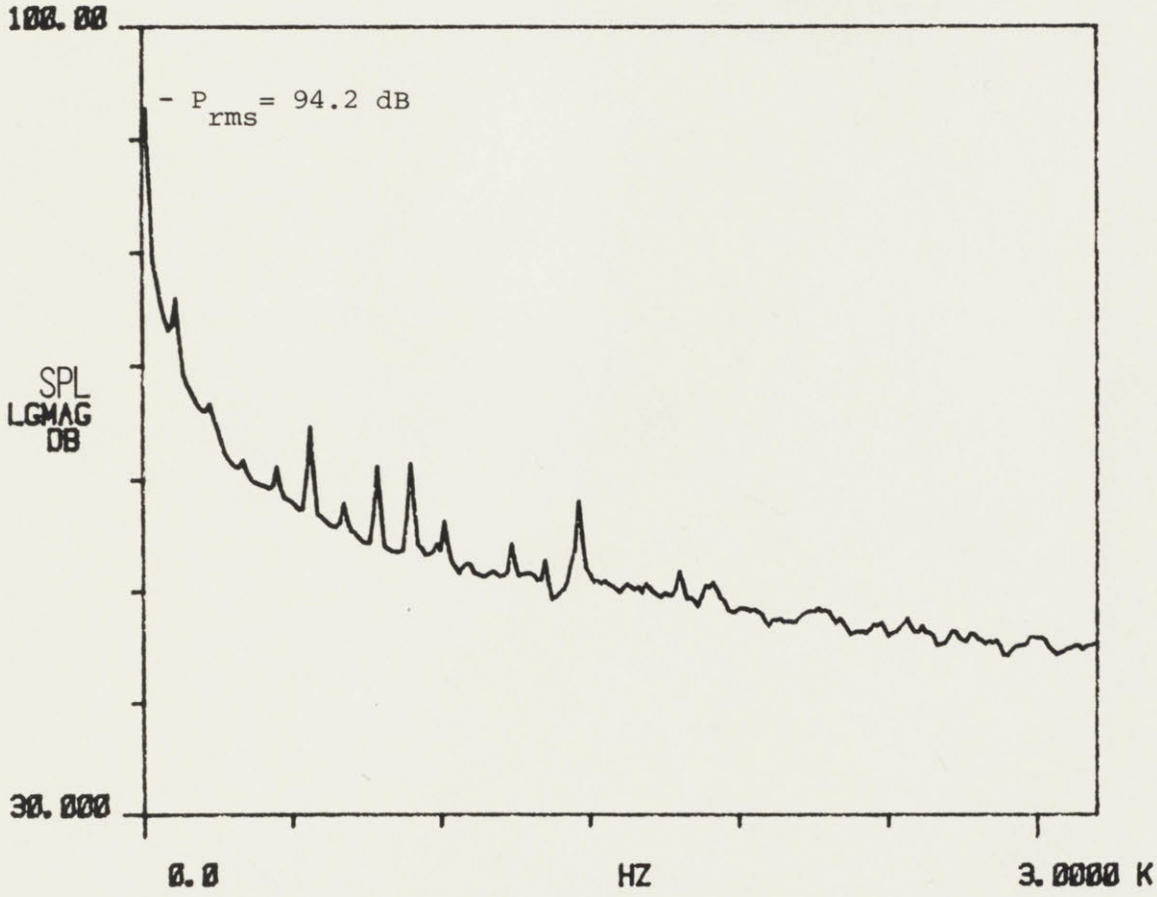

Fig C.43 Off Axis Microphone From Loading Test in the Tower Wake (turbine draws .24 hp)

Cylinder Test

Tape 7 Counter 960

2 blades 1990 RPM

U = 22.5 MPH

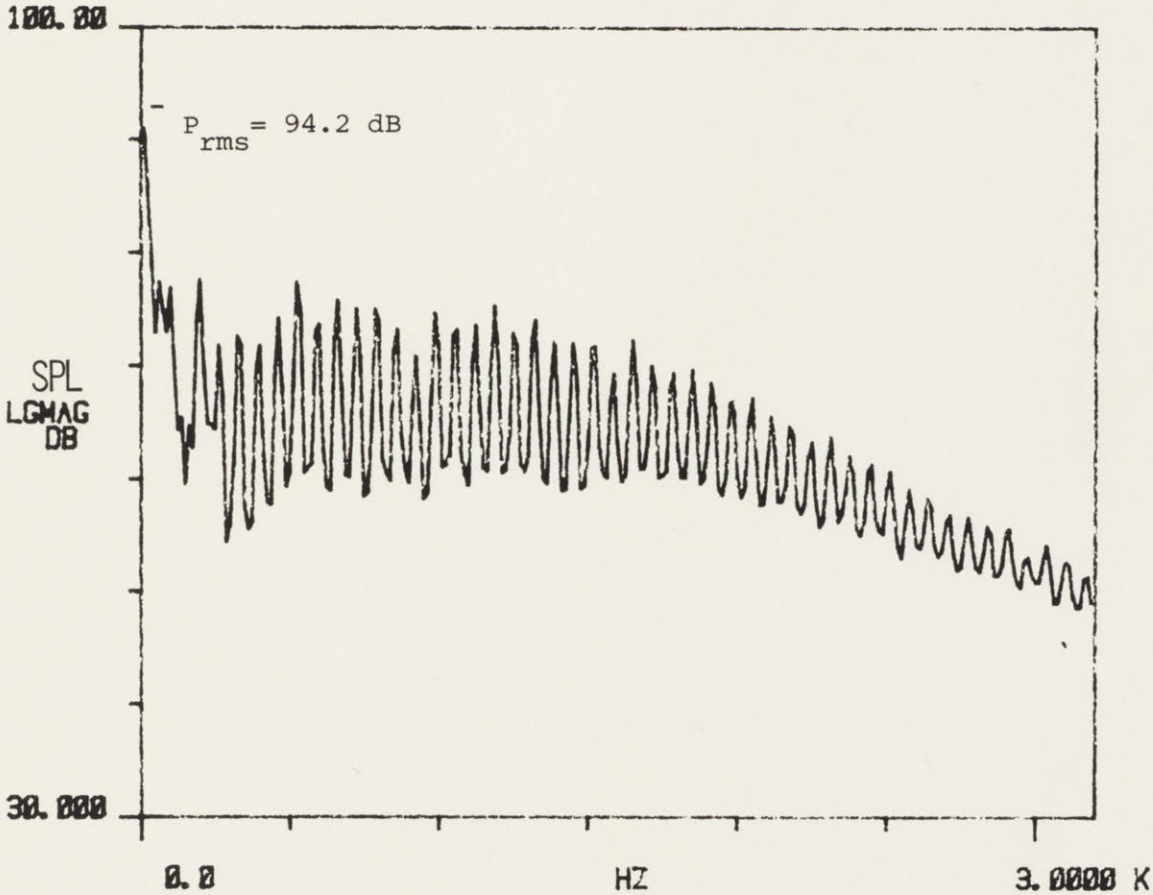

Fig C.44 On Axis Microphone From Cylinder Test
5/8" cylinder
10 diameters upstream of rotor plane

Cylinder Test

Tape 7 Counter 1240

2 blades 1990 RPM

U = 22.5 MPH

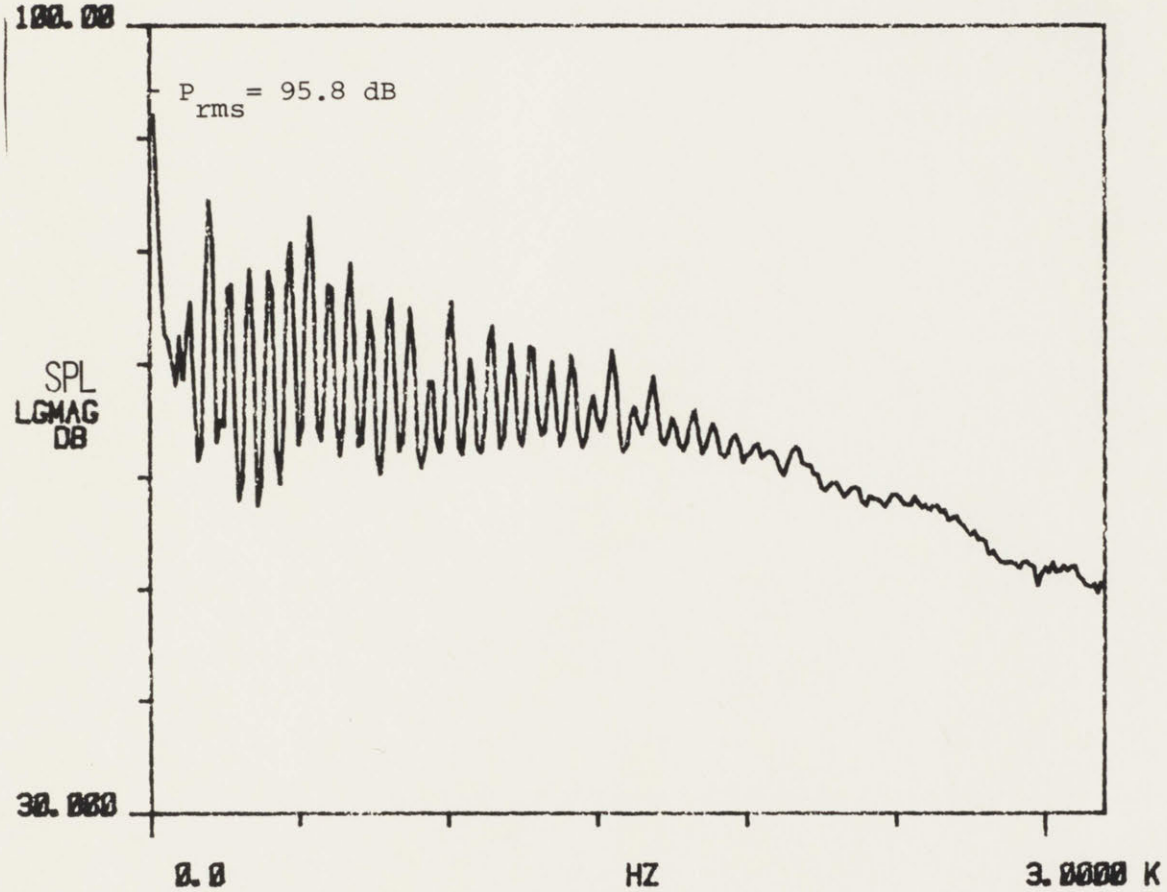

Fig. C.45 On Axis Microphone From Cylinder Test
1.25 " cylinder
10 diameters upstream of rotor plane

Cylinder Test

Tape 7 Counter 1520

2 blades 1970 RPM

U = 22.5 MPH

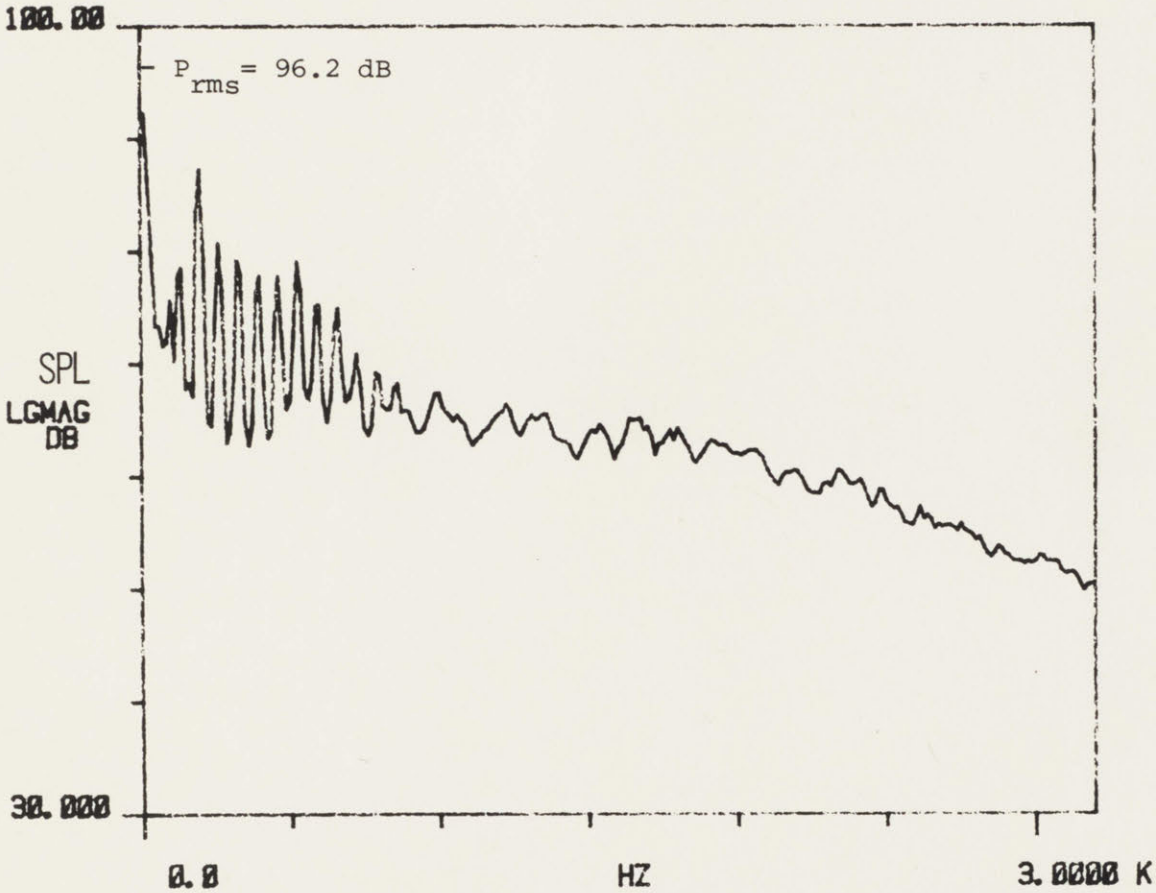

Fig C.46 On Axis Microphone From Cylinder Test
2 " cylinder
10 diameters upstream of rotor plane

Cylinder Test

Tape 4 Counter 172

2 blades 1750 RPM

U = 22.5 MPH

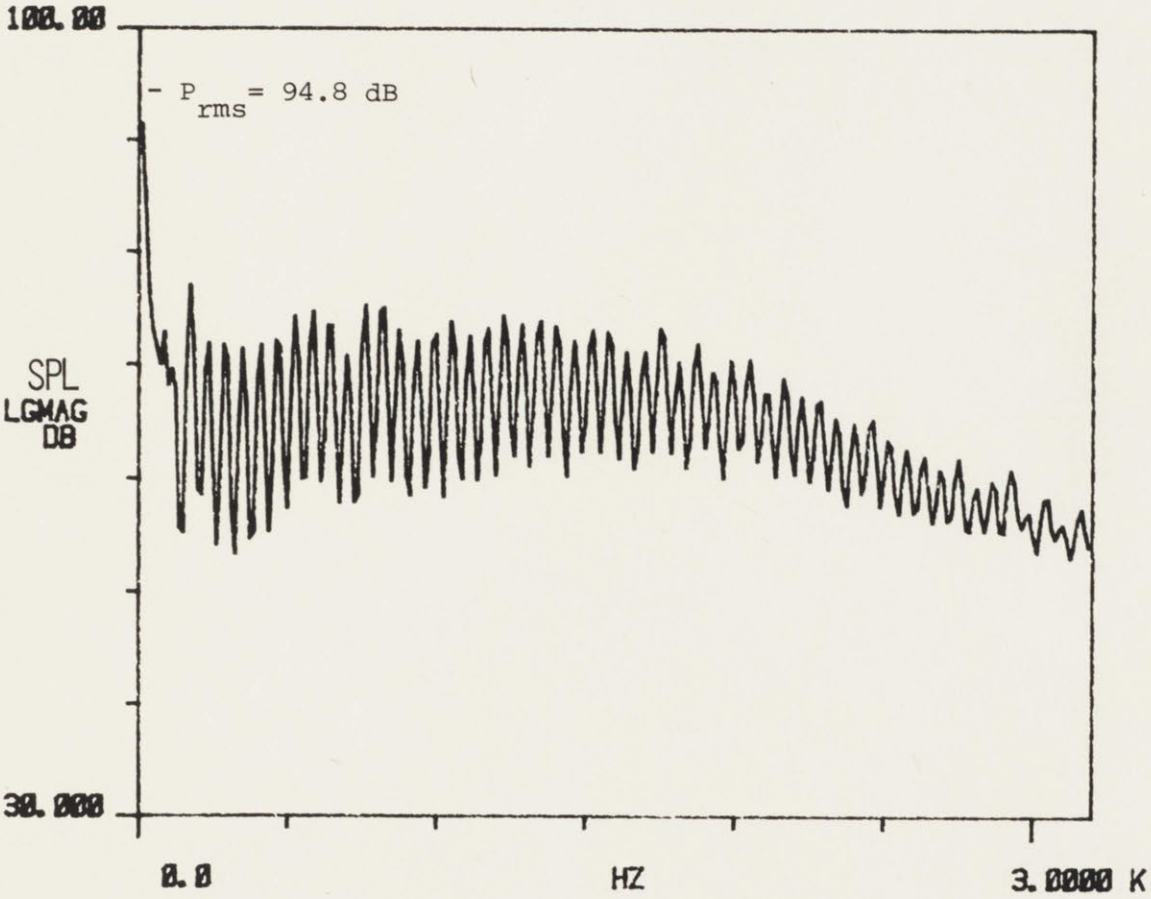

Fig C.47 On Axis Microphone From Cylinder Test
5/8 " cylinder
5 diameters upstream of rotor plane

Cylinder Test

Tape 4 Counter 172

2 blades 1750 RPM

U = 22.5 MPH

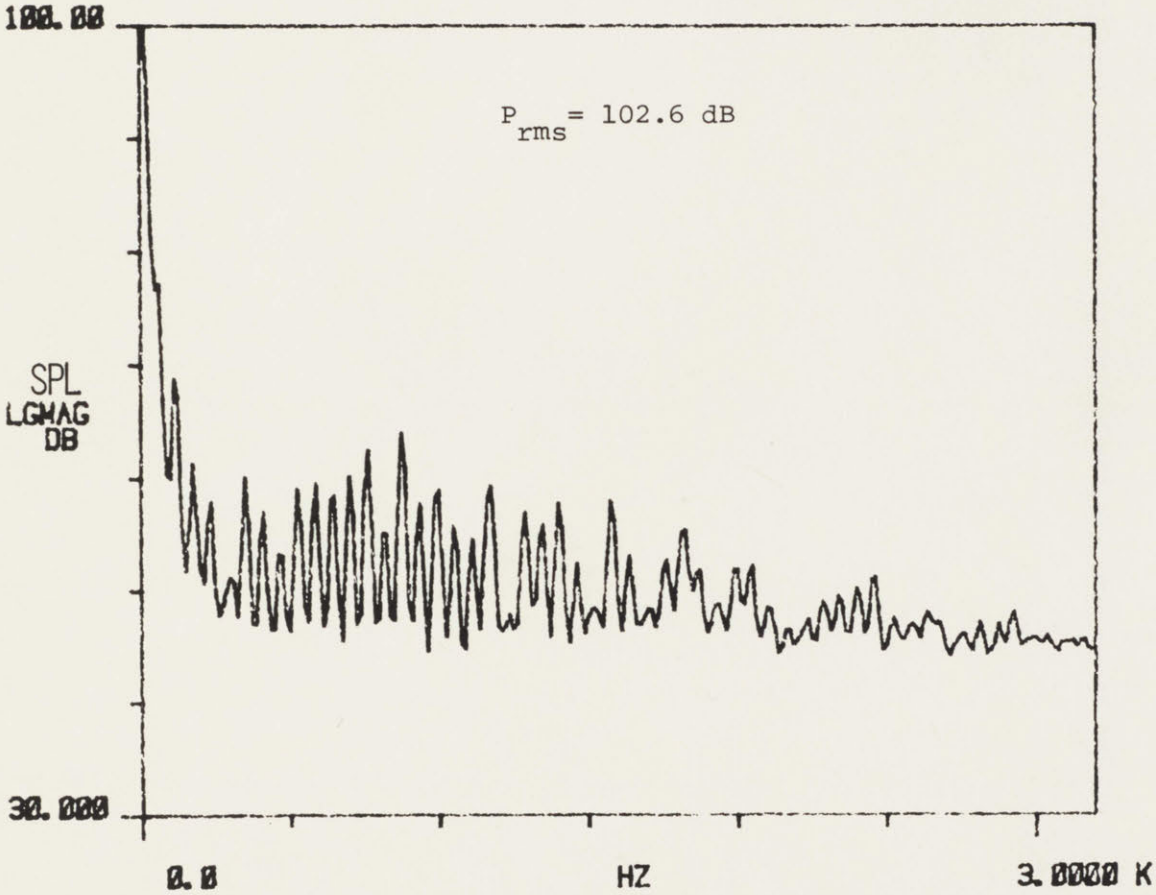

Fig C.48 Off Axis Microphone From Cylinder Test
5/8" cylinder
5 diameters upstream of rotor plane

Cylinder Test

Tape 4 Counter 385

2 blades 1740 RPM

U = 22.5 MPH

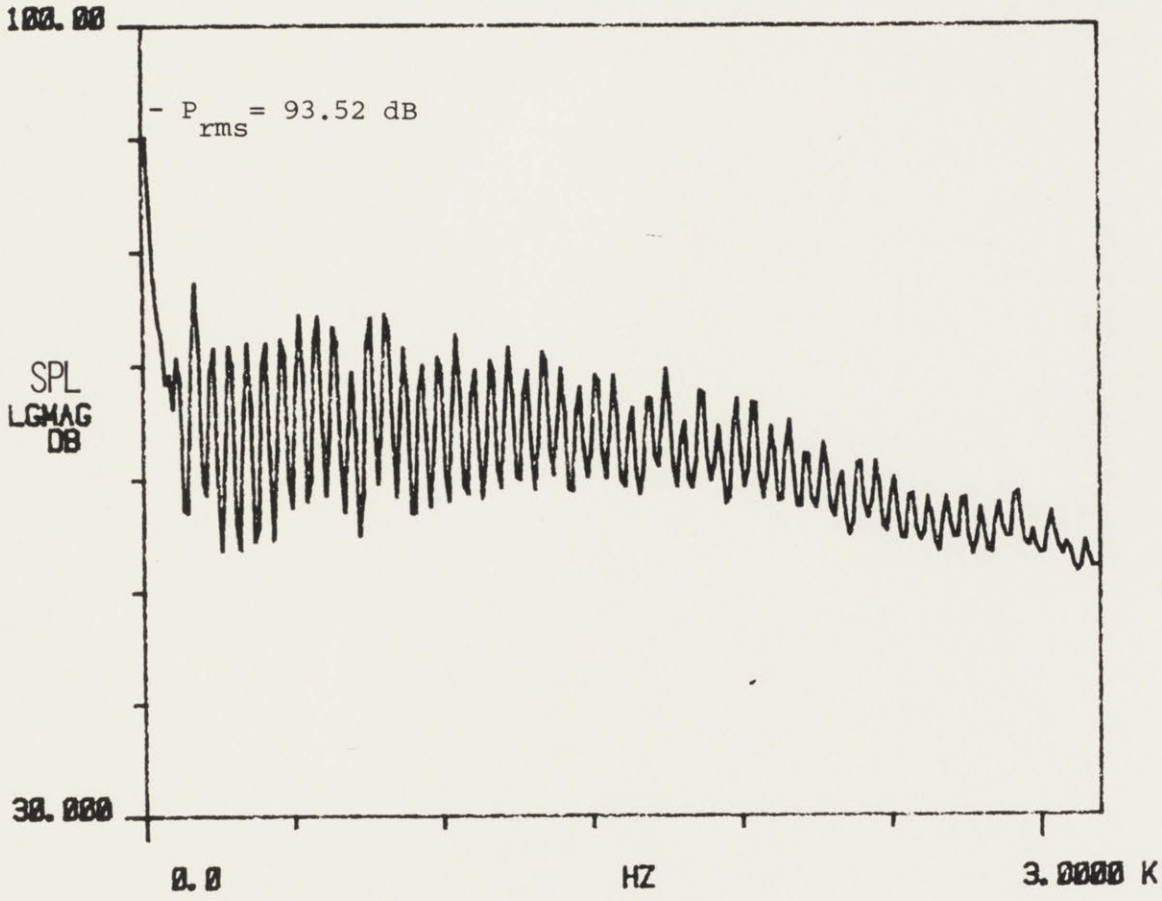

Fig C.49 On Axis Microphone From Cylinder Test

5/8 " cylinder
10 diameters upstream of rotor plane

Cylinder Test

Tape 4 Counter 385

2 blades 1740 RPM

U = 22.5 MPH

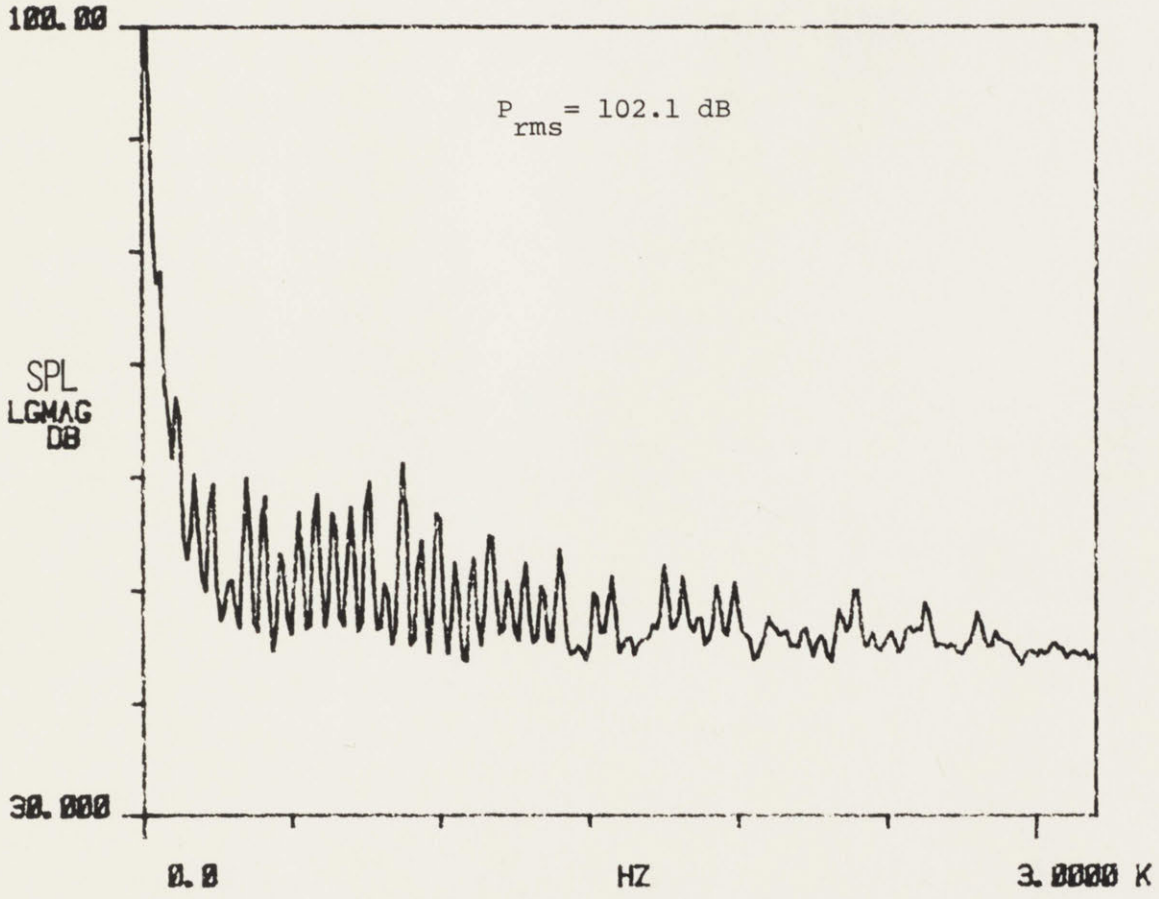

Fig C.50 Off Axis Microphone From Cylinder Test

5/8 " cylinder
10 diameters upstream of rotor plane

Cylinder Test

Tape 4 Counter 595

2 blades 1740 RPM

U = 22.5 MPH

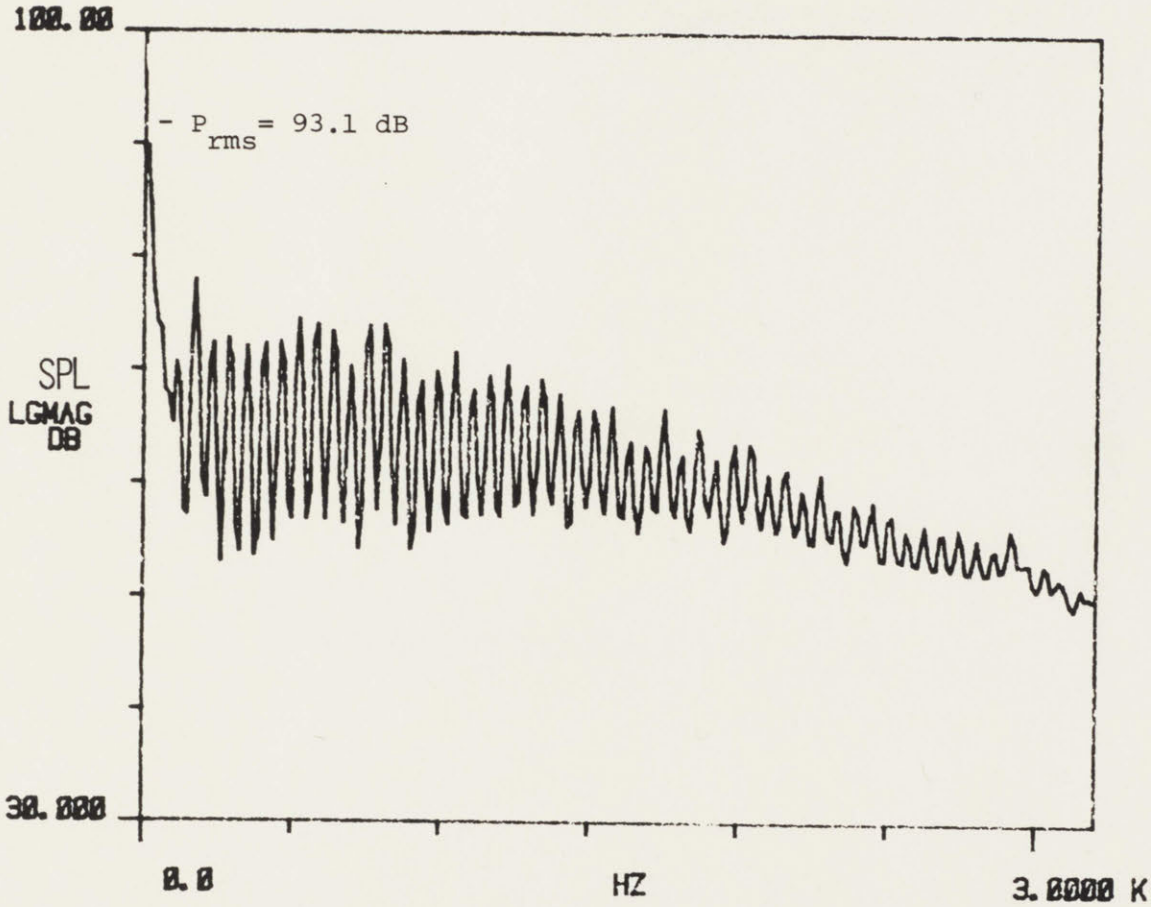

Fig C.51 On Axis Microphone From Cylinder Test

5/8" cylinder
15 diameters upstream of rotor plane

Cylinder Test

Tape 4 Counter 595

2 blades 1740 RPM

U = 22.5 MPH

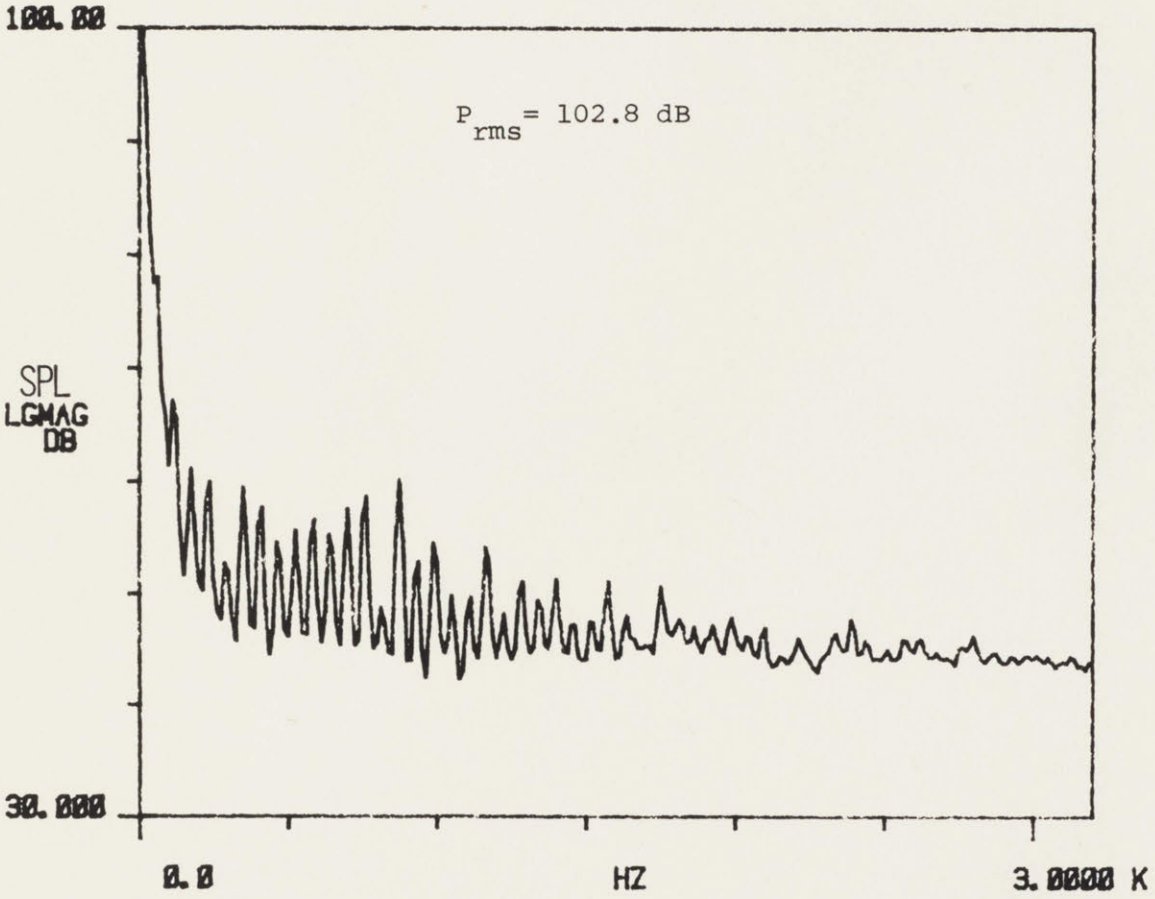

Fig C.52 Off Axis Microphone From Cylinder Test

5/8 " cylinder
15 diameters upstream of rotor plane

Cylinder Test

Tape 4 Counter 798

2 blades 1740 RPM

U = 22.5 MPH

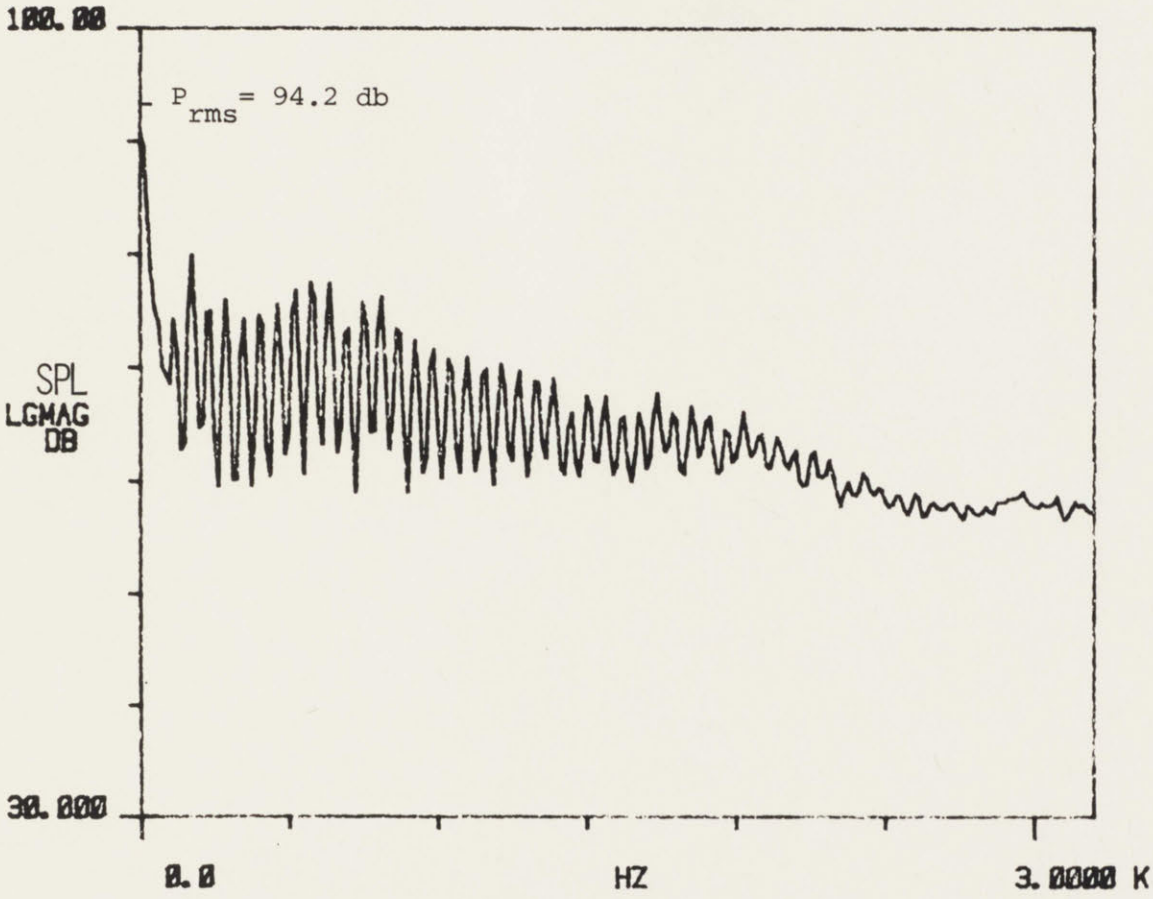

Fig C.53 On Axis Microphone From Cylinder Test

1.25 " cylinder
5 diameters upstream of rotor plane

Cylinder Test

Tape 4 Counter 798

2 blades 1740 RPM

U = 22.5 MPH

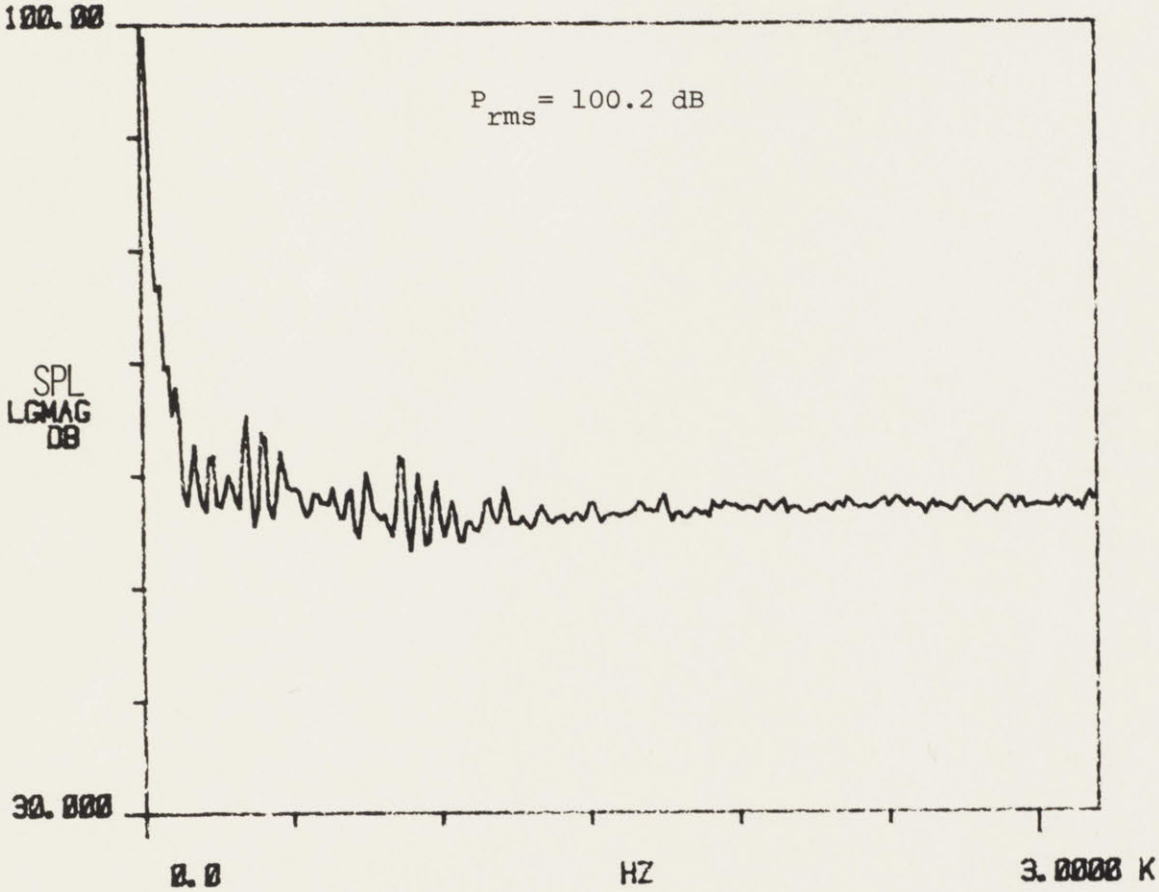

Fig C.54 Off Axis Microphone From Cylinder Test

1.25 " cylinder
5 diameters upstream of rotor plane

Cylinder Test

Tape 4 Counter 1007

2 blades 1740 RPM

U = 22.5 MPH

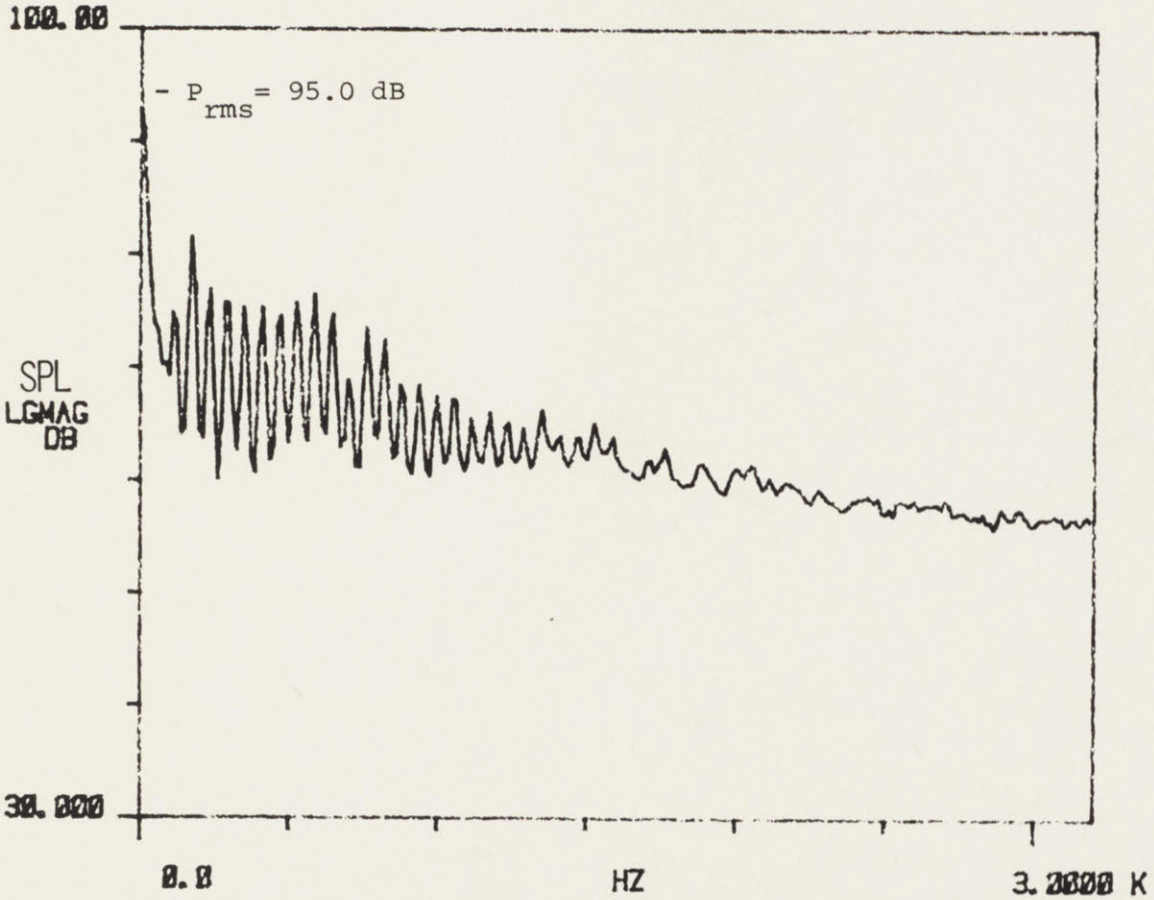

Fig C.55 On Axis Microphone From Cylinder Test

1.25 " cylinder
10 diameters upstream of rotor plane

Cylinder Test

Tape 4 Counter 1007

2 blades 1740 RPM

U = 22.5 MPH

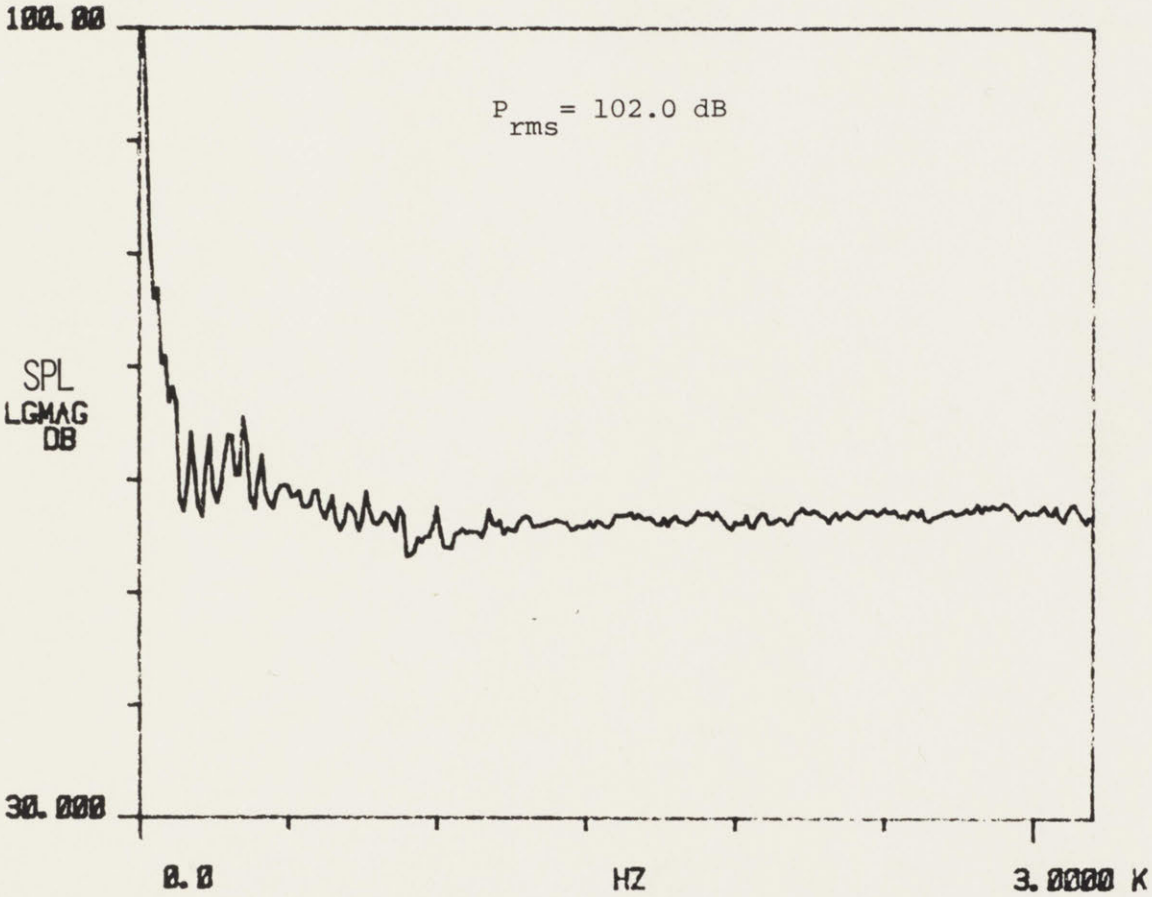

Fig C. 56 Off Axis Microphone From Cylinder Test
1.25 " cylinder
10 diameters upstream of rotor plane

Cylinder Test

Tape 4 Counter 1243

2 blades 1740 RPM

U = 22.5 MPH

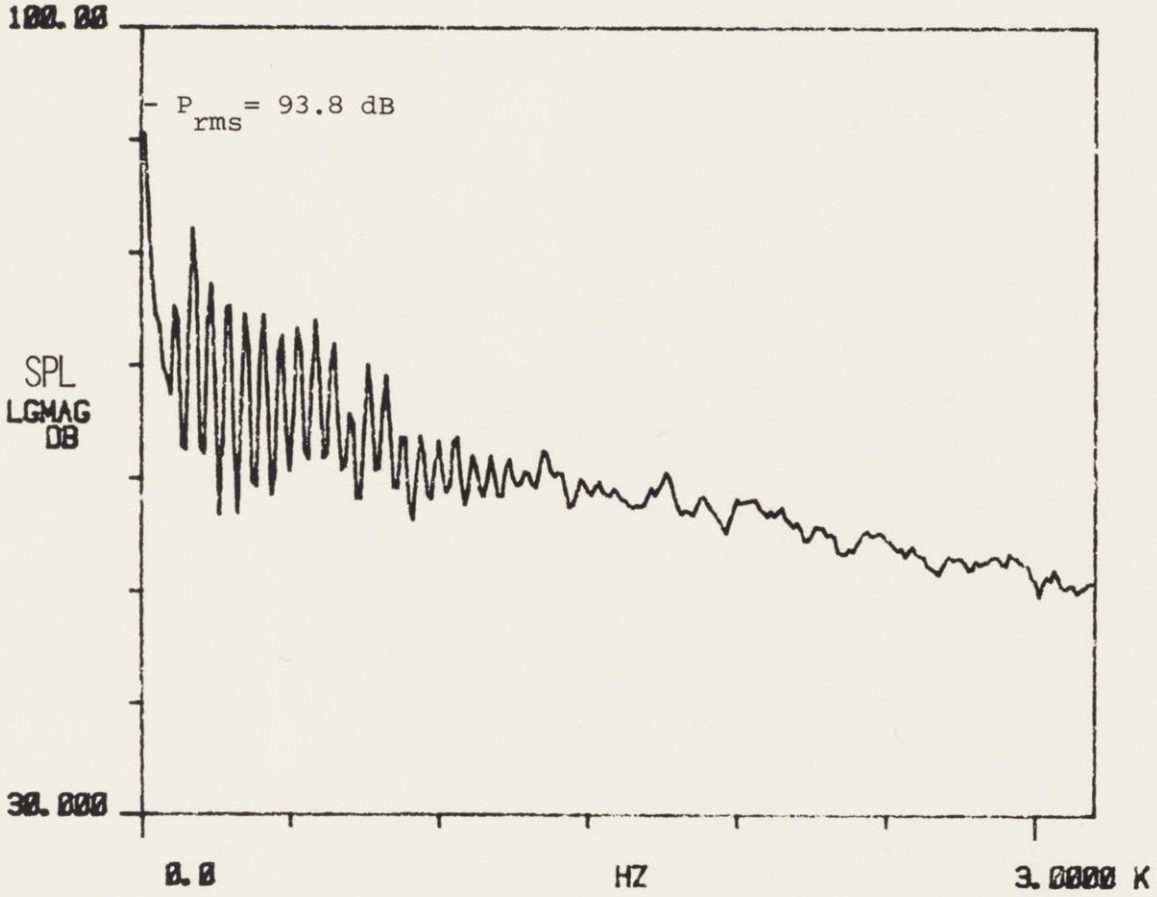

Fig C.57 On Axis Microphone From Cylinder Test

1.25 " cylinder
15 diameters upstream of rotor plane

Cylinder Test

Tape 4 Counter 1243

2 blades 1740 RPM

U = 22.5 MPH

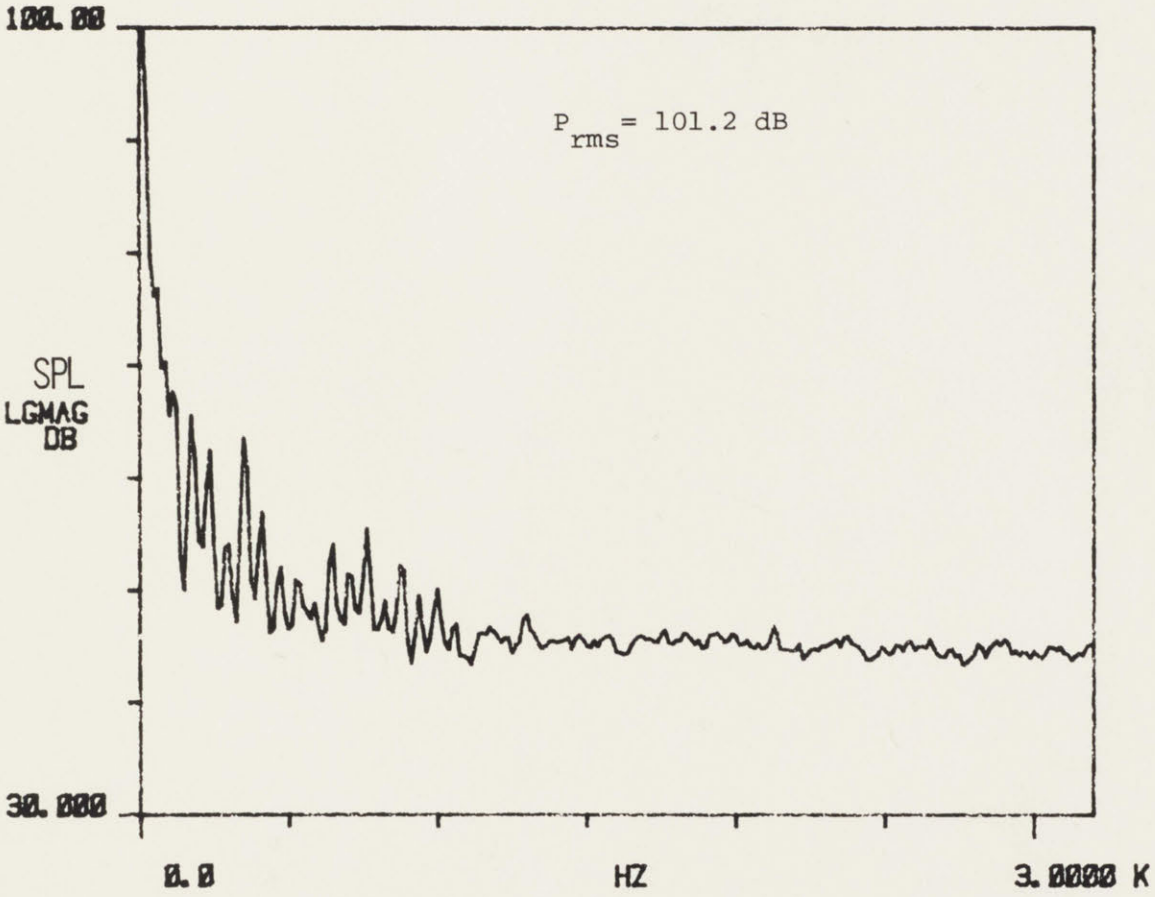

Fig C.58 Off Axis Microphone From Cylinder Test

1.25 " cylinder
15 diameters upstream of rotor plane

Cylinder Test

Tape 4 Counter 1444

2 blades 1740 RPM

U = 22.5 MPH

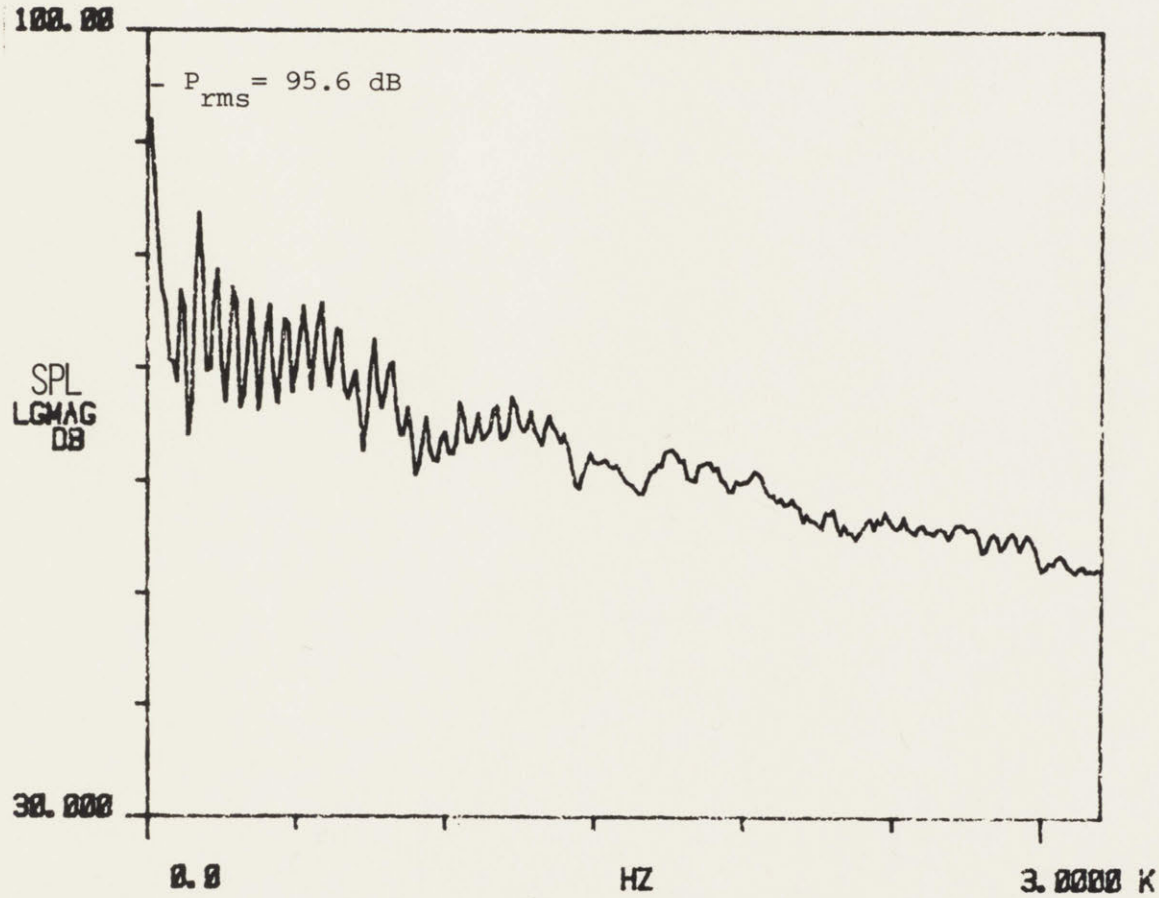

Fig C.59 On Axis Microphone From Cylinder Test

2 " cylinder
5 diameters upstream of rotor plane

Cylinder Test

Tape 4 Counter 1444

2 blades 1740 RPM

U = 22.5 MPH

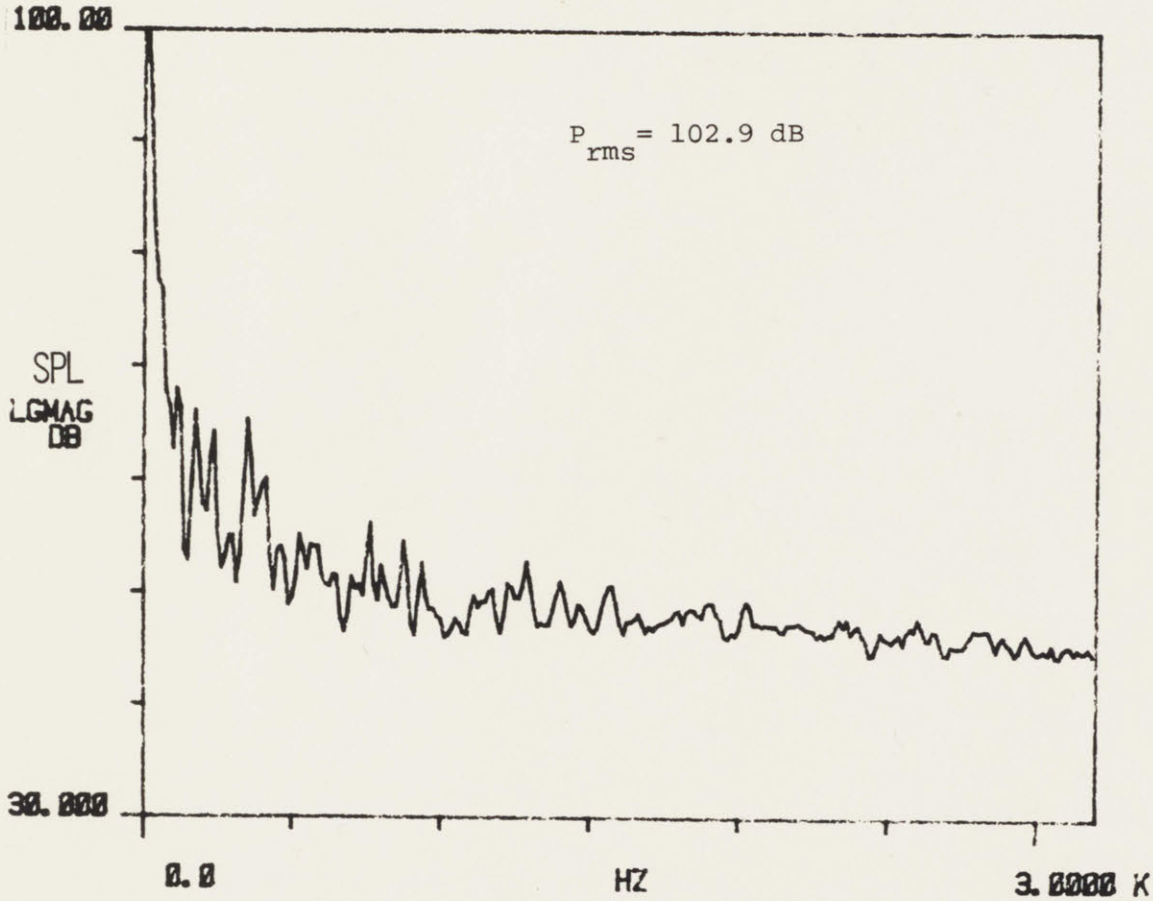

Fig C.60 Off Axis Microphone From Cylinder Test

2 " cylinder
5 diameters upstream of rotor plane

Cylinder Test

Tape 4 Counter 1654

2 blades 1740 RPM

U = 22.5 MPH

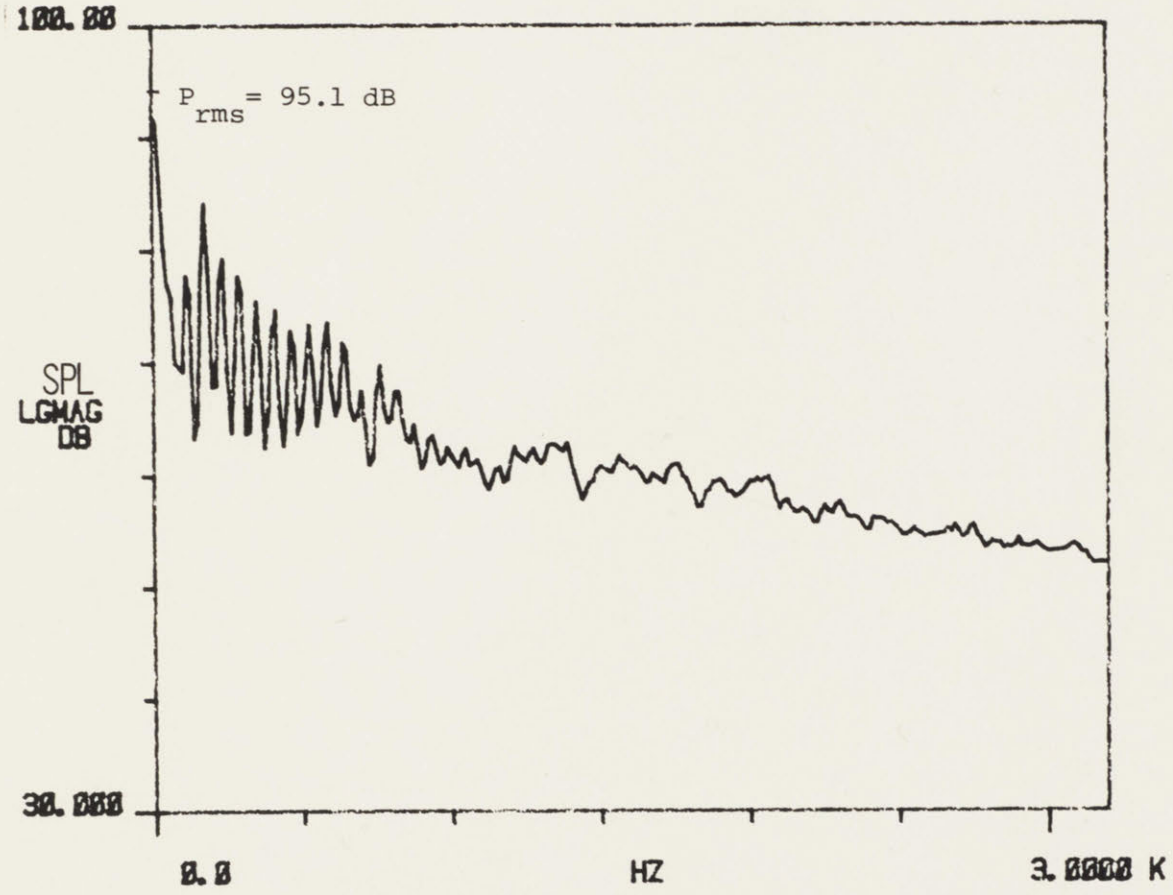

Fig C.61 On Axis Microphone From Cylinder Test

2 " cylinder
10 diameters upstream of rotor plane

Cylinder Test

Tape 4 Counter 1654

2 blades 1740 RPM

U = 22.5 MPH

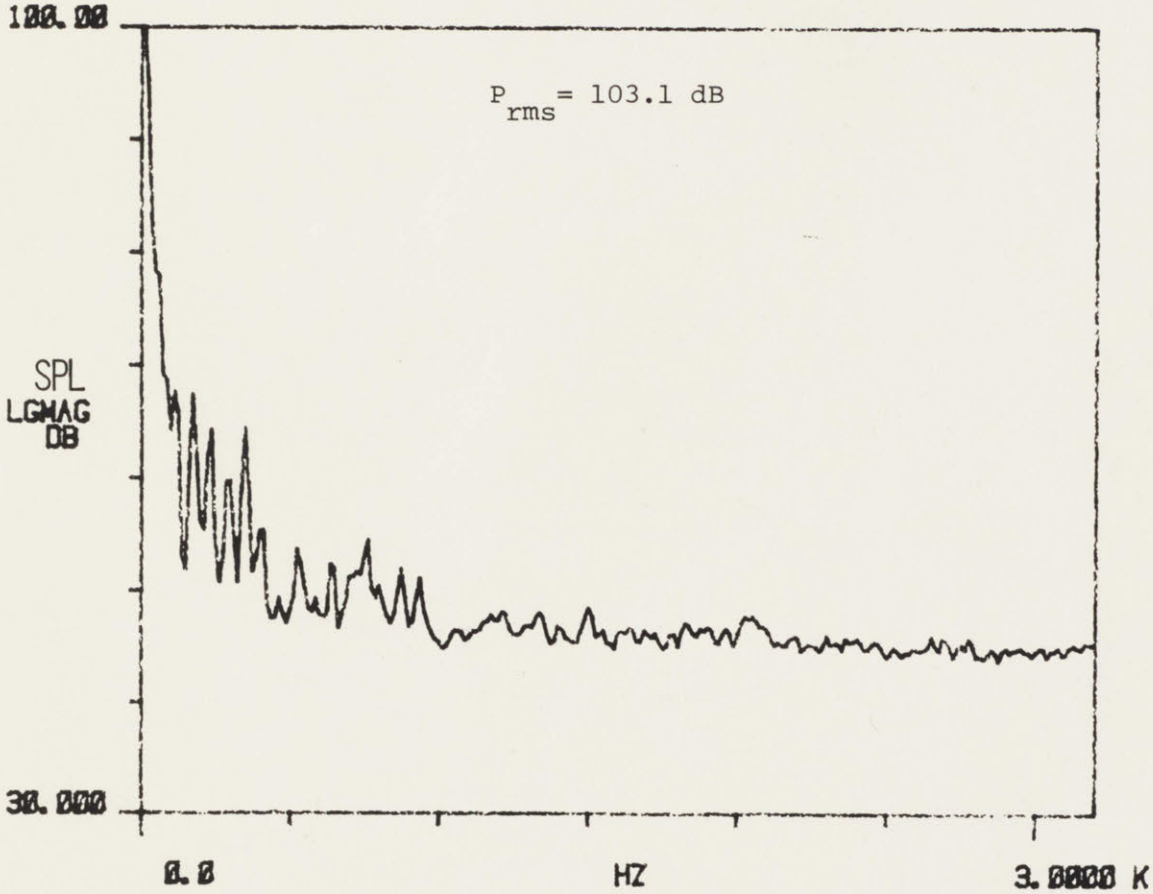

Fig C.62 Off Axis Microphone From Cylinder Test

2 " cylinder
10 diameters upstream of rotor plane

Cylinder Test

Tape 5 Counter 171

2 blades 1720 RPM

U = 22.5 MPH

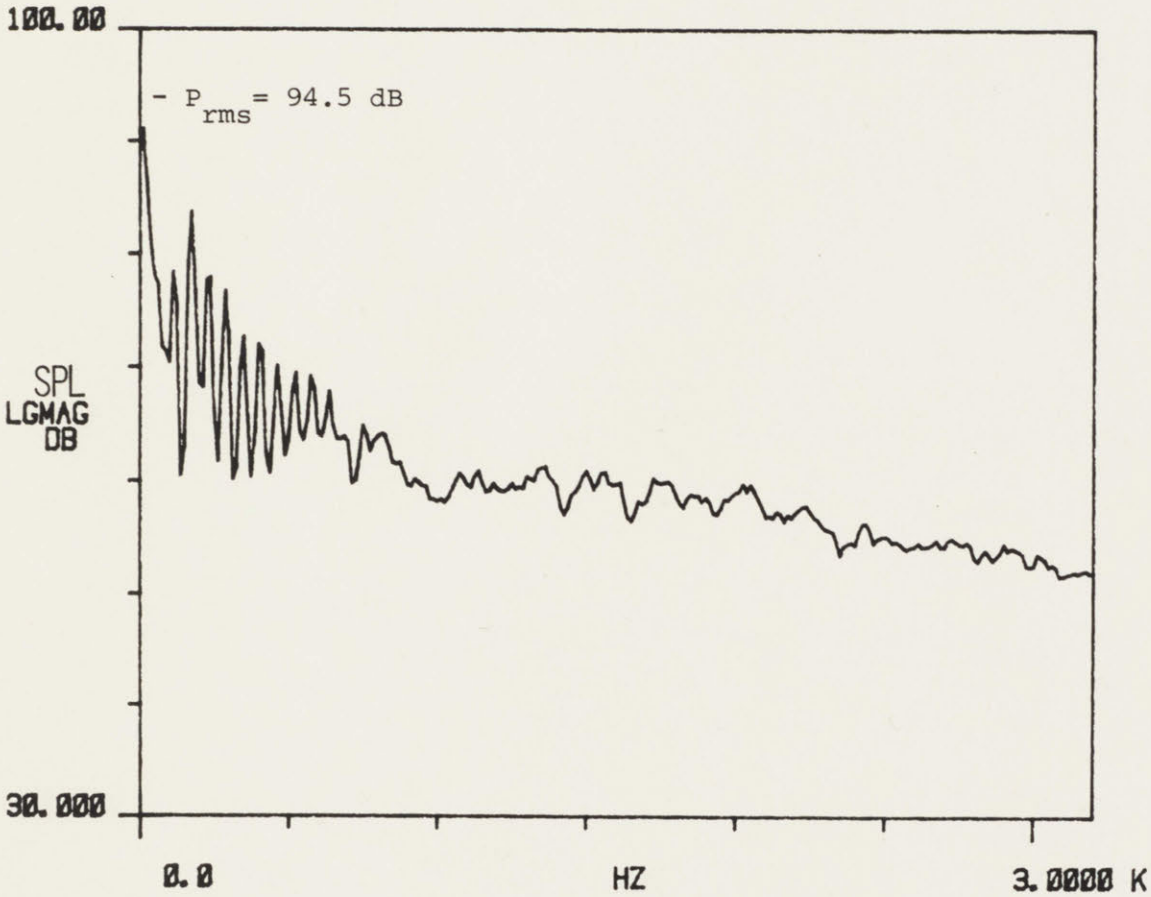

Fig C.63 On Axis Microphone From Cylinder Test

2 " cylinder
15 diameters upstream of rotor plane

Cylinder Test

Tape 5 Counter 171

2 blades 1720 RPM

U = 22.5 MPH

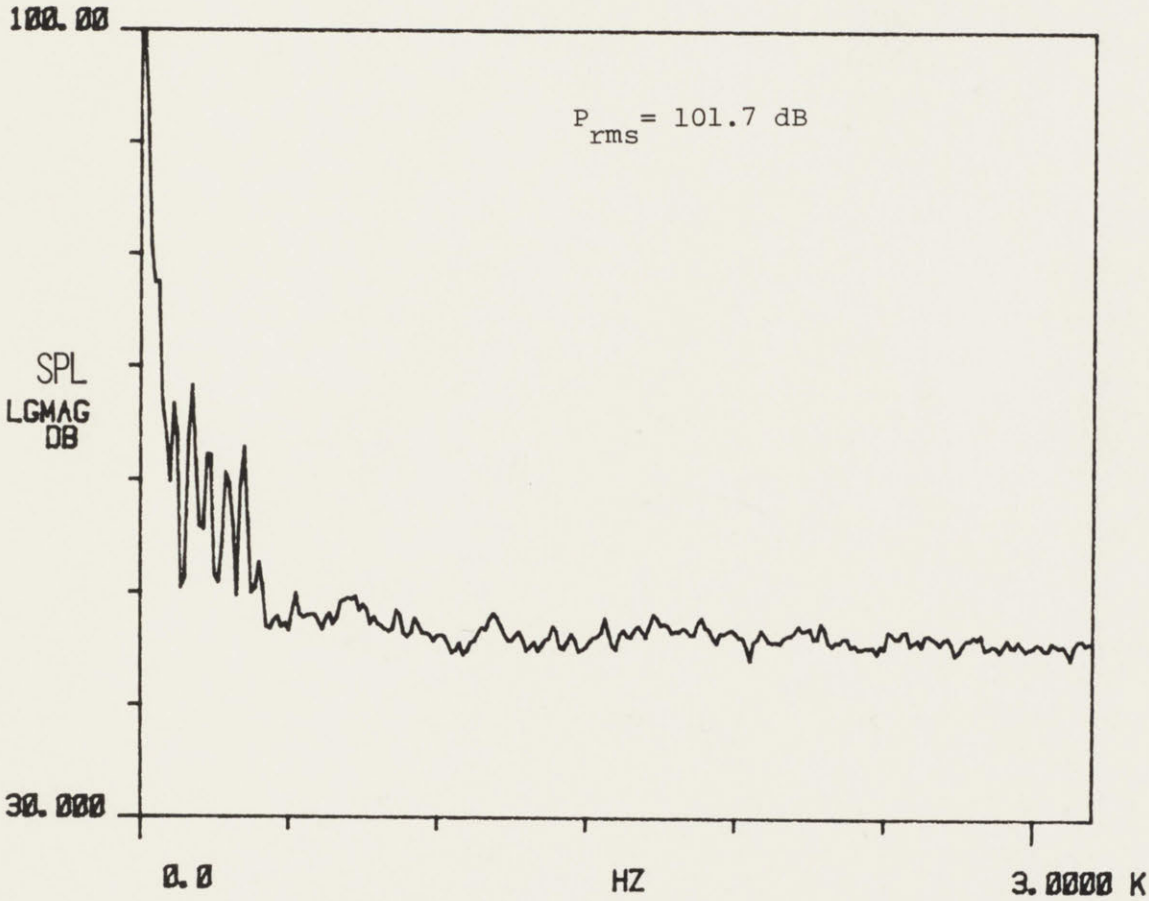

Fig C.64 Off Axis Microphone From Cylinder Test

2 " cylinder
15 diameters upstream of rotor plane

Boundary Layer Test

Tape 7 Counter 1990

2 blades 1990 RPM

U = 22.5 MPH

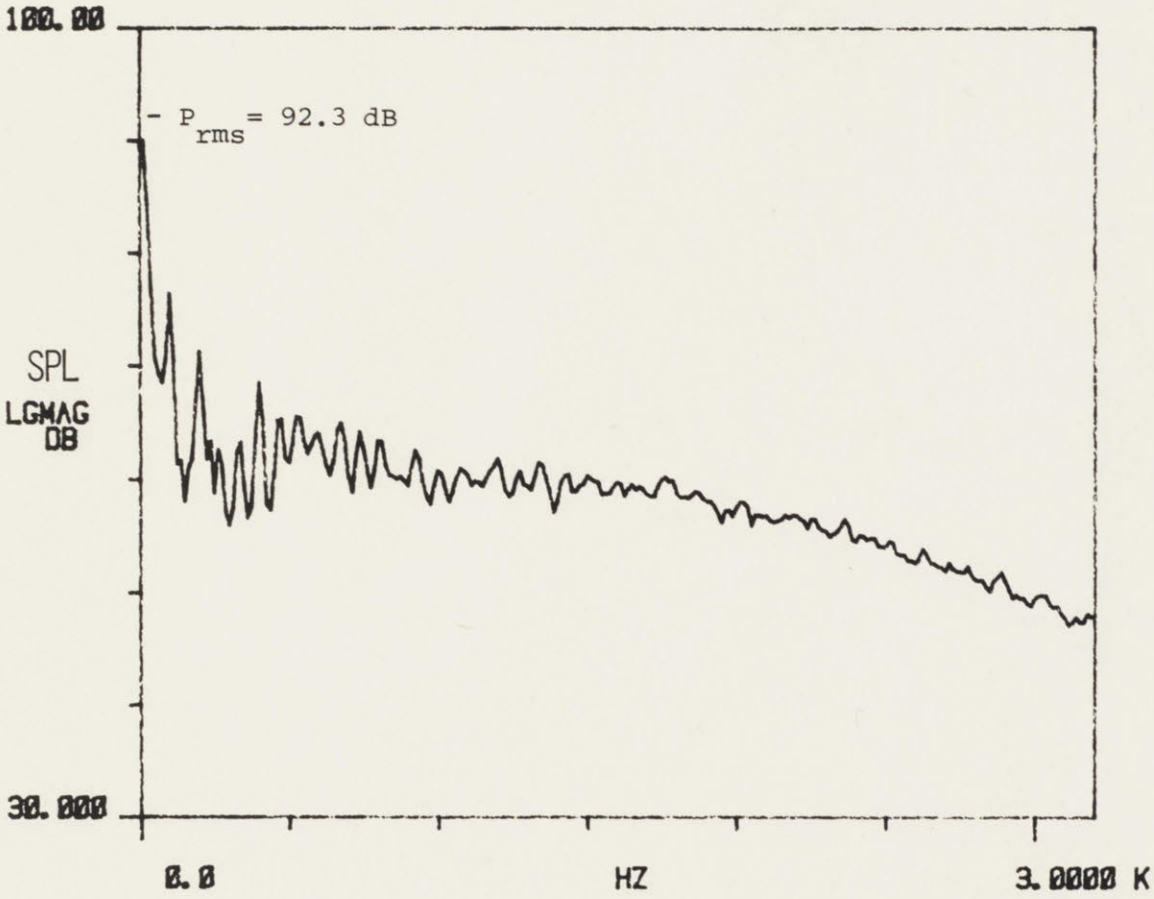

Fig C.65 On Axis Microphone For Boundary Layer #1

Boundary Layer Test

Tape 7 Counter 460

2 blades 1990 RPM

U = 22.5 MPH

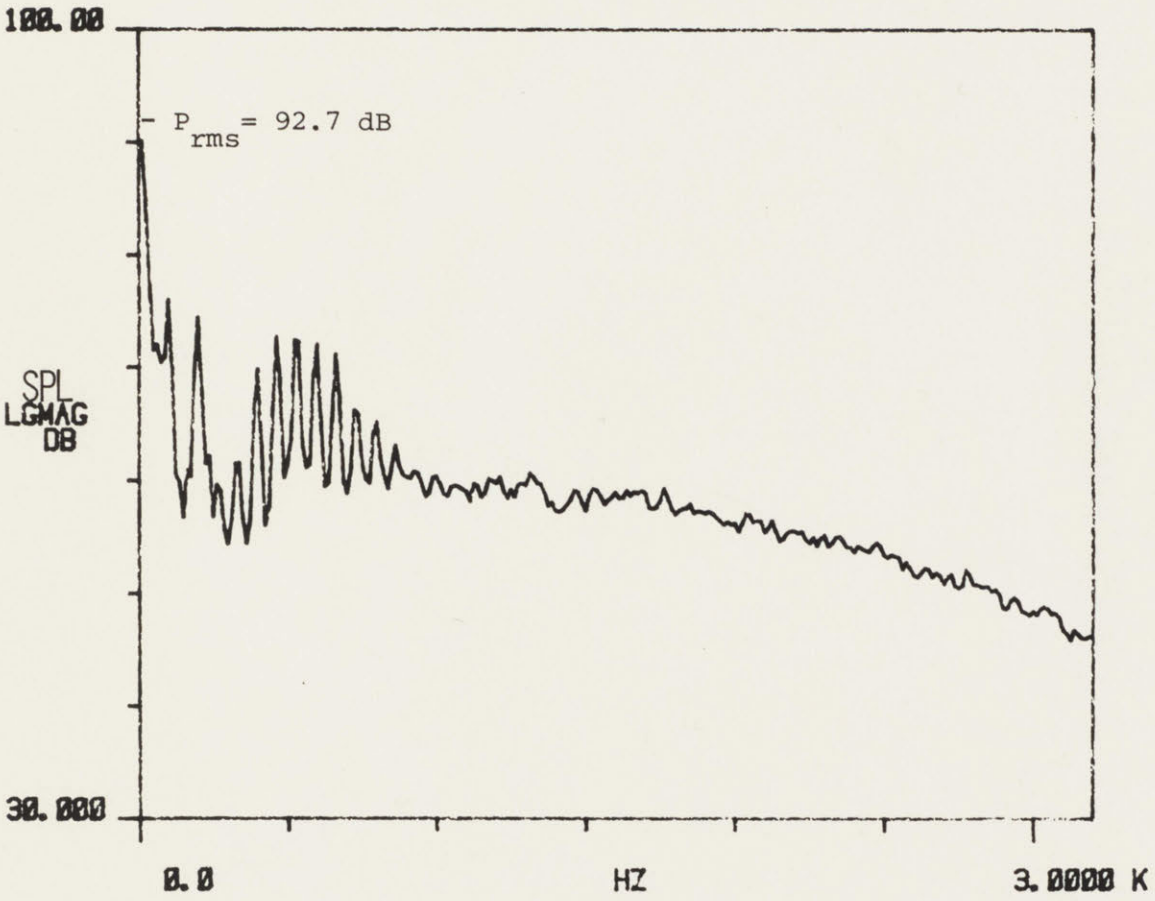

Fig C.66 On Axis Microphone For Boundary Layer #2

Boundary Layer Test

Tape 3 Counter 1393

2 blades 1610 RPM

U = 22.5 MPH

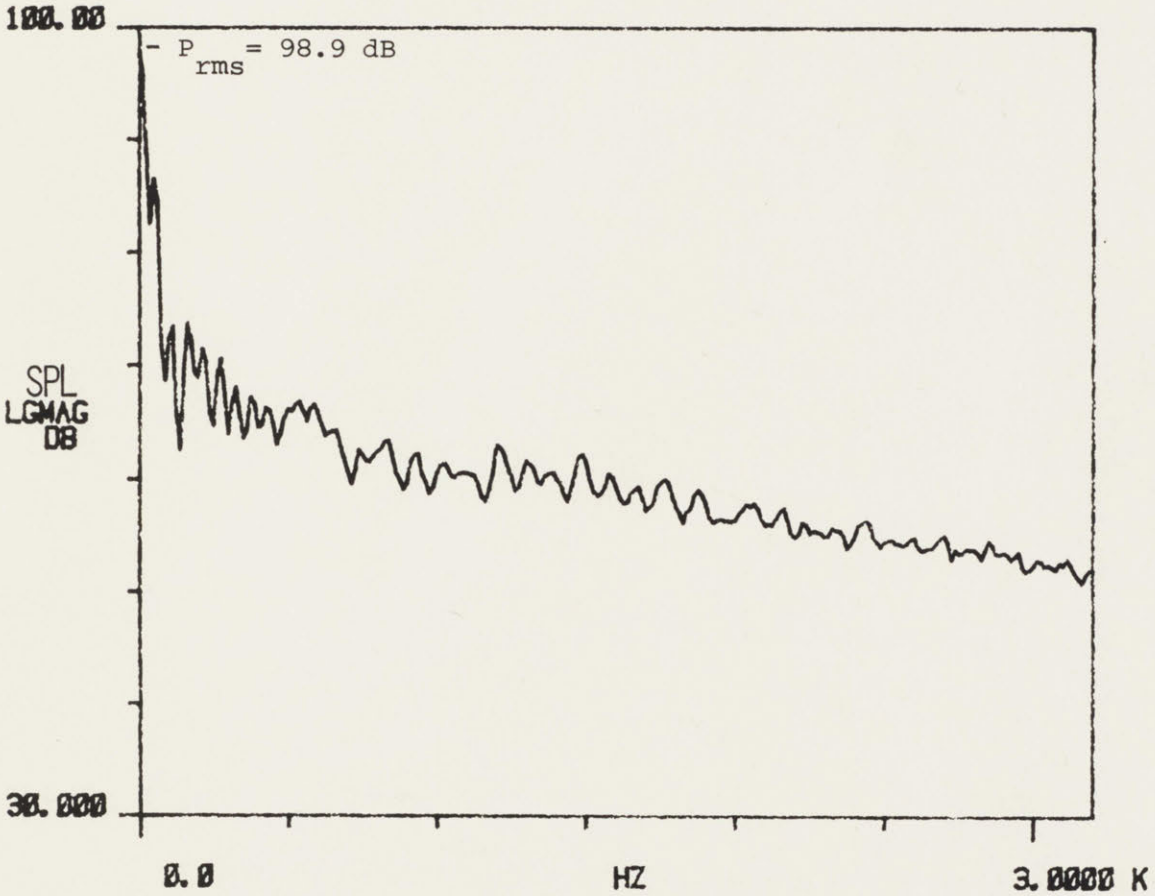

Fig C.67 On Axis Microphone For Boundary #3
(oncoming turbulence not measured)

Boundary Layer Test

Tape 3 Counter 1393

2 blades 1610 RPM

U = 22.5 MPH

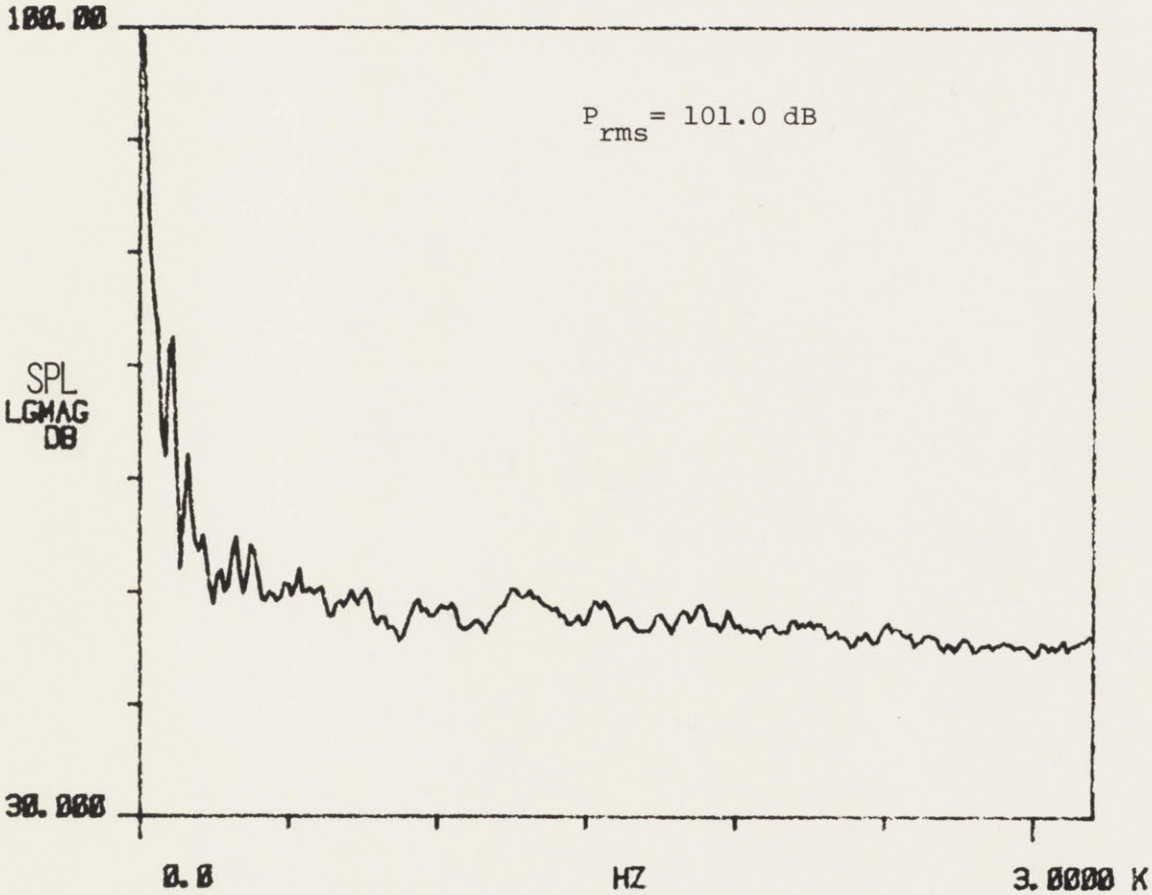

Fig C.68 Off Axis Microphone For Boundary Layer #3
(oncoming turbulence not measured)

Boundary Layer Test

Tape 3 Counter 1527

3 blades 1660 RPM

U = 22.5 MPH

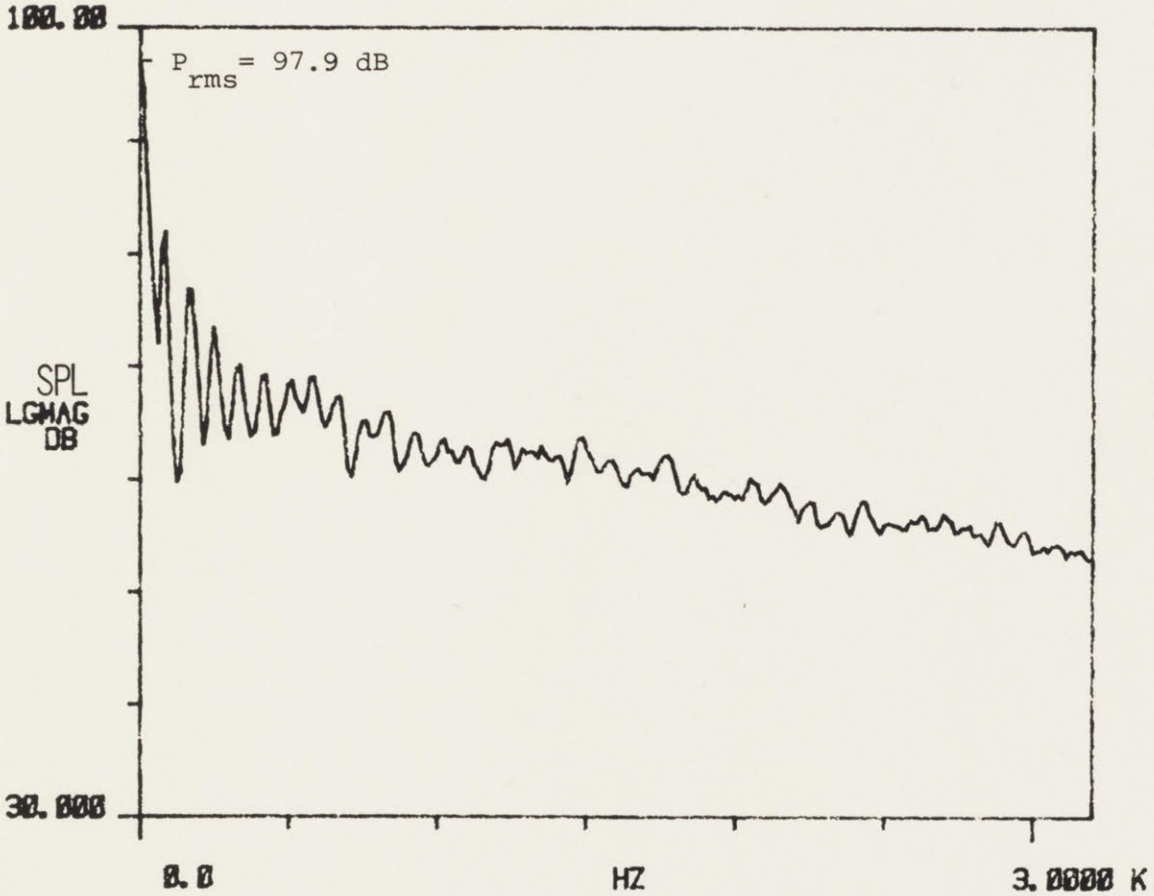

Fig C.69 On Axis Microphone For Boundary Layer #3
(oncoming turbulence not measured)

Boundary Layer Test

Tape 3 Counter 1527

3 blades 1660 RPM

U = 22.5 MPH

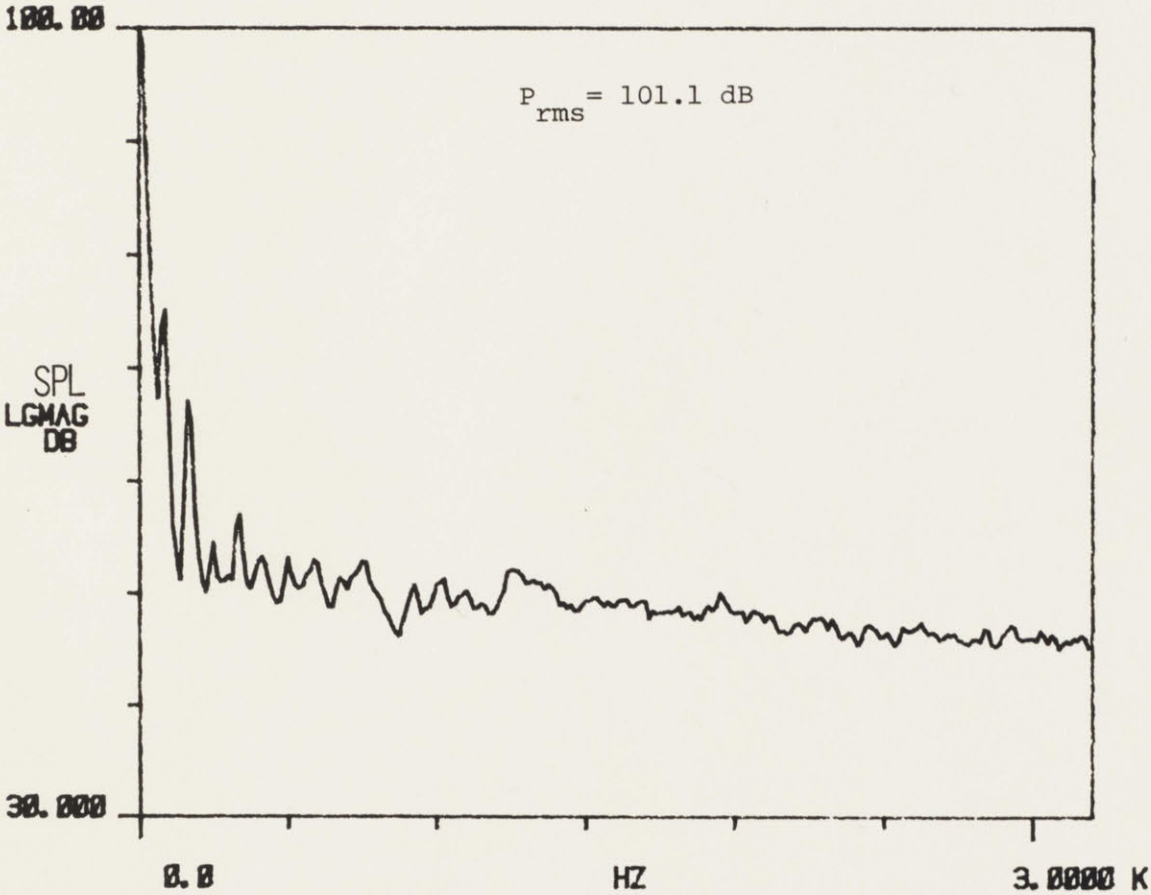

Fig C.70 Off Axis Microphone For Boundary Layer #3
(oncoming turbulence not measured)